KINETIC STUDY OF TWO PENTAMERIC LIGAND-GATED ION CHANNELS

By
Alessandro Marabelli

Submitted for the degree of Ph.D

University College London
Neuroscience, Physiology & Pharmacology

Supervised by
Prof. Lucia G. Sivilotti

'I confirm that the work presented in this thesis is my own. Where information has been derived from other sources, I confirm that this has been indicated in the thesis'.

Alessandro Marabelli
June 2014

Abstract

The Cys-loop or nicotinic superfamily is an important group of ligand-gated ion channels. The pentameric channels in this family commonly mediate fast synaptic transmission in *eukaryotes* (cf. nicotinic acetylcholine, γ-aminobutyric acid receptor and glycine receptor). Related channels are also found in *prokaryotes* and these channels include *Gloeobacter violaceous* ligand-gated ion channel (GLIC) and *Erwinia chrysanthemi* ligand gated ion channel (ELIC). Cys-loop channels share a common structural fold and are thought to activate in a similar way: the ligand binds at the interface between the extracellular domains of adjacent subunits and causes the receptor to undergo a conformational change. This is conveyed to the transmembrane region of the receptor where it results in the opening of the channel pore.

The energy landscape of the channel protein can be characterised by determining a kinetic mechanism, which explicitly details the functional states that the channel can visit and quantifies the transition rates between them. This is possible in ion channels because the current generated by a single channel molecule can be detected with high temporal resolution. Establishing a detailed kinetic mechanism allows a better understanding of the structure function relation for the protein, because it allows us to determine which step of the activation is affected when we change agonist or when we mutate the channel protein itself. The aim of my work was to establish the kinetic mechanism that best describes two homomeric ligand-gated ion channels, the α3 glycine receptor and ELIC receptor. This work involved recording single channel currents and the currents elicited by fast agonist applications and analysis by direct model fitting to the data.

The physiological role of α3 glycine receptor is not currently known. The α3 expression is concentrated in areas involved in pain processing, such as the superficial dorsal horn (Harvey *et al*., 2004), suggesting that this isoform could be involved in the nociceptive pathway. Characterising the kinetics of a synaptic receptor is important also in understanding synaptic transmission, because it is the lifetime of the activated channel that is largely responsible for setting the time course of synaptic currents. We investigated the activation mechanism of this channel in HEK293 cells by maximum likelihood fitting of single-channel data, at a wide range of glycine concentrations. The mechanism we propose suggests that α3 channels can open only when more than 3 binding sites are occupied by glycine, and only after the channel undergoes a

conformational change (‘flip’) that links binding to gating. The scheme can describe adequately macroscopic currents from fast concentration jumps experiments.

The function of the prokaryotic channel ELIC is unknown, but ELIC is important as it has been recently crystallized (Hilf and Dutzler, 2008) in non-conductive state (the highest resolution structure currently available for a non-conductive state). Establishing a kinetic mechanism for this channel is particularly important, because combining structure and function offers the best possibility to investigate how the perturbation induced by the binding of the transmitter opens the channel. We investigated the activation mechanism of this channel in HEK293 cells by maximum likelihood fitting of single-channel data, at a wide range of propylamine concentrations. The mechanism we propose suggests that ELIC can open from partially primed conformational states, and only after the channel undergoes a conformational change (‘priming’), which links binding to gating. The scheme describes adequately both macroscopic currents from fast concentration jumps experiments and single channel activity.

Table of Contents

List of Tables

List of Figures

Abbreviations

5-HT3A	Serotonin receptor
ACh	Acetylcholine
AChBP	Acetylcholine binding proteins
AChR	Acetylcholine receptor
AP^r	Ampicillin-resistance gene
ATCC	American Type Culture Collection
ATP	Adenosine tri-phosphate
BGH poly A	Bovine growth hormone poly A
cDNA	Complementary DNA
CMV	Cytomegalovirus
CNS	Central nervous system
Cys	Cysteine
DMEM	Dulbecco`s modified Eagle`s medium
DNA	Deoxyribonucleic acid
ECD	Extracellular domain
eGFP	Green fluorescent protein
ELIC	*Erwinia chrysanthemi* ligand gated ion channel
GABA	γ-aminobutyric acid
$GABA_A$	GABA receptor
GLIC	*Gloeobacter violaceous* ligand-gated ion channel
GluCl	Glutamate-gated chloride
Gly	Glycine
GlyR	Glycine receptor
HEK293	Human embryonic Kidney 293
hGlyRs-α1	Human α1 glycine receptor

HPLC	High Performance Liquid Chromatography
ICD	Intracellular domain
IPSC	Inhibitory postsynaptic current
J&W	*Jones & Westbrook*
KCC	K-Cl cotransporter
LFERs	Linear free-energy relationship
LGICs	Ligand-gated ion channels
MWC	*Monod-Wynan-Changeux*
nAChR	Nicotinic acetylcholine receptor
NEO(R)	Neomycin-resistance gene
NKCC	Na-K-Cl cotransporter
NMR	Nuclear magnetic resonance
PCR	Polymerase chain reaction
pdfs	Probability density function
pLGIC	Pentameric ligand-gated ion channel
P_{open}	Open probability
pre-mRNA	Precursor messenger Ribonucleic acid
R_s	Series resistance
TMD	Transmembrane domain
TRP	Transient receptor potential

Chapter 1: Introduction

1.1 Aims of the work

The aim of my work was to characterise the kinetic mechanism of two members of the pentameric ligand-gated ion channels (pLGIC) family, the α3 glycine receptor (GlyR) and ELIC, a prokaryotic receptor, to better understand the structure function relation of the pLGIC family. This was done using single channel recording, direct model fitting to the data and fast agonist application current recording. Studying how different agonists and mutations in the receptor influence the kinetic activation mechanism is the best way to understand the function of the different domains and the effects of mutations.

The physiological role of α3 glycine receptor is not currently known, however, α3 expression is concentrated in areas involved in nociceptive processing, such as the superficial dorsal horn (Harvey *et al*., 2004). The kinetic mechanism of synaptic channels sets the time course of synaptic currents. Thus characterising the kinetics of a synaptic receptor is important in understanding synaptic transmission.

ELIC is a prokaryotic channel and a member of the pLGIC family. ELIC has been recently crystallized (Hilf and Dutzler, 2008) in non-conductive state. The availability for ELIC of a high resolution structure makes it particularly important to establish a kinetic mechanism for this channel, as combining structure and function offers the best possibility to investigate how the perturbation induced by the binding of the transmitter opens the channel. Given that it is likely that the gating motions are conserved across the pLGIC family (as the domain folds are), extrapolating these findings to other receptors in the superfamily will help understand the structural basis of channelopathy mutations, and give a basis for rational drug design in this channel superfamily.

1.2 Ion Channels

The boundary of the cell, the cytoplasmic membrane, is a lipid bilayer that separates the living cell from its environment and contains all the vital components within the cytoplasm. This structure, however, is impermeable to polar compounds and hence mechanisms, such as transporters and ion channels, had to evolve for the active and passive diffusion of polar compounds between the two environments. Ion channels are membrane spanning proteins that are present in all organisms. Part of the ion channel forms a hydrophilic pore that opens

and allows ions to flow along the electrochemical gradient. The channel pore is usually selectively permeable and allows a restricted class of ions to flow passively down their electrochemical gradient at a very high rate (>10^6 ions per second). Different channels have different selectivity; some of them are very selective and permeable only to a single ion, while other ion channels allow more ionic species to pass through the pore.

Channels are activated by a variety of different stimuli, which gate the pore and change the conformation of the channel (open or closed). Some channels can be activated by changes in membrane potential, other by physical stimuli (temperature, stretch), whereas others are activated by extracellular or intracellular chemical signals. *Ligand-gated ion channels* (LGICs) are activated by the binding of chemicals, often acting as neurotransmitters. LGICs are divided into subfamilies, according to subunit topology and coding sequences: Cys-loop receptors, glutamate receptors and the ATP-gated channels. (Le Novere and Changeux, 1999).

1.3 The Cys-loop family

1.3.1 Introduction

In this section I will provide a general review of channels in the Cys-loop or nicotinic family. Cys-loop receptors are ligand gated ion channels that take their name from the presence of a characteristic loop formed by a disulfide bond between two cysteine (Cys) residues, which are separated by 13 highly conserved amino acids in the N-terminal extracellular domain (the β6-β7). This loop is conserved in almost all members of this superfamily, which include classical vertebrate receptors such as acetylcholine nicotinic (ACh), serotonin receptor (5-HT3A), glycine receptor (GlyR), γ-aminobutyric acid receptor ($GABA_A$), invertebrate receptors such as many nicotinic receptors, glutamate and histamine-gated chloride channels and zinc-activated channel (ZAC) (Le Novere and Changeux, 1999; Davies *et al*., 2003). Additional group of related proteins are the prokaryotic channels ELIC and GLIC, where the Cys-loop is absent (Hilf and Dutzler, 2008; Bocquet *et al.*, 2009; Hilf and Dutzler, 2009; Nury *et al.*, 2010)and the soluble acetylcholine binding proteins (AChBP) found in molluscs (Brejc *et al.*, 2001; Celie *et al.*, 2004).

All the members of the Cys-loop family are pentamers, whose five constituent subunits are arranged pseudo-symmetrically around a central channel pore. Receptors can be formed by

one single subunit type or by a combination of different subunits, and are referred to as homomeric and heteromeric receptors respectively. Channels are selective for either cations or anions, and as a result of that mediate excitatory or inhibitory synaptic potentials.

The topology of the subunits is similar for all the members of the pLGIC. Each subunit comprises an extracellular part formed by the N-terminal domain (ECD), a transmembrane domain (TMD), formed by four α-helical transmembrane sequences (M1-M4), and a large, variable intracellular loop between TM3 and TM4. This contains an amphipathic helix but is mostly unstructured (Grenningloh *et al*., 1987; Finer-Moore and Stroud, 1984) (Figure 1.1).

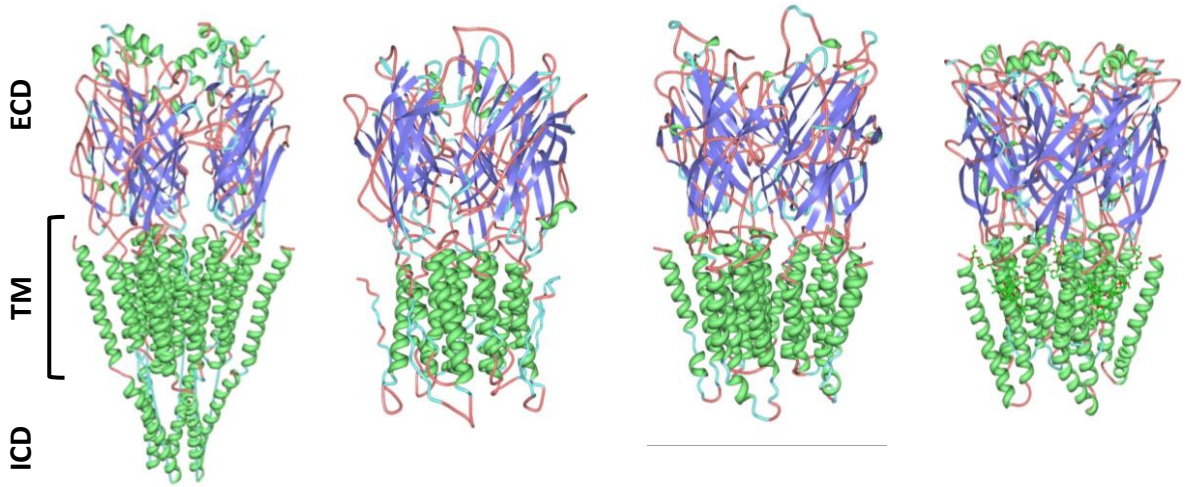

Loop C Torpedo acetylcholine (ACh) (Unwin, 2005)

Erwinia chrysanthemi (ELIC) (Hilf and Dutzler, 2008)

Cyanobacterium Gloebacter violaceus (GLIC) (Hilf and Dutzler, 2009)

Caenorhabditis elegans glutamate-gated chloride channel α (GluCl) (Hibbs and Gouaux, 2011)

Figure 1.1 Structures of pLGIC receptors
Ribbon structures of the Torpdepo nicotinic acetylcholine receptor (nAChR) (Protein Data Bank (PDB): 2BG9), of the prokaryotic receptor ELIC (PDB:2VL0), GLIC (3EHZ) and GluCl (PDB 3RIF), view from the membrane plane. ECD is the Extracellular domain, TMD is the transmembrane domain and the ICD is the Intracellular domain. The structures were made using the program PyMOL (www.pymol.org).

The first ligand-gated ion channel (LGIC) member of the Cys-loop family to be characterized in detail was the acetylcholine receptor (AChR) at the neuromuscular junction. Indeed up to about 10 years ago, most of what is known about the structure of the members of the Cys-loop family was based on Nigel Unwin's cryo-electron microscopy of *Torpedo* muscle-type AChR (Unwin, 2005). More recently other proteins related to the Cys-loop family, such as

the soluble AChBP (homopentamers which contains only the extracellular domain) and channels from prokaryotic and invertebrate organisms have been crystallized. The Table 1.1 summarises the main structures available so far on the pLGIC.

Table 1.1 Main structures for the pLGICs family

Receptor	Structure	Resolution	Conformation	Reference
AChBP	Crystals	2.7 Å	no channel	(Brejc *et al*., 2001)
Torpedo ACh	Cryo-EM	4 Å	closed channel	(Unwin, 2005)
ELIC	Crystals	3.3 Å	closed channel	(Hilf and Dutzler, 2008)
GLIC	Crystals	2.9 Å	open channel	(Bocquet *et al*., 2009; Hilf and Dutzler, 2009)
GluCl	Crystals	3.3 Å	open channel	(Hibbs and Gouaux, 2011)
Torpedo ACh	Cryo-EM	6 Å	open/closed channel	(Unwin and Fujiyoshi, 2012)
Glycine α1	NMR		Transmembrane domain only	(Mowrey *et al.*, 2013)
$GABA_A\beta3$	Crystals	3 Å	closed channel	(Miller and Aricescu, 2014)
5-HT3A	Crystals	3.5 Å	closed channel	(Hassaine *et al.*, 2014)

1.3.1.1 N-Terminal Domain

The N-terminal domain forms the ligand binding domain in the extracellular space and contains the 13 amino acids disulfide linked Cys-loop. Most of the molecular details for the N-terminal domain have been extrapolated from the 2.7 Å structure of the snail's AChBP, which is not an ion channel (Brejc *et al*., 2001). The more recent structures of prokaryotic receptors such GLIC (Bocquet *et al*., 2009) and ELIC (Hilf and Dutzler, 2008), and from an invertebrate Glutamate-gated chloride (GluCl) receptor (Hibbs and Gouaux, 2011) support the assumption that the general fold of the subunits is conserved in the superfamily (Figure 1.2). Nevertheless, it must be noted that there is relatively little sequence homology across the family, in particular between the channels that have provided good structural information and those which are important in mammalian synaptic transmission.

For instance, AChBP subunits share ≈25% sequence identity with the N-terminal of the muscle nAChR subunits and ≈15-20% homology with the other Cys-loop receptors (Sixma and Smit, 2003; Sixma, 2007), but lack the transmembrane and intracellular domains found in

the actual channels. Because AChBP can bind agonists, toxins and competitive antagonists that bind to nAChR, they have been used to model the agonist binding region, despite the relatively low homology (Karlin, 2002; Sixma and Smit, 2003; Ulens *et al*., 2006). Each AChBP subunit (Brejc *et al*., 2001) is formed by a sandwich like structure of 10 β-strands, with an inner sheet located towards the central axis of the pentamer made of six strands (β1, β2, β3, β5, β6 and β8) and an outer sheet formed by four strands (β4, β7, β9 and β10) located distally from the central axis. This structure is conserved in the agonist binding domain of the α1 muscle ACh subunit (Dellisanti *et al*., 2007), GLIC (Hilf and Dutzler, 2009), ELIC (Hilf and Dutzler, 2008) and GluCl (Hibbs and Gouaux, 2011). There is also a short α-helix between β strands 3 and 4, at the part of the extracellular domain (ECD) that is furthest from the membrane. The cylinder formed by the five extracellular domains has an external diameter of 80Å, and an internal diameter of 18Å with a height of 60Å (Sixma and Smit, 2003).

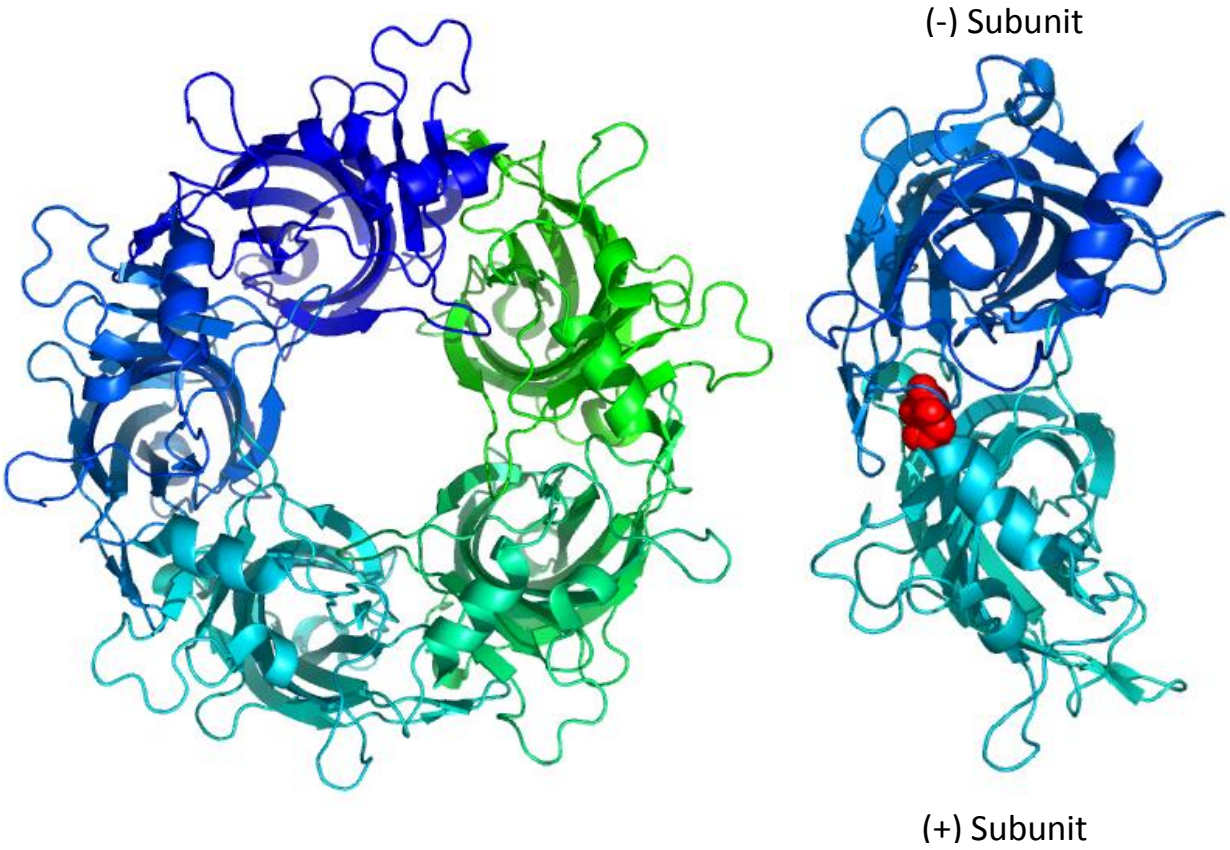

Figure 1.2 N Terminal domain
The N terminal domain of five subunits of GlucCl, view from the top are coloured separately. The binding site between the subunit interface, in red the agonist glutamate. The structures were made using the program PyMOL.

The agonist binding site is located at the interface between two subunits (Brejc *et al*., 2001; Bocquet *et al*., 2009; Hibbs and Gouaux, 2011; Celić *et al*., 2003; Sine, 2002), which are termed the principal and the complementary subunits (Figure 1.2). The principal subunit provides the anticlockwise part of the site and contributes loops A, B and C, whereas the complementary subunit forms loop D, E, F and G. This nomenclature was introduced by Galzi and Changeux (1995) on the basis of early mutational studies. Within each loop, only a few residues can face into the binding pocket, but other nearby residues may play other important roles, such as maintaining the pocket structure or stabilising conformational changes.

All the binding sites of the members of the Cys-loop family, with ZAC as the only exception, contain aromatic residues, which are thought to form a cation-π interaction with the ligand. In different Cys-loop receptors, the cation-π interaction appears to be provided by different aromatic side chains (Trp, Phe or Tyr) (Beene *et al*., 2002; Xiu *et al*., 2009; Lummis *et al*., 2005; Pless *et al*., 2008; Hibbs and Gouaux, 2011). Each of these aromatic side chains are located in one of the three loops on the principal subunit and form an "aromatic box".

1.3.1.2 Transmembrane domain

Each subunit has four α-helices (M1-M4) that span the membrane. The first structural information on the TMDs came from Unwin's work on Torpedo AChR (Unwin, 1995; Miyazawa *et al*., 1999; Miyazawa *et al*., 2003; Unwin, 2005). The best resolution reached by this analysis of cryo-electron microscopy images of the nAChR was 4Å (Miyazawa *et al*., 2003). Recently, structural information at higher resolution has been obtained from prokaryotic pLGICs (Bocquet *et al*., 2009; Hilf and Dutzler, 2008; Hilf and Dutzler, 2009; Nury *et al*., 2010). The structures show the four TMDs of each subunit arranged symmetrically around the central pore. The inner ring is formed by M2 helices from the five subunits, which is shielded from the membrane by the other TMD arranged in a clockwise orientation (Miyazawa *et al*., 1999; Miyazawa *et al*., 2003). Charged amino acids are present only at the beginning and end of each M1, M3 and M4 domains, satisfying the need of the helices to be hydrophobic (Miyazawa *et al*., 2003).

M1 is in contact with the lipid environment and may contact M2 as well. The importance of M1 has been shown using several mutations that produce non-functional receptors or changes

in EC_{50} (Akabas and Karlin, 1995; Zhang and Karlin, 1997; Dang *et al*., 2000; Greenfield *et al*., 2002; Lobitz *et al*., 2001; Lobo *et al*., 2004; Spitzmaul *et al*., 2004). M1 may be involved in transmitting movement from the ligand binding site in ECD to the M2, through interactions with the M2 helix following activation (Dang *et al*., 2000; Unwin *et al*., 2002; Miyazawa *et al*., 2003; Cymes and Grosman, 2008). The region that links the ECD to M1 plays an important role in the gating process. Indeed, mutations in this region have been shown to affect receptor gating (Castaldo *et al*., 2004; Kash *et al*., 2004; Zhang and Karlin, 1997). In addition to that, the intracellular end of M1 and the M1-M2 linker is likely to be exposed to the pore, as it contains residues responsible for cation/anion selectivity (Filippova *et al*., 2004).

Electron microscope images of the nAChR pore (Miyazawa *et al*., 2003) show that the channel comprises a ring of five aligned M2 α-helices, one from each of the five subunits. The pore structure may be stabilized by contacts between the different M2 helices and by the contacts at the beginning and end of M1 and M3 helices, which support the actual channel lining (Miyazawa *et al*., 2003). M2 is approximately 40Å long and it extends beyond the membrane (Miyazawa *et al*., 2003). The pore is wider at the external end and each helix has a bend in the middle. The channel gate is located in M2 between residues 6'-9', where the helices tilt toward the centre of the pore (Miyazawa *et al*., 2003; Leonard *et al*., 1988; Unwin, 2005).

The pore is highly symmetrical due to equal side by side hydrophobic interaction between residues 9', 10', 13' and 14'. These residues form several levels of contacts. Thus, the side chain of the 9' and 13' residues interact with those of the 10' and 14' residues of the adjacent M2 domain (e.g. 9' with 10' and 13' with 14'). These interactions create a hydrophobic girdle that is 3Å wide at its narrowest point in the closed channel (Miyazawa *et al*., 2003).

New information about the channel pore comes from crystal structures of prokaryotic pLGICs (Hilf and Dutzler, 2008; Hilf and Dutzler, 2009; Bocquet *et al*., 2007) and invertebrate GluCl (Hibbs and Gouaux, 2011). The structures confirmed both that the M2 helices of GLIC and ELIC are bordered by rings of charges, homologous to nAChR (Imoto *et al*., 1988), and that the extracellular half of the pore is mainly composed of hydrophobic residues, whereas the intracellular half of the pore is composed of polar side chains of serine and threonine that provides a hydrophilic environment (Hilf and Dutzler, 2008; Hilf and

Dutzler, 2009). A ring of glutamate residues (-2') in the intracellular pore entry define the narrowest part of the channel (Hilf and Dutzler, 2009), and resemble a narrow selectivity filter. The smallest diameter of the GluCl pore is 4.6 Å, which is defined by the hydrophobic girdle of -2' (Hibbs and Gouaux, 2011), and it is smaller than that estimated for $GABA_A$ and GlyR 5.2-6.2 Å (Bormann *et al*., 1987; Mowrey *et al*., 2013). Recently, the isolated transmembrane domain of the human α1 glycine receptor (hGlyRs-α1) has been determined by using nuclear magnetic resonance (NMR) and electron micrographs (Mowrey *et al*., 2013). The M2 of the hGlyRs-α1 is formed by 21 residues from -2' to 18', because the residues subsequent to the 18' in M2 are nonhelical (Mowrey *et al*., 2013). This is in contrast with the structure of the TMD of α2β4 and α7 nAChR, which show a longer M2 of 23 residues from -2' to 20' (Bondarenko *et al*., 2012; Bondarenko *et al*., 2013) (Figure 1.3)

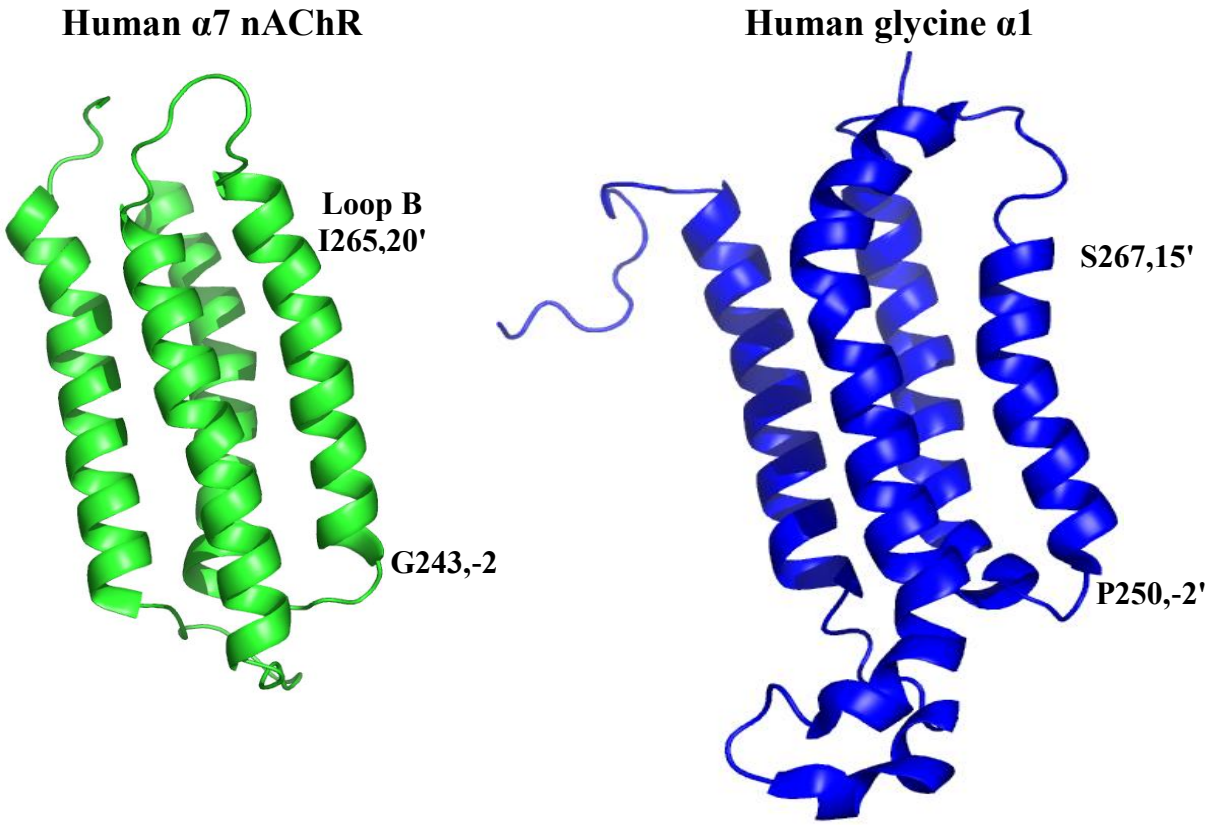

Figure 1.3 Transmembrane domains
The TMD of one subunit of human α7 nAchR (green, (Bondarenko *et al*., 2013)) and human glycine α1 (blue, (Mowrey *et al*., 2013)), view from the side. The structures were made using the program PyMOL.

In Cys-loop receptors, the -2/2 region of the pore has been proposed to provide the charge selectivity filter (Imoto *et al*., 1988; Corringer *et al*., 1999; Keramidas *et al*., 2004; Hibbs and

Gouaux, 2011). The key residues for anion permeation are -1' Ala and -2' Pro and -1' Glu for cations (Thompson *et al*., 2010; Sunesen *et al*., 2006; Hibbs and Gouaux, 2011). Mutations in the TM2 affect the modulation of glycine and $GABA_A$ receptors by general anaesthetics (Dupre *et al*., 2007; Mihic *et al*., 1997), zinc (Lynch *et al*., 1998) and protons (Wilkins *et al*., 2005).

Structural data show that M2 is shielded from the lipid bilayer by M3 and M4, which are α-helical, though there are water-accessible clefts in between the TMD α-helices (Miyazawa *et al*., 2003). The M3 helix is straight in all the ligand gated receptors imaged so far, except for the TMD of Glycine receptors, which have a kink at Ala288 that changes the axis direction by approximately 33˚ (Mowrey *et al*., 2013).

M3 and M4 play a role in receptor function, as shown by the fact that mutations in M3 and M4, have effects on channel assembly (Guzman *et al*., 2003), on converting ivermectin from positive allosteric modulator to antagonist (Collins and Millar, 2010), on the potentiation by allosteric modulators (Young *et al*., 2008) and on single-channel kinetics of nAChRs (Bouzat *et al*., 2000; Bouzat *et al*., 2002; Wang *et al*., 1999; Lasalde *et al*., 1996). These regions also affect receptor expression on the cell surface (Butler *et al*., 2009; Villmann *et al*., 2009).

1.3.1.3 The loops in the TMD and the intracellular domain

The M1-M2 loop in the glycine α1 receptor is formed by only five amino acids (TM1-Asp-Ala- Ala-Pro-Ala-TM2). It has been suggested that this loop links the binding signals with channel gating (Lynch *et al*., 1997; Czajkowski, 2005), but evidence for an exclusive role of this (or other domains) in signal transduction is lacking. Evidence from substituted cysteine accessibility data indicates that this region lies along the ion-conducting pathway, suggesting a possible role in ion selectivity (Imoto *et al*., 1988; Galzi *et al*., 1992; Filippova *et al*., 2004; Keramidas *et al*., 2000). It has been shown that the intracellular domain between M1 and M2 also influences the desensitisation properties (Saul *et al*., 1999) and the zinc potentiation of GlyR (Lynch *et al*., 1998).

The M2-M3 loop forms part of the interface between ECD and TMD, and as such is also likely to have a role in the conformational change that transmits binding energy in channel opening (Lynch *et al*., 1997). The loop is formed by the helical part of the domain that

extends outwards of the membrane (Miyazawa *et al*., 2003; Ma *et al*., 2005). The position of this loop is controversial, because the models proposed by Unwin (Miyazawa *et al*., 2003; Unwin *et al*., 2002) are different compare to the crystal structures available for the pLGIC (Hilf and Dutzler, 2008, 2009; Hibbs and Gouaux, 2011; Hassaine *et al.*, 2014; Miller and Aricescu, 2014). Mutations in this region disrupt the activation of nicotinic acetylcholine, GABA and Glycine receptors (Campos-Caro *et al*., 1996; Grosman *et al*., 2000a; Grosman *et al*., 2000b; Lewis *et al*., 1998; Saul *et al*., 1999; Lape *et al*., 2012). Two of the best characterised residues in this loop are Arg271 and Lys276 in the α subunit of GlyR. Mutations of these residues to Gln/Leu and Glu, respectively, cause hyperekplexia in man (Shiang *et al*., 1993; Elmslie *et al*., 1996). In the case of the Arg271 mutations, all that we know is that there is a reduction in the channel sensitivity to glycine (Rajendra *et al*., 1994). An in depth single channel study in our lab showed that the Lys276 mutation slows and impairs channel gating by glycine (Lape *et al*., 2012). Other effects of these mutations include transforming beta-alanine and taurine from agonists into competitive antagonists (Rajendra *et al*., 1995), converting picrotoxin from channel blocker to an allosteric potentiator (Lynch *et al*., 1995) and reducing the single channel conductance of the receptor (Langosch *et al*., 1994).

The intracellular domain (ICD) is mostly formed by the loop between TM3 and TM4. This is poorly conserved in length and sequence across Cys-loop members (Le Novere and Changeux, 1999) and it does not show secondary structure, apart from a single α helix of 23 residues (Unwin, 2005). Interestingly, homologous receptors in bacteria do not possess the intracellular region between TM3 and TM4 (Hilf and Dutzler, 2008; Bocquet *et al*., 2007). Deletion of the intracellular region does not compromise expression of vertebrate channels (Jansen *et al*., 2008), suggesting that this region is not essential for receptor expression in recombinant systems. On the contrary, receptor function is influenced by this intracellular region (Baptista-Hon *et al.*, 2013). The cytoplasmic loop is involved in intracellular modulation by internal molecules and is thought to interact with kinases and phosphatases and to undergo ubiquitination at specific sites (Lynch, 2004). These interactions can modulate receptor activity, assembly and trafficking (Akk and Steinbach, 2000; Bouzat *et al*., 1994; Melzer *et al*., 2010; Meyer *et al*., 1995; Kneussel and Betz, 2000; Kneussel and Loebrich, 2007). Unwin's data show that the intracellular domain forms a structure with fenestrations lined with charged residues, which are likely to be the intracellular portal to the pore. This is confirmed by the effect of mutations in this region on channel conductance, (Kelley *et al*.,

2003; Peters *et al*., 2004; Gee *et al*., 2007; Livesey *et al*., 2008; Hales *et al*., 2006; Carland *et al*., 2009).

1.3.2 Activation of Cys-loop receptors

Once a receptor has bound its specific neurotransmitter, the signal has to travel from the ECD binding pocket to the gate, which is located approximately 60Å from the pocket. The signal triggers conformational changes that open the channel pore and allow ions to permeate the channel. Thus, the last step in any activation mechanism is the channel opening. Linear free-energy relationship analysis (LFERs) (Leffler, 1953; Leffler and Grunwald, 1963) showed that channel opening is the result of a conformational wave which starts at the binding site. This progresses to the transmembrane domain and terminates at the gate (Grosman *et al*., 2000a; Grosman *et al*., 2000b), the opposite wave describes the closing of the channel.

Binding happens at the interface between adjacent subunits, loops A-C on the principal side and loops D-F on the complementary side (Corringer *et al*., 2000). The binding process does not always involve all the residues present in the binding site. X-ray crystallography studies have indicated the different ways in which the agonist positions itself inside the binding pocket, which is box like. Once the agonist enters inside the pocket, it is trapped by the inward movement of loop-C, which closes the pocket (Celie *et al*., 2004; Hansen *et al*., 2005; Gao *et al*., 2005). The loop-C is uncapped in the absence of agonist (Unwin, 2005) and when an antagonist is present, the loop-C moves outwards (Hansen *et al*., 2005). Moreover, it has been suggested that the closure of the Loop-C is an important determinant for agonist efficacy (Hibbs *et al*., 2009; Brams *et al*., 2011).

On the basis of the 4 Å structure of the nAChR (Unwin, 2005), it was suggested that loop-B could facilitate reorientation of β-sheets during the activation, because it connects the inner and outer β-sheets . Functional studies of ACh receptors have shown that loop-B contacts loop-A and loop-C on the principal binding face (Grutter *et al*., 2003; Mukhtasimova *et al*., 2005; Lee and Sine, 2004). The importance of loop-A has been revealed using rate equilibrium free energy relationship, which showed how loop-A stabilised the closed state of the receptor and moves early on in activation (Chakrapani *et al*., 2003).

The agonist binding domain is linked covalently to the TMD by the pre-M1 region between β10 and M1. In addition to that, the bottom of the ECD comprises loop 2 (between β1 and

β2), the Cys-loop (loop 7), and loop 9 (between β8 and β9). These extend towards the TMD contacting the linker between M2 and M3 α helices (Grosman *et al*., 2000a; Lee and Sine, 2005; Rovira *et al*., 1999). The local changes in the agonist binding site are propagated to the rest of the protein, by rotations of the outer β sheet, repacking the β sandwich. The rotations bend the outer β sheet toward the pore axis, while the position of the inner β sheet is unchanged.

The most recent view on activation of the nicotinic AChR proposes that once ACh binds to the α-subunit causes a concerted rearrangement in the ligand binding domain. This involves an outwards, radial tilting of the extracellular portion the of β-subunit helices where it interacts with the ends of α-helices. This accommodation permits channel opening by widening the pore and by increasing the polarity in the gate region (Unwin and Fujiyoshi, 2012). Originally, the pore opening was thought to be the result of a clockwise rotation of the five M2 (Law *et al*., 2005, Unwin, 2005). However, recent functional mapping of the M2 residues suggested a rigid body tilting of the M2 domain outwards (Cymes and Grosman, 2008; Cymes *et al*., 2005; Paas *et al*., 2005). Each M2 can exhibit distinct movements (Unwin and Fujiyoshi, 2012), some tilt outward and others straighten from a bent conformation. As they move, M2 helices change their interaction with M1 and M3 (Unwin, 2005; Miyazawa *et al*., 2003). Such movements are possible because M2 makes limited contact with M1 and M3, and M1-M2 and M2-M3 loops contain glycine residues that allow flexibility for M2 movement (Miyazawa *et al*., 2003).

It is hoped that high resolution structures from ELIC and GLIC (Hilf and Dutzler, 2009; Bocquet *et al*., 2009; Hilf and Dutzler, 2008) and GluCl (Hibbs and Gouaux, 2011) will provide good models of eukaryotic channel activation, due to their conservation of motifs and both tertiary and quaternary folds and structures. Several differences are observed between the structure of the closed ELIC and open GLIC and GluCl (Bocquet *et al*., 2009; Hibbs and Gouaux, 2011; Hilf and Dutzler, 2008) that may be related to channel gating. In GLIC and GluCl downward motion of the β1-β2 loop is present, along with a displacement of both the Cys-loop (β6-β7) and the M2-M3 linker away from the central pore axis. These movements are accompanied by an outward tilt of the five M2 α helices, which increase the diameter of the pore. In GLIC (open conformation), the M2-M3 loops have moved outwards, pulling the tops of the attached M2 α-helices with them. This tilts the helices outward and separates the

hydrophobic girdle (Bocquet *et al*., 2009; Hilf and Dutzler, 2008), confirming speculations based on nAChR data. In contrast with the nACh receptors, the ELIC, GLIC and GluCl structures show less contact between the loops of the agonist binding domain and the M2-M3 linker of the TMD.

1.4 Glycine receptors

Glycine is an important fast inhibitory neurotransmitter in the brainstem and spinal cord, where it is believed to regulate locomotor behaviour. Glycine was first proposed to be a neurotransmitter on the basis of an analysis of its distribution and concentration in the spinal cord by Aprison and Werman (1965). Additional studies discovered that glycine hyperpolarizes adult spinal neurons (Werman *et al*., 1967). This effect is abolished by strychnine and it is due to an increase in Cl^- conductance (Werman *et al*., 1968; Curtis *et al*., 1967; Curtis *et al*., 1968). The Cl^- flux shifts the membrane resting potential towards the Cl^- equilibrium potential. Depending on the position of the Cl^- equilibrium potential versus the cell resting potential, this results in either hyperpolarisation or depolarisation. In embryonic neurons, the intracellular Cl^- ($[Cl^-]_i$) concentration is set by the cation chloride co-transporter NKCC1, $[Cl^-]_i$ is high and glycinergic currents depolarise the cell, because the reversal potential of Cl^- is less negative than the resting membrane potential (Delpire, 2000; Wu *et al*., 1992; Reichling *et al*., 1994). The depolarization triggers Ca^{2+} influx, which has an important role in developmental processes, such as synaptogenesis and neuronal differentiation (Ye, 2008). In the mature cell, there is a developmental switch to another cation chloride co-transporter, KCC2, which lowers the $[Cl^-]_i$ concentration. In the adult central nervous system (CNS), the activation of GlyRs causes hyperpolarisation, because the Cl^- equilibrium potential is more negative than the cell resting potential (Rivera *et al*., 1999; Hubner *et al*., 2001).

The passage of charged ions through ion channels generates current that can be recorded using the patch clamp technique. GlyR subunits form ion channels whose main conductance level is higher for homomers vs. heteromers, 47 pS and 31 pS respectively (Burzomato *et al*., 2004; Beato *et al*., 2004). Moreover, several conductance levels have been reported for each form of the GlyR, between 20-90 pS (Bormann, 1986; Bormann *et al*., 1993; Lewis *et al*., 1998), and it is possible to observe direct transition between levels. Different results in the number of the conductance levels reported may be due to different experimental conditions,

such as recording configurations (cell-attached versus outside-out for example), methods of analysis, species (human versus rat clones) and possibly the whim of expression systems (Beato *et al*., 2004; Burzomato *et al*., 2004; Bormann *et al*., 1993; Marabelli *et al*., 2013; Pitt *et al*., 2008; Krashia *et al*., 2011).

1.4.1 GlyR isoforms

GlyRs are pentamers (Langosch *et al*., 1988) that can assemble as homomers or heteromers. The rat spinal cord GlyR was originally purified by affinity chromatography on amino strychnine agarose columns (Pfeiffer and Betz, 1981; Pfeiffer *et al*., 1982; Lynch, 2004). Three major polypeptides associated with GlyRs were purified, with masses of 48 kDa, 58 kDa and 93 kDa (Pfeiffer *et al*., 1982). The 48 kDa protein, which associates with strychnine or glycine, was named α subunit (α1), as it was thought to be the main ligand-binding subunit. The 58 kDa protein did not associate with glycine or strychnine (Graham *et al*., 1985), and it was named β subunit (Grenningloh *et al*., 1990a). The biggest polypeptide, within the protein complex, was found to be a cytoplasmatic protein, known as gephyrin, which links the receptor with the cytoskeleton (Schmitt *et al*., 1987).

Two additional subunit isoforms were cloned by homology screening in rat. The two isoforms were named α2 (Akagi *et al*., 1991; Kuhse *et al*., 1991) and α3 (Kuhse *et al*., 1990). Genes homologous to those encoding α2 and α3 subunits, were identified in man and mouse (Grenningloh *et al*., 1990b). Another isoform, α4, was identified in mice (Matzenbach *et al*., 1994), chick (Harvey *et al*., 2000) and zebrafish (Devignot *et al*., 2003). This subunit does not exist in rats and humans. The human α1 and β genes have an 80-90% sequence identity to the corresponding rat genes, whereas the α1 and β genes have a sequence similarity of about 47-48% to each other (Grenningloh *et al*., 1990b; Handford *et al*., 1996).

There are other α variants, which arise from alternative splicing of subunit pre-mRNA or from gene polymorphisms. The α1ins is a variant of the rat α1 subunit, which contains eight additional amino acids in the intracellular loop (Malosio *et al*., 1991a). Two splicing variants are described for the α2 subunit, α2A and α2B (Kuhse *et al*., 1990; Kuhse *et al*., 1991). Alternative splicing of the human α3 gene was described, α3K and α3L, which differ in the presence of a 15 amino acids segment in the intracellular loop. The human α3L is identical to the rat α3 subunit (Kuhse *et al*., 1990; Nikolic *et al*., 1998), in addition another α3 variant has

been identified in rat (Meier *et al*., 2005). Only one form of the β subunit is known (Grenningloh *et al*., 1990a).

When expressed in heterologous expression systems (i.e. Human embryonic kidney cells 293), all α subunits assemble to form homopentameric receptors. If different α subunits are expressed simultaneously the receptor composition may simply reflect the relative abundance of each subunit (Kuhse *et al*., 1993). On the other hand, the β subunit cannot form functional receptors on its own and can form functional heteromeric receptors only if co-expressed with α subunits (Kuhse *et al*., 1993). The stoichiometry of most heteromeric Cys-loop channels is unknown, for the αβ GlyRs, there is evidence that supports a stoichiometry of 3α:2β (Langosch *et al*., 1988; Kuhse *et al*., 1993; Burzomato *et al*., 2003; Durisic *et al*., 2012) as well as evidence that favours a subunit ratio of 2α:3β (Grudzinska *et al*., 2005). Accurate determination of channel stoichiometry is relevant to understand channel function (Webb and Lynch, 2007; Lynch, 2009).

1.4.2 Distribution of GlyRs in the CNS

GlyR isoforms are developmentally regulated and are expressed in distinct regions of the CNS and this may have a physiological significance. In situ hybridization studies showed that α1 transcripts are absent from cortical regions (Malosio *et al*., 1991b), but abundant in the spinal cord and brainstem of adult rats. In the superior and inferior colliculi, the cerebral deep nuclei and the hypothalamus, levels of α1 are much lower (Malosio *et al*., 1991b; Sato *et al*., 1992; Garcia-Alcocer *et al*., 2008). Transcripts for α1 become detectable around embryonic day (E) 14 in spinal cord and around postnatal day (P) 5 in the brain, and transcription peaks in both at P15 (Malosio *et al*., 1991b).

The α2 transcript is found in the rat brain and spinal cord mainly at the embryonic stage (Malosio *et al*., 1991b). In adults, α2 is undetectable in the spinal cord, but is still present at high levels in the cortex, hippocampus, thalamus (Malosio *et al*., 1991b; Sato *et al*., 1992) Two splice variants of the α2 isoform, α2A and α2B, have been found during early brain development (Kuhse *et al*., 1991). Both are expressed between E19 and P0 in the cortex, thalamus and hippocampus (Kuhse *et al*., 1991). The messenger ribonucleic acid (mRNA) levels for both splice variants drop quickly after maturation, when only α2B is still detectable (Racca *et al*., 1998).

During development the decrease of α2 mRNA is accompanied by an increase in α1 and α3 isoforms (Malosio *et al*., 1991b; Legendre, 2001; Kuhse *et al*., 1990), with levels of α1 transcripts higher than α3. In adult, the α3 GlyR subunit is present in the superficial laminae of the mouse dorsal horn (Harvey *et al*., 2004), olfactory bulb and hippocampus (Malosio *et al*., 1991b).

The β subunit is widely expressed in the E14 brain and increases in the adult (Grenningloh et al., 1990a; Fujita et al., 1991; Malosio et al., 1991a; Singer et al., 1998; Legendre, 2001)(Legendre, 2001; Malosio *et al*., 1991b; Singer *et al*., 1998; Fujita *et al*., 1991; Grenningloh *et al*., 1990a). The β mRNA is much more widely expressed than individual α subunits, and interestingly, it is found in brain regions which lack α subunits (Malosio et al., 1991a)(Malosio *et al*., 1991b). The physiological meaning of this wider expression is not clear, since β subunits cannot assemble with anything other than GlyR subunits.

Functional GlyR distribution was studied using different approaches, including in vitro autoradiography of [^{3}H]-strychnine (Zarbin *et al*., 1981; Probst *et al*., 1986; Young and Snyder, 1973)or [^{3}H]-glycine (Bristow *et al*., 1986) and immunocytochemistry studies for the GlyR anchoring protein gephyrin (Araki *et al*., 1988; Triller *et al*., 1985; Racca *et al*., 1997), both in wild type animals and in transgenic animals carrying deletions of the GlyR subunits or of Gly transporters (Harvey *et al*., 2004; Betz *et al*., 2006). The results obtained with those methods are in good agreement, and show that GlyRs are present in the caudal part of the adult CNS, at high levels in the grey matter of the spinal cord, medulla and pons, and at lower levels in the midbrain, thalamus, hypothalamus and hippocampus (Legendre, 2001; Lynch, 2004). In some nuclei of the brainstem, such as the trigeminal nuclei, cuneate nucleus, reticular nuclei and cochlear nuclei, GlyRs are discretely localized and present at high levels (Probst *et al*., 1986). GlyRs were also detected in the cerebellum (Araki *et al*., 1988; Takahashi *et al*., 1992), olfactory bulb (van den Pol and Gorcs, 1988) and retina (Pourcho, 1996). These observation were confirmed by recording glycinergic synaptic transmission, in the spinal cord (Takahashi and Momiyama, 1991), in brainstem auditory and motor nuclei (Moore and Caspary, 1983; Stevens *et al*., 1996), in the cerebellum (Dieudonne, 1995), retina (Protti et al., 1997) and hippocampus (Chattipakorn and McMahon, 2002).

Furthermore, GlyRs are often localized together with $GABA_A$ receptors ($GABA_ARs$). Presynaptic buttons containing both transmitters were found, in the spinal cord (Todd, 1990; Todd, 1996), in the brainstem (Dumba *et al*., 1998) and in the cerebellum (Crook *et al*., 2006). Often the presence of mixed GABA-glycine synapses is associated with the presence of both $GABA_ARs$ and GlyRs in the postsynaptic membrane (Crook *et al*., 2006; Todd *et al*., 1996; Jonas *et al*., 1998; Hamill *et al*., 1983; Dumoulin *et al*., 1999; Dumoulin *et al*., 2001).

1.5 Prokaryotic Receptors

Phylogenetic analysis, suggests that the common ancestor of the Cys-loop family can be found in prokaryotes (Tasneem *et al*., 2005) such as *Cytophaga hutchinsonii, Bradyrhizobium japonicum, Magnetospirillum magnetotaticum, Erwinia chrysanthemi, Microbulbifer degradans, Methylococcus capsulatus, Methanosarcina* and *Gloeobacter violaceus*. Channels from two of these species were discovered and characterised, ELIC from *Erwinia chrysanthemi* and GLIC from *Gloeobacter violaceus*. A common mechanism of channel gating is likely to operate in the pLGIC family members from prokaryotes and eukaryotes. This hypothesis is supported by the fact that there is sequence conservation between prokaryotic and eukaryotic channels (Tasneem *et al*., 2005). In addition to that, the structures of ELIC and GLIC appear very similar to the eukaryotic structure, thus it is quite reasonable to think that the gating mechanism is also similar.

1.5.1 ELIC

ELIC is a channel from the plant pathogen *Erwinia chrysanthemi*, which has been recently crystallized in a closed conformation (Hilf and Dutzler, 2008). The role of ELIC in the bacterium is unknown. It is only recently that ligands that activate ELIC have been discovered and they include cysteamine, propylamine, bromopropylamine, GABA and putrescine (Zimmermann and Dutzler, 2011). The most potent agonist was cysteamine (EC_{50} 370 μM) and the least potent putrescine (EC_{50} 16 mM). The fact that GABA is an ELIC agonist has been taken to validate the role of ELIC as a model for $GABA_A$ receptors (Spurny *et al*., 2012). Recently, several compounds that inhibit or modulate Cys-loop receptor were found to be inhibitors of ELIC (Thompson *et al*., 2012). Proadifen and α-endosulfan were the most potent, with an *IC*50 of 8 and 17 μM. Other antagonist such as dieldrin, picrotoxin and rimantadine, were much weaker.

ELIC is cation selective with negligible permeability to anions (Zimmermann and Dutzler, 2011). Ion conductivity of ELIC has been characterised in *Xenopus* oocytes and lipid bilayers, with a single channel conductance of 84 pS and 96 pS, respectively (Zimmermann and Dutzler, 2011). Using single channel recording, under asymmetric condition (different monovalent cations on either side of the membrane), currents reverse at 0 mV, suggesting that ELIC does not discriminate between different monovalent cations (i.e. Na^+ and K^+) (Zimmermann and Dutzler, 2011). Cation selective Cys loop channels are known to be somewhat permeable to divalent cations, which often interact with the pore, decreasing or blocking conductance in a voltage dependent way (Dani and Eisenman, 1987; Adams *et al*., 1980). Furthermore, divalent cations can also modulate channel gating in nicotinics (Sine *et al*., 1990; Mulle *et al*., 1992; Vernino *et al*., 1992). Similar results have been obtained for ELIC, whose agonist responses are affected by divalent cations such as Ca^{2+}, Mg^{2+}, Sr^{2+}, Ba^{2+} and Zn^{2+}, either as channel blockers or as negative modulators of channel gating (Zimmermann et al., 2012).

1.5.2 ELIC closed structure

The crystal structure of ELIC has been determined at 3.3 Å resolution (Hilf and Dutzler, 2008). ELIC dimensions are 95 Å x 110 Å, and resemble the nAChRs (bearing in mind that ELIC intracellular domain is 9 amino acids in length). The five subunits that form the channel are arranged around a symmetry axis that defines the ion pathway. On the extracellular side the subunits form a wide aqueous cylinder with a diameter of about 16 Å, which is lined by charged and hydrophilic residues. The vestibule gets narrower at the membrane interface to form a partly hydrophobic pore, which has a diameter of 7 Å. The narrowness of the diameter, together with the fact that ELIC was crystallised without agonist bound, strongly indicates that the structure is that of a closed conformation.

The general structure of ELIC is very similar to that of other channels in the Cys-loop superfamily and to AChBP. In this section I will therefore list only the differences. In ELIC the ECD is a β sandwich and the segment that is an α-helix in eukaryotic channels lacks a clear secondary structure. In addition to that, ELIC (as GLIC) does not have the two cysteines that form the disulfide bridge in the Cys-loop channels, the Cys-loop that gives the superfamily its name. Nevertheless, the central part of the Cys-loop is quite conserved.

The ligand binding site is located in a pocket at the interface between two different subunits, which in AChBP is covered on one side by an extended loop region that connects β9-β10. The tip of this loop is mobile and has a high mobility in the absence of agonist (Hansen *et al*., 2005). In ELIC crystal structure this loop is poorly defined, confirming the idea that the ELIC structure is in a closed state. The ELIC binding site contains conserved aromatic amino acids, as the acetylcholine binding pocket, but the exact position of these residues is not conserved (Tasneem *et al*., 2005). The aromatic residues contribute to form an aromatic binding pocket for compounds whose binding is stabilized by cation-π interactions.

The wide and hydrophilic extracellular vestibule of ELIC leads into a narrow pore, formed by residues of the M2 helix. Similar to AChRs (Revah *et al*., 1991; Wilson and Karlin, 2001), ELIC contains large hydrophobic residues in the center of the pore which contribute to channel closing, and physically obstruct the channel. In the extracellular part of the pore, which extends toward the center of the membrane, there are two interruptions by bulky side chains that occlude a hydrophobic cavity. The cavity is restricted by 16' Phe246 and 9' Leu239, at the extracellular and intracellular side respectively. The hydrophobic side chain of these two residues would prevent the diffusion of ions and the whole of this area probably serves as gate in the closed conformation. Below the 9' residue, a hydrophilic channel of about 6 Å is present. The channel is formed predominantly of acidic residues which attract cations despite the presence of positively charged residues in the extracellular vestibules.

Many questions remain for including whether the non-conductive state of ELIC in the crystal structure is resting, desensitised or neither (Hilf and Dutzler, 2008; Gonzalez-Gutierrez and Grosman, 2010). The possibility that ELIC is in a desensitised state is supported by the fact that no structural rearrangement was observed in the transmembrane domain in ELIC structures resolved in the presence and the absence of the agonist (Hilf and Dutzler, 2008; Zimmermann and Dutzler, 2011), even though the presence of the agonist in the binding pocket was confirmed by a plausible electron density there.

Moreover, crystal structures of ELIC mutants with slowed desensitisation bound to agonist, confirmed the possibility that ELIC is in a desensitized state (Gonzalez-Gutierrez *et al*., 2012). Mutating the pore of muscle AChR to resemble that of ELIC (by introducing a ring of phenylalanines at position 16') reduces by 95% the peak amplitude of current responses elicited by saturating agonist. Gonzalez-Gutierrez and Grossman (2010) hypothesized that the

mutant AChR (and therefore ELIC) can enter a unique, non-activatable, long lived refractory state from the resting state without ligands bound, and indeed that most of the channels are in this unique state at rest. This refractory state was argued to be distinct from the normal desensitised state, as mutating position 16' of GLIC M2 to Phe slows apparent entry into desensitization during sustained agonist (low pH) applications. These mutations in the AChRs correspond to the positions Leu239, Phe246 and Asn250 in ELIC receptors

1.6 Mechanisms

Once the neurotransmitter binds to the channel, it triggers a wave of conformational changes, which start from the agonist binding site and ends in channel opening (Chakrapani *et al*., 2004; Czajkowski, 2005). Events such as binding and gating can be studied by characterizing the channel activation mechanism using single channel recordings. A kinetic mechanism represents the process of channel activation as a chemical reaction that takes reversible steps.

The first mechanism of ligand gated ion channel activation was postulated in 1957 by del Castillo and Katz (1957) on frog endplate nicotinic receptors, scheme 1. They postulated a two step process, which accounts for the effects of partial agonists and competitive antagonists.

$$A+R \underset{k_{off}}{\overset{k_{on}}{\rightleftharpoons}} AR \underset{\alpha}{\overset{\beta}{\rightleftharpoons}} AR^*$$

Scheme 1

The mechanism postulates that the channel can exist in one of three discrete states. It can be shut, R and AR, or open, AR*. Where R denotes receptor and A ligand. The letters near the arrows show the name for the transition rate constants. The ratios of the rate constants are the equilibrium constants that are sufficient to describe the process at equilibrium. The first step is the binding and is described by the equilibrium dissociation rate constant K_d (ratio between k_{off} and k_{on}). The second step is the channel opening, subsequently called " gating", and is defined by the equilibrium constant for the conformational change, *E* (ratio between β and α). The del Castillo and Katz mechanism provided a conceptual frame for interpreting data, and it was a milestone in receptor pharmacology. However, it is too simple to describe the real activation mechanism of any Cys-loop receptor, as it assumes a single binding step, a single bound shut state and a single open state. Thus other, more complex, mechanisms for describing the activation of Cys-loop receptors have been postulated.

*The Monod Wyman Changeux (*MWC) mechanism shown below is the adaptation of a general model originally proposed by Monod, Wyman and Changeux in 1965 for oxygen binding to haemoglobin (Monod *et al*., 1965). The model has two simple rules: the protein adopts two conformations and each conformation has a different affinity for the ligand (Monod *et al*., 1965), scheme2. Since its proposal the MWC mechanism has been widely used to describe the activation mechanisms of many proteins, including ion channels. In the Cys-loop superfamily it has also been intensely used to describe the activity of muscle ACh receptors (Auerbach, 2012; Karlin, 1967).

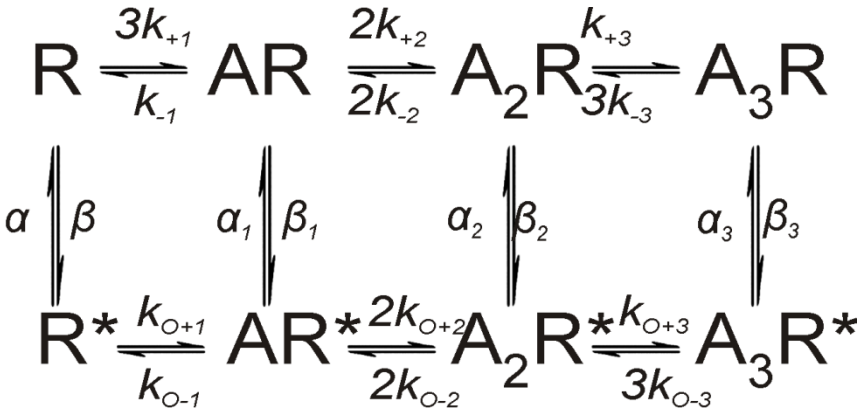

Scheme 2

The MWC mechanism assumes that the receptor can reversibly adopt two global conformational states, open or closed, and each conformation has a different affinity for the ligand. In the MWC mechanism, conformation changes are concerted across all subunits and binding sites. The scheme 2 contains four shut states (R, and A_nR, where A is the agonist and n =1 2, or 3) from which the receptor can open to the open states (R* and A_nR*). Note that opening is possible also from the unliganded resting state ("spontaneous openings"). Another feature of this model is that it allows transitions from one open state to another. The affinity is set by the state of the receptor (open or closed) and not by the number of agonist molecules bound, this can be formalized as follow

$$k_{+1}=k_{+2}=k_{+3};\ k_{-1}=k_{-2}=k_{-3};\ k_{o+1}=k_{o+2}=k_{o+3};\ k_{o-1}=k_{o-2}=k_{o-3}$$

The cycles in the mechanism introduce the constraint of microscopic reversibility or detailed balance. A consequence is that changes in the efficacy of opening must change monotonically from left to right as more agonist binds.

Jones and Westbrook mechanism. The Jones-Westbrook mechanism (J&W) was proposed by (Jones and Westbrook, 1995) to describe the activation of GABA receptors. In this mechanism, the receptor can either open or enter a short-lived desensitized state, from each of the resting states that are bound to agonist. In Scheme 3 the agonist binding sites are allowed to interact with each other, and change their affinity with the level of ligation.

Scheme 3 contains three shut states from which the receptor can open or desensitise. R denotes resting states, A the agonist, D desensitised states and R* open states. This model does not allow transition from one open state to another. Because there are no cycles that introduce the constraint of microscopic reversibility, the efficacy of opening can change freely as more molecules of agonist bind. The D states are short lived shut states, rather than the slow components of macroscopic desensitization.

The J&W is a good model to describe the behaviour of GABA channels (Jones and Westbrook, 1995) and of glycine receptors such as α1β and α3 (Burzomato *et al*., 2004; Marabelli *et al*., 2013), as we shall see in Chapter 3. However the position of the short lived desensitised states (as an alternative to opening from the resting states) does not lend itself to a clear physical interpretation of these states.

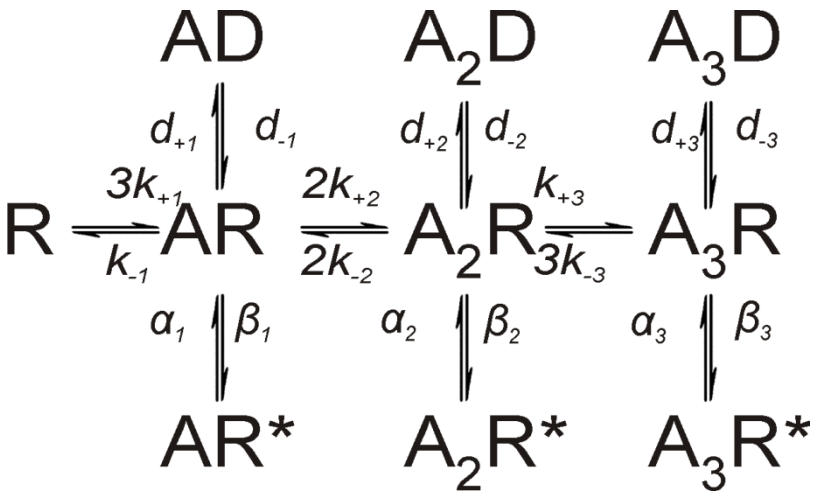

Scheme 3

"Flip" mechanism. The Flip mechanism (Scheme 4) was proposed by Burzomato *et al.* (2004) to interpret single channel activity of α1β heteromeric GlyR. The flip mechanism postulates the existence of an additional shut state, called the flipped state, which represents a concerted conformational change (i.e., all five subunits move together) that occurs before the

channel opens (Burzomato *et al*., 2004). In flip-type models, the agonist binding sites are independent and the binding affinity depends only on the state of the receptor (i.e. resting or flipped), and not on the level of ligation. In that respect, the flip mechanism resembles the MWC model. Hence, the scheme specifies only two equilibrium constants for binding, one for the resting conformation (R) and one for the flipped conformation (F), regardless of how many sites are already occupied.

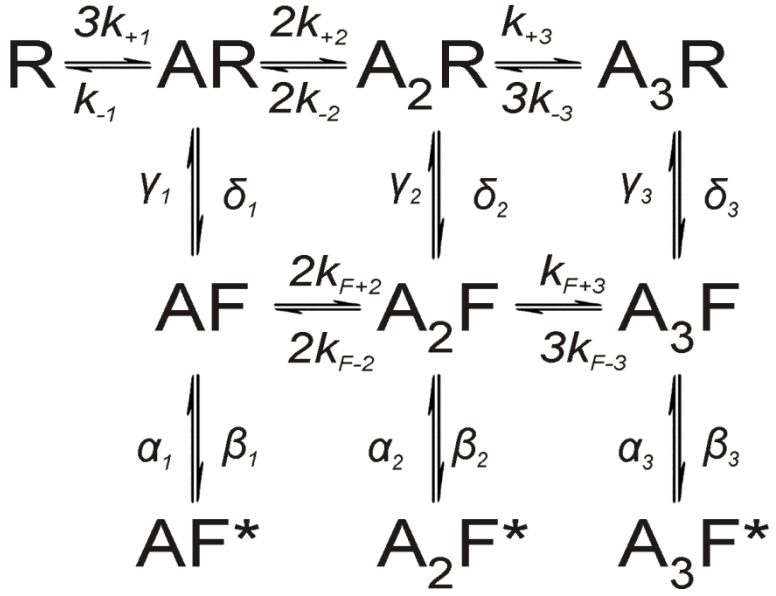

Scheme 4

This mechanism postulates that agonist binding favours this early flip conformational change and that this conformational change is concerted. Channel opening can occur from any of three liganded shut states, and the efficacy of gating can vary freely as more agonist molecules bind. A physical interpretation for the flip states (suggested by their position on the trajectory between resting and open) is that they represent the receptor when the extracellular domain has closed onto the agonist, but the conformational change has not yet reached the channel gate.

The flip mechanism was successful in explaining the activation mechanism of glycine receptor α1 homomeric and heteromeric (Burzomato *et al*., 2004), α2 (Krashia *et al*., 2011), α3 (Marabelli *et al*., 2013), the GlyR of the *spasmodic* mouse strain (Plested *et al*., 2007) and for describing the action of partial agonists both on glycine and muscle ACh nicotinic receptors (Lape *et al*., 2008).

Primed mechanism. The first mechanism of this class was proposed by (Mukhtasimova *et al*., 2009) to explain the complex structure of unliganded channel openings in gain of function of the 9' mutant of the nACh receptor, and in particular the presence of more than one open time component in spontaneous openings. Note that the mechanisms examined so far would allow only one open state for this type of opening (or indeed, for fully-bound receptors).

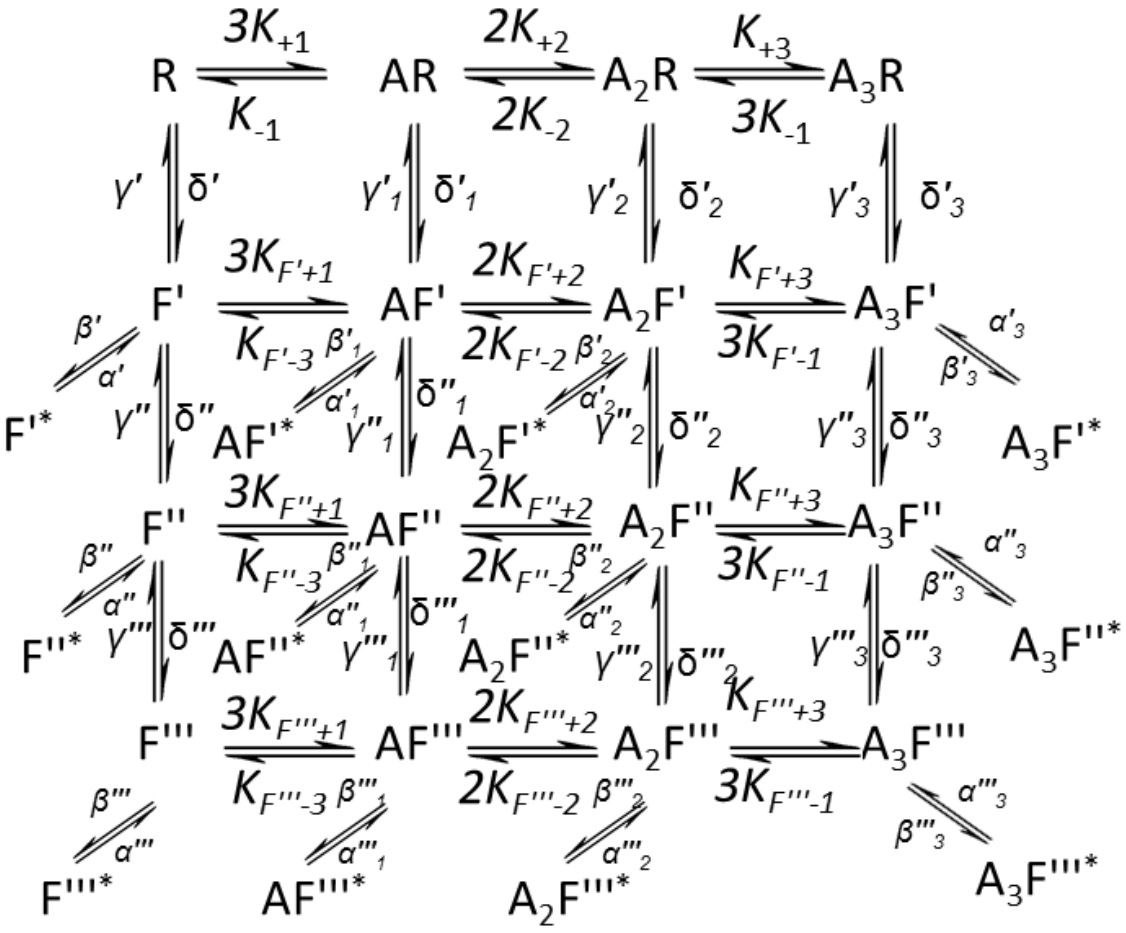

Scheme 5

In the primed mechanism (Mukhtasimova *et al*., 2009) subunits do not flip in a concerted fashion (flip) but rather independently from each other (represented as multiple horizontal layers in scheme 5, above). Using dysulfide trapping, Mukhtasimova and colleagues (2009) showed that the capping of each binding site initiates priming and that openings can then occur from each of these partially primed channels. The full primed mechanism for a receptor with three binding sites is rather complicated and only a subset could be reliably investigated

(Lape *et al*., 2012). In this mechanism the agonist binding sites are independent and the binding affinity depends only on the state of the receptor (i.e. resting or primed).

Hence the scheme specifies two equilibrium constants for binding, one for the resting conformation (R) and one for the primed conformation (F'), regardless of how many sites are already occupied. This was done by applying constraints to the rate constants, as in the flip mechanism. Scheme 5 has three open states and three primed states, which are accessible from all the liganded resting states. As more agonist molecules bind, both the pre-opening conformation change to the primed state and the opening of the channel from the primed state becomes more favourable. Thus, it is plausible to expect a monotonic increase in the primed equilibrium constant *F*'. The gating equilibrium constants are allowed to vary freely. In the gain of function nicotinic channel, the most stable openings come from the most primed states, whereas the singly primed states triggers brief openings. The primed model was successful in describing the single channel activity of the K276E hyperekplexia mutant of GlyRs (Lape *et al*., 2012), and of the prokaryotic receptor ELIC (Marabelli *et al* submitted, see Chapter 4).

Chapter 2: Methods

2.1 Preparation of plasmid cDNAs

All the experiments were done on ion channels heterologously expressed in Human Embryonic Kidney-293 cells (HEK293) (see 2.2). The amplification and cloning of the glycine receptor α3 subunit was done by Paul Groot-Kormelink, as described in Beato *et al.* (2002) and Burzomato *et al*. (2003). Briefly, two pairs of primers were used, one pair to amplify the gene and the second pair to attach restriction sites and the Kozak consensus sequence upstream of the start codon (Figure 2.1). Two Polymerase chain reactions (PCR) were performed, the fragment obtained was purified and cloned into the respective restriction sites of the pcDNA3 vector (Invitrogen), and sequenced fully on both strands. The pcDNA3 plasmid for ELIC was kindly provided by the Dutzler group, Biochemisches Institut, Zürich University.The GenBank accession number is AJ310838 for the rat α3 glycine receptor subunit and ADN00343.1 for ELIC.

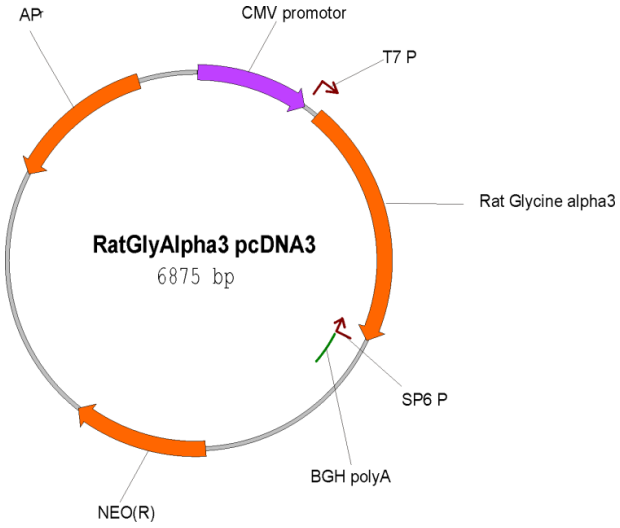

Figure 2.1 Schematic diagram of the rat glycine receptor α3/pcDNA3
The rat glycine receptor α3 has been cloned downstream of the viral promoter cytomegalovirus, (CMV). The CMV promoter will drive the expression of the α3 receptor subunit transfected into a mammalian cell, such as HEK293. The plasmid contains also two prokaryotic promoters, T7 and SP6P, and Ampicillin resistance gene (AP^r,), Neomycin resistance gene (NEO(R)) and the bovine growth hormone polyA (BGH poly A). The ELIC plasmid is the same except for the replacement of the Rat glycine alpha3 receptor with ELIC coding sequence.

2.2 HEK 293 cells culture and transfection

HEK293cells, obtained from the American Type Culture Collection (ATCC), were maintained in a humidified incubator at 37°C (95% air/5% CO_2). The growth medium was Dulbecco's modified Eagle's medium (DMEM; Gibco, Invitrogen) supplemented with

sodium pyruvate (0.11 g/liter), heat-inactivated fetal bovine serum (10% vol/vol), and penicillin G (100 U/ml)/streptomycin sulfate (100 µg/ml; all from Invitrogen). Cells were passaged every 2-3 days (i.e. before they became more than 90% confluent). Cells were washed once with Hanks` balanced salt solution (Gibco UK) and detached from the bottom of the flask by approximately 30 s exposure to 1 ml 0.05% trypsin (Gibco UK) at 37°C. Cells were suspended from the flask by adding 4 ml growth medium. The cell suspension was centrifuged (2 min, 157 g) and the supernatant discarded. The pellet was dispersed in 1 ml of DMEM, to yield a cell suspension which was diluted into a new flask.

Glass coverslips (13 mm) were coated with 0.01% poly-L-lysine (Sigma-Aldrich) and sterilised by autoclaving for 20 mins at 123˚C. HEK293 cells were then seeded onto the coated coverslips in 35 mm culture dishes containing 2 ml growth medium. HEK293 cells were transfected using the Ca^{2+}-phosphate co-precipitation method (Groot-Kormelink *et al*., 2002) to express the ion channel of interest and enhanced green fluorescent protein (eGFP) as a marker of transfection. All plasmids used were pcDNA3 (Invitrogen, The Netherlands). Cells were transfected with a mixture of plasmids containing inserts encoding either receptor subunit(s), or eGFP (Clontech, UK). When the level of channel expression was too high, non-coding vector pcDNA3 plasmid ("empty vector") was added to the mixture, keeping the total amount of plasmid transfected constant at 3 µg complementary DNA (cDNA) per dish (table 2.1). For a full description of the plasmid ratio approach to optimising expression see Groot-Kormelink *et al.* (2002).

Table 2.1 Transfection mixtures

Receptor Type	**Receptor cDNA (%)**	**Empty Vector (%)**	**eGFP (%)**
α3 Glycine	82	0	18
ELIC	5-82	0-77	18

The cDNA mixture was added to a $CaCl^2$ solution (340 mM) at a 1:5 volume ratio. The precipitate was formed by mixing the resulting DNA/$CaCl^2$ solution with an equal volume of HEPES buffered saline (280 mM NaCl; 2.8 mM Na2HPO4; 50mM HEPES; pH adjusted to 7.2 with NaOH). The two solutions were mixed and immediately added to the Petri dishes, one drop at a time. Each dish (containing 2 ml growth medium) was transfected with a total of 3 µg cDNA (72µl, DNA concentration 500 ng/µl). Cells were then incubated overnight at 37°C in a 95% air/5% CO^2 atmosphere. About 8 hours after transfection, cells were washed

with Hanks` balanced salt solution and incubated in 2 ml growth medium. Recordings were performed between 4 h and 48 h after transfection.

2.3 Solutions

Electrophysiological recordings were performed at 19–21°C in transfected cells using different patch clamp configurations, such as cell-attached, excised outside-out and whole cell. The composition of extracellular solutions are summarised below (Table 2.2, in mM):

Table 2.2 Extracellular solutions used for electrophysiological recording

Bath glycine (E1)	**Bath ELIC (E2)**	**Bath ELIC (E3)**
20 Na-gluconate		
102.7 NaCl		
2 KCl	150 KCl	150 KCl
2 $CaCl^2$	0.5 $BaCl^2$	0.05 or 0.2 $CaCl^2$
1.2 $MgCl^2$		
10 HEPES	10 HEPES	10 HEPES
20 TEA-Cl		
15 sucrose		
14 glucose		
pH 7.4 with NaOH	pH 7.4 with KOH	pH 7.4 with KOH
osmolarity 320 mOsm	osmolarity 310 mOsm	osmolarity 310 mOsm

Electrodes were backfilled with intracellular solution. The composition of intracellular solutions are summarised below (Table 2.3, in mM):

Table 2.3 Intracellular solutions used for electrophysiological recording

Glycine single channel (I1)	**Glycine Whole Cell (I2)**	**ELIC (I3)**	**ELIC (I4)**
20 Na-gluconate	121.1 K-gluconate	150 KCl	150 KCl
102.7 NaCl			
2 KCl			
2 $CaCl^2$	1 $CaCl^2$	0.5 $BaCl^2$	0.05 $CaCl^2$
1.2 $MgCl^2$	1$MgCl^2$		
10 HEPES	10 HEPES	10 HEPES	10 HEPES

20 TEA-Cl	16 TEA-Cl		
15 sucrose			
14 glucose	2 MgATP glucose		
0.05-10 glycine			
	11 EGTA		10 EGTA
pH 7.4 with NaOH	pH 7.2 with KOH	pH 7.4 with KOH	pH 7.4 with KOH
osmolarity 320 mOsm	osmolarity 325 mOsm	osmolarity 310 mOsm	osmolarity 320mOsm

Both extracellular and intracellular solutions for glycine were prepared using high performance liquid chromatography (HPLC)-grade water (VWR International) in order to reduce contamination by glycine. All the solutions listed in the table above were filtered through a 0.2-μm Cyclopore track-etched membrane (GE Healthcare) to remove impurities.

2.4 Electrophysiological recordings

2.4.1 Single channel currents: cell-attached or outside-out configuration

Single channel currents were recorded in the cell-attached or outside-out configurations with thick-walled borosilicate glass pipettes (with filament; Harvard Apparatus). Before filling, pipettes were coated near the tip with Sylgard (Dow Corning) and fire-polished to a final resistance of 6–15 MΩ (with solutions E1, I1 or I2, glycine receptor experiments) and a final resistance of 8–12 MΩ (with solutions E2, E3, I3 and I4, ELIC receptor experiments). The bath level was kept as low as possible, in order to reduce noise. Single channel experiments were performed in cell-attached configuration at a pipette potential of +100 mV and -60 mV in outside-out configuration. Currents were recorded with an Axopatch 200B amplifier (MDS Analytical Technologies), with no correction for junction potential, as this was calculated to be at most +1 mV (Clampex 10.2; MDS Analytical Technologies). Currents were filtered at 10 KHz (4-pole low-pass Bessel filter; Axopatch 200B amplifier), digitized (sampling rate 100 kHz) and stored directly on the computer hard drive using Clampex 10.2 software. For off-line analysis, data were filtered again digitally (low pass Gaussian filter) using the program Clampfit 10.2 to achieve a final cut-off frequency of 3– 6 kHz (calculated including the prefiltering).

For recording in the cell-attached configuration, pipettes were filled with extracellular solution containing agonist dissolved to the concentration required. In outside-out recordings, agonists were bath-applied.

2.4.2 Dose- response curves: whole-cell patch clamp recordings and U-tube drug application system

Whole-cell patch-clamp recordings were used to obtain dose-response curves for different agonists. Agonist solutions were applied to the cells via a custom built U-tube delivery system (Krishtal and Pidoplichko, 1980). The U-tube is a U-shaped glass tube with a small, smooth-edged drug outlet hole at the tip. One branch of the U-tube is connected to a vacuum pump and the other to a reservoir containing the agonist solution. In control conditions, the pump is set to suck the drug solution and a small amount of bath solution into a collection trap. The drug application is achieved by interrupting the connection between the U-tube and the vacuum pump, thus allowing a stream of drug solution to flow into the bath. The U-tube was made from a thick-walled borosilicate glass capillary (Drummond), bent into a U-shape by heating; the hole at the tip was produced by applying positive pressure to the inside of the capillary while heating the tip. The hole was then polished using a Bunsen burner, so that the edges were smooth and the final diameter was 10-30 μm. Every U-tube was tested before use, and at regular intervals, as follows. The bath was filled with extracellular solution E2 and an electrode was placed close to the bottom of the bath; then a 50% diluted extracellular solution was applied. The different composition of the two solutions caused a change in junction potential, inducing a current through the electrode. Monitoring the time course of the onset of the junction potential allowed us to measure the exchange time of application. U-tubes were used only if the 20-80% rise time of the exchange time was better or equal to 50 ms. Note that the effective real exchange at the cell would be much slower, because the cell is bigger than the open electrode tip.

Electrodes were pulled from thin-walled borosilicate glass capillaries (with filament; Harvard Apparatus) and fire polished to reach a resistance of 3 to 5 MΩ, when back-filled with intracellular solution I 3. Transfected cells were identified for the purpose of whole-cell recording by their expression of eGFP and their fluorescence observed exposing to Expo x-cite®120 lamp (X-cite®) light, excitation 457-487 nm, bandpass filter 472 nm. Once the whole-cell configuration was achieved, membrane capacitance (25±6 pF) and series resistance, (R_S), (5-8.5 MΩ) were measured at -30 mV holding potential and compensated by

about 60-75%. R_s was monitored throughout all experiments, and recordings were discarded if R_s changed more than 25%.

Macroscopic whole-cell currents were recorded with an Axopatch 200B amplifier, filtered at 5 KHz and digitised (at rate of 20 KHz) directly on the hard drive of a computer using Clampex software.

A full concentration-response curve was obtained for each cell, applying in random order different concentrations of agonist. A response to a standard concentration of agonist (approximately EC_{50}) was elicited every second application of agonist, to monitor for rundown. The amplitude of current elicited by the standard was plotted against time from the start of recording, and fitted with a straight line. The slope was used to correct intervening currents for rundown. Recordings were discarded if the rundown was not linear, or if it was bigger than 35%, or if the fitted parameters of the concentration response curve were poorly defined.

The full concentration-response curve was fitted empirically with the Hill equation:

$$I = I_{\max} \frac{[A]^{n_H}}{[A]^{n_H} + EC_{50}{}^{n_H}} \qquad \text{[eq. 2.1]}$$

where I is the measured current, Imax is the maximum current, [A] is the agonist concentration, nH is the Hill coefficient and EC_{50} is the agonist concentration for 50% of the maximum response. Each experiment was fitted separately by least squares, using the program CVFIT (http://www.ucl.ac.uk/Pharmacology/dcpr95.html). The curve parameters estimated by the program are Imax, n_H and EC_{50}. Results are given as mean ± standard deviation of the mean (SD of the mean) from the individual fits.

In order to produce figures, each curve was normalised to its fitted Imax and the normalized curves were pooled. The average concentration-response curve was then re-fitted with the Hill equation and displayed in the figures.

2.4.3 Fast concentration jumps: outside-out patches and the fast theta-tube/pjezo drug application system

Fast concentration jumps of agonist were applied to outside-out patches via a piezo driven theta glass tube (Hilgenberg, Malsfed, Germany). Theta glass capillaries were pulled, and their tips were cut to a final diameter of about 150 μm with a diamond pencil under visual

control (using a 10 X binocular microscope). The two barrels were then connected to a solution reservoir by using polyethylene (PE) microtubing (Portex ®). The tubing was inserted into the back ends of the theta tube barrels and shifted towards the tip, then the space between the pipette wall and the microtubes was filled with glue (two component Araldite®Instant). The applicator was fixed to a piezo stepper (Burleigh Instruments, NY, USA) that was driven by voltage commands to generate a translation that took the patch (downstream of the applicator) from the control solution stream into the agonist solution. Voltage commands for the stepper were square pulses of appropriate duration, applied at 5 or 10 s intervals and filtered (low-pass eight-pole Bessel; −3 dB frequency 5 kHz) in order to make the movement smooth and reduce oscillations.

The application setup was tested before and after each experiment, by applying a pulse of dilute extracellular solution (30% water: 70% normal extracellular solution) onto an open tipped patch pipette and monitoring the time course of onset of the junction potential. This was done before every experiment, in order to optimize the position of the electrode cf. the applicator, and repeated at the end of the experiment (after the patch was lost) to ensure the quality of the step response.

During these tests, low positive pressure was applied to the recording pipette, in order to avoid diffusion of the external solution into the tip. The rise and decay time for open tip currents was measured as the time from 20-80% of the peak response using Clampfit software. Experiments in which the open tip response had a 20–80% exchange time slower than 150 μs for Glycine channels and 200 μs for ELIC were rejected.

Outside-out patches were obtained with thick-walled borosilicate pipettes (with filament; Harvard Apparatus) fire-polished to a final resistance of 8–12 MΩ when filled with intracellular solution (I2, I3 and I4). All outside-out recordings were performed at a nominal pipette holding potential of -100 mV (junction potential was calculated to be 13 mV for the α3 receptor and 0 mV for ELIC). Macroscopic currents were recorded with an Axopatch 200B, digitized with a Digidata 1322A, and saved directly on a computer via the Clampex software (5 kHz filtering, 20 kHz sampling rate).

In order to study the kinetics of macroscopic currents, 10–50 sweeps were recorded in response to pulses of agonist, applied at intervals of at least 10 s. Responses for each patch were averaged, excluding failures or responses that contained patch breakdowns. Only experiments in which the rundown between the first and last three responses was <5% were

included in the analysis. For ELIC recordings, the time course of deactivation and activation was fitted from 80-20% with the sum of one or more exponentials. For α3 glycine receptor recordings, the time course of the deactivation was fitted as for ELIC, but the rise time was measured as the time from 20-80% of the peak response. Results are reported as the mean ± SD of the mean.

2.5 Kinetic analysis of the data

2.5.1 Overview of the analysis of single-channel data

The first step in the analysis of single channel records is the idealisation of the trace, to convert the experimental record into a list of openings and closings, with the duration of each event and the corresponding amplitude. This is an approximation of the true channel activity, because some of the original transitions are missed in the analysis process, i.e. channel openings and closings shorter than the resolution (30 μs in my experiments on the α3 glycine receptor and between 25-40 μs for ELIC).

The second step is to construct stability plots for fitted amplitudes and for open times, shut times and open probability (P_{open}), in order to characterise the channel behaviour and make sure that the recording was stable. For the recordings that satisfy this scrutiny, dwell time histograms are plotted and fitted with exponential probability density functions, using the EKDIST program ((Colquhoun, 1995); www.onemol.org.uk). The ensemble of all this information provides a description of the activation behaviour of the receptor that can be used to perform a kinetic investigation.

We start the kinetic investigation by postulating and subsequently testing a series of plausible activation mechanisms that explain the channel behaviour. The simplest activation mechanism possible for a ligand-gated channel consists of two states, a single shut state and a single open state, linked by a single opening/closing step, with rates of reaction described by rate constant values (dimension of frequency, s^{-1}). The first realistic mechanism for a ligand-gated channel is only slightly more complex and (eq. 2.2) was proposed by del Castillo and Katz (1957). This mechanism identifies two steps in the activation, the binding of the agonist A (to a resting closed receptor R) and the conformational change of the agonist-bound receptor AR (also closed) to the open state AR*, the gating step.

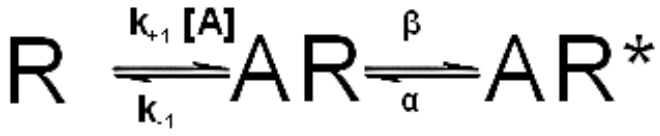

[eq. 2.2]

The rate constants in the mechanism describe the frequency of transitions from one state to another. The binding of the agonist to the channel is described by a concentration dependent rate, namely the association rate constant k_{+1} times the agonist concentration [A]. This is followed by the conformational change that brings the channel to open. The frequency of the transition from a closed channel with agonist bound AR to an open channel AR* is described by the rate constant β. All the reaction steps in the mechanism are reversible. Channel closing, and the unbinding of the agonist are described by rate constants α and k_{-1}, respectively. Thus a kinetic mechanism incorporates a number of open/closed states and rate constants to describe the receptor behaviour. Desensitised states are omitted from the mechanisms, because they are largely eliminated from the single channel data during analysis (see Chapter 2.5.6).

As the next step, I carried out global fits of several postulated kinetic mechanisms to stretches of idealised single channel data obtained at a range of agonist concentrations, using the HJCFIT program. HJCFIT calculates the rate constants values that maximize the likelihood that the data analysed can be generated by a receptor behaving according to the given putative mechanism. Those are the rate constants that produce the best fit of a particular mechanism to the observed experimental behaviour. Because we have only *postulated* a mechanism, we need then to test whether the mechanism fitted does describe the behaviour of the channel. This can be judged by the agreement between the data (in various displays) and the predictions of the mechanism itself. The aim of the analysis is to obtain the *simplest* mechanism that will describe the data and is realistic in the light of what we know about the structure of the receptor (i.e., number of binding sites occupied to get a maximum response and presence of intermediates states).

2.5.2 Idealisation of the single-channel traces

Digitised single-channel current recordings were processed with the SCAN software using time course fitting in order to reconstruct the opening and shutting events that give rise to the recording (Colquhoun, 1995).

Transitions between open and shut current levels are very fast, and can be assumed to be effectively instantaneous, but are filtered by the amplifier circuits and by our choice of signal conditioning filter. Thus, in our recordings the transitions are rounded. Knowing how the filtering distorts the square signal allows the program to calculate the original signal. In such a way, SCAN calculates a theoretical time course of the current and fits it to the actual data. The time of the transitions and the amplitude of the current are optimised during a least-square fit to the experimental record, until the fit is satisfactory and the calculated output is superimposed on the data. A simultaneous determination of amplitude and duration is possible for pulse widths that are long enough to reach full amplitude. In this case, the error for the estimation of the width is constant and the precision in the estimation of the amplitude increases for longer pulses. When the pulse width is short (cf. the filter rise time) the current in the experimental record does not reach full amplitude, and the estimation error for both amplitude and width increase. If the duration is fitted constraining the amplitude to zero for shuttings and that for openings to be the same as the amplitude of the nearest long opening or as the average of all the previous ones, the error in the estimated duration depends weakly on width. It is obvious that this procedure is appropriate only for records in which only one, stable conductance is present, and the amplitude is the same for all openings.

The "time course fitting" method is slow and laborious in comparison to other idealization methods such as the "Half-Amplitude Threshold" method. In this method, channel amplitude is estimated and a threshold is set at 50% of the full amplitude. Every crossing of the threshold is interpreted as an opening or closing transition; events that do not reach the threshold due to filtering are missed. There are two advantages in using the time-course-fitting method. First, the time resolution of measurements is greater than can be obtained with the threshold-crossing method. Second, it is the only well-tested method for dealing with records that contain multiple conductance or subconductances.

2.5.3 Imposing the resolution

It is inevitable that the shortest openings and shuttings will remain hard to distinguish from noise and therefore undetected when the single-channel record is idealized, because of the limited experimental bandwidth. Those missed short events distort the apparent duration of open and shut times. Openings will appear longer if they contain undetected short shut times, because they are concatenated together, if they have the same amplitude, and the same happens for shuttings separated by undetected short openings.

Thus it is important to adopt a rational consistent strategy that allows us to apply a correction for missed events. The first step is to impose retrospectively a consistent resolution on the idealised data (Sakmann and Neher, 1995). Resolution is defined as the shortest event duration (t_{res}) that can be trusted to be always detected. When the idealization is completed, the value of t_{res} can be chosen and the idealized record revised. Openings shorter than t_{res} are removed, thus shutting separated by openings shorter than t_{res} are concatenated and are treated as single shut times and the same procedure is applied to shuttings shorter than t_{res}. In this way a new idealized recorded is produced and is the input for the next analysis step.

2.5.4 Stability plots and amplitude histogram

The single-channel recordings described here were made at equilibrium, so it is important to check that the channel activity is not changing with time, because any changes can make the corresponding distributions meaningless. This is done by displaying information contained in the idealised record as *stability plots*, for amplitudes, for open time, shut time, and open probability, P_{open} (Figure 2.2).

Stability plots of open time, shut time and P_{open} (Weiss and Magleby, 1989) are constructed using a moving average of these values and plotted against the interval number at the centre of the averaged value (Figure. 2.2 A). A standard procedure is to average the duration of 50 consecutive values and then increment the starting point by 25, in such a way the samples overlap, smoothing the graph. Each P_{open} value is calculated as the ratio of the total open time to the total length (open + shut). Care must be taken not to over interpret the P_{open} stability plot. Even if the P_{open} is stable overall, it is quite common to observe drops when the record contains a very long shut period. However, even if the very long shut period reduces the overall P_{open}, it affects only one point of the stability plot.

Histograms of the distribution of single-channel current amplitudes were also constructed (Figure. 2.2B) Amplitude measurements are useful to characterize channel types, e.g. types with different subunit composition often have different amplitudes. Amplitudes can be reliably measured only for openings longer than twice the rise time of the filter of the recording system. These distributions were than fitted by a single Gaussian or a mixture of Gaussians, to estimate the conductance level(s) (even though amplitude distributions are only approximately Gaussian, (Sakmann and Neher, 1995).

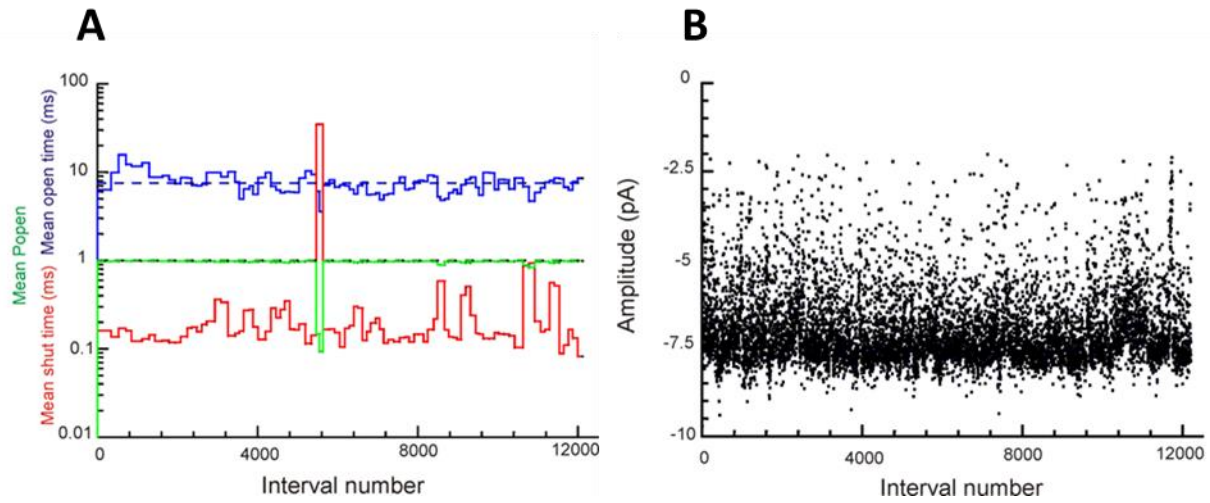

Figure 2.2 Stability plots.
Single channel amplitude (A), mean open time (blue), Popen (green) and shut time (red) for a typical patch (B). These plots are inspected to be sure that single channel properties do not vary with time.

2.5.5 Dwell time distribution and probability density function

Apparent open and shut time histograms can be plotted from idealized data after a resolution has been imposed. The distributions are plotted with a logarithmic time axis and a square root of the number of events/bin as vertical axis. Displayed in such way, the exponential components appear as curves with a peak and the peak position corresponds directly to the time constant of the exponential.

Dwell time intervals are continuous variables, so the probability distribution can be specified as probability density function (pdf). The pdfs describing single channel open/shut time intervals are mono or multi exponential and could be empirically fitted to the experimental histograms in the EKDIST program. The number of exponential components in each distribution is the first clue to the minimum number of states visited by the channel. Furthermore, from the dwell time distributions, it is possible to identify which of the shut time components are concentration-dependent. This allows us to devise a criterion for determining the sections of trace that are most likely to originate from a single channel molecule (see below). These sections are the ones that can be used in the second stage of kinetic analysis.

2.5.6 Bursts and clusters.

For ligand-gated ion channels that undergo desensitisation, there is no practical way of counting the number of channels in the patch. The duration of a shut time between two successive openings cannot be interpreted, if the number of the channels in the patch is unknown. In other words, it is impossible to be sure that a particular single channel current originates from the same channel molecule that produced the previous one. Only sequences of events that originate from the same channel are kinetically meaningful. Hence to perform kinetic analysis, all the openings in a group should come from the same channel. This can be achieved by dividing openings into groups (bursts or clusters, see below) using a critical shut time (t_{crit}). The shut times within these groups are interpretable, and they reflect transition among the states of the mechanism (eq. 2.1). The t_{crit} was chosen empirically, using the shut time distributions and the results of fitting them with a mixture of exponential pdfs.

Two different kinds of single-channel activity can be seen. At low agonist concentration, channel activity occurs as bursts, groups of few openings separated by long shut times. Each burst is likely to represent an activation of a channel molecule (e.g. what happens between binding and unbinding of the agonist; (Edmonds *et al*., 1995). In a hypothetical patch that contains a single ion channel molecule that follows the del Castillo-Katz mechanism (eq. 2.1), the long shut interval between two bursts is the time it takes for the channel to rebind an agonist molecule (a time that is longer at the lower concentrations) plus the time that it takes to enter the burst states, which represent oscillations between AR (shut bound state) and AR* (open state).

We use the fitted shut time pdf to find a suitable t_{crit}, by the following criteria. The time constants of the within-bursts shut times should be similar across different patches, irrespective of agonist concentration (Figure 2.3). This follows from the fact that only the duration of the interburst shut time should be affected by the number of channels in the patch. The duration of the interburst shut times is also concentration-dependent because these events are terminated by agonist binding. These shut times are potentially shortened by the presence of more than one channel in the patch, and therefore they are not used in the fitting as such. Nevertheless, they provide some information that we can exploit, in that they tell us that the real shut times (between activations of the *same* channel) have to be at least as long as the observed long shut times. This boundary condition is incorporated in our analysis by using a special sort of initial and final vectors (CHS vectors) in the likelihood calculations at burst concentrations (Colquhoun *et al*., 1996).

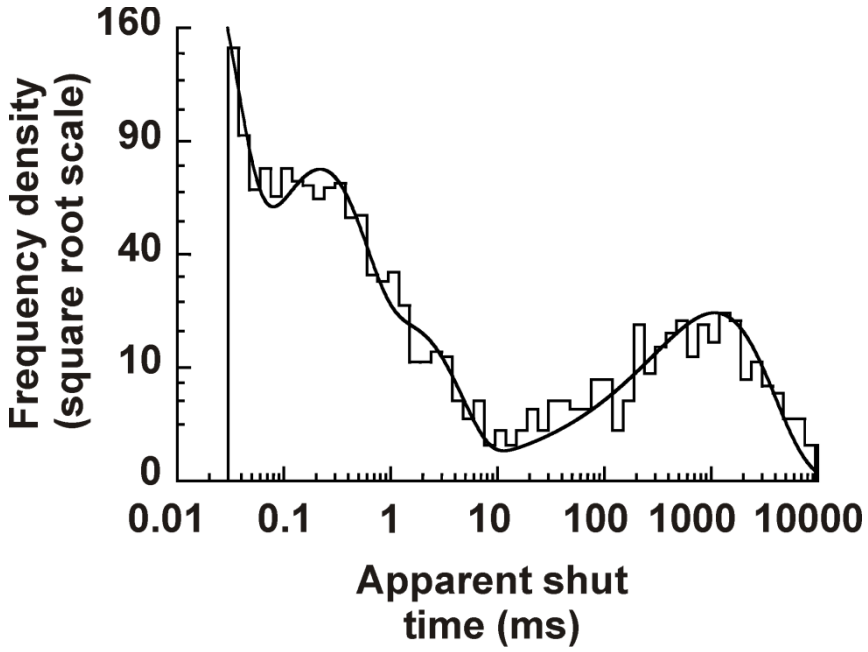

Figure 2.3 α3 GlyR shut time distribution obtained at 50 μM glycine
The continuous line is the fit with a mixture of exponentials. A t_{crit} of 10 ms was chosen to separate the longer shut times (e.g. interburst events, about 1000 ms) from the shorter ones, which are identified as intraburst.

In summary, intra and inter burst components of the pdf can be identified by checking whether their time constants change with agonist concentration across different patches. An appropriate t_{crit} is the value that best divides the intra-burst component from the inter-burst component. Different methods have been suggested to define the t_{crit} for bursts (Jackson *et al*., 1983; Magleby and Pallotta, 1983; Clapham and Neher, 1984; Colquhoun and Sakmann, 1985). This is done by discriminating a slower component (area a_s and mean t_s) and a fast component (a_f and mean τ_f). When the time constants, t_f and t_s are very different, all the methods give more or less the same solution for t_{crit}, so it will make little difference which method is used. All the methods gave similar solutions for the α3 glycine receptor, thus we decided to define the t_{crit} of bursts using Jackson method (Jackson *et al*., 1983).

At high concentrations of agonist, Sakmann *et al*. (1980) observed that bursts of openings can be grouped together into clusters of bursts, with long gaps between clusters. These long gaps are likely to reflect sojourns in long lived desensitised states. In such recordings it is possible to say that all the events in a cluster originate from the same ion channel. This is because clusters are long and have relatively high P_{open}, and if they originate from more than one

channel, double openings would be very likely to occur. Hence all of the shut times within a cluster can be interpreted in terms of kinetics, even when the number of channels in the patch is not known. In the shut time distribution, inter clusters shut time are clear separated from the shorter intra cluster shuttings, which are the greater proportion of the shuttings (Figure 2.4). Hence t_{crit} can be easily chosen as the value that separates the long isolated shut times from the rest of the distribution.

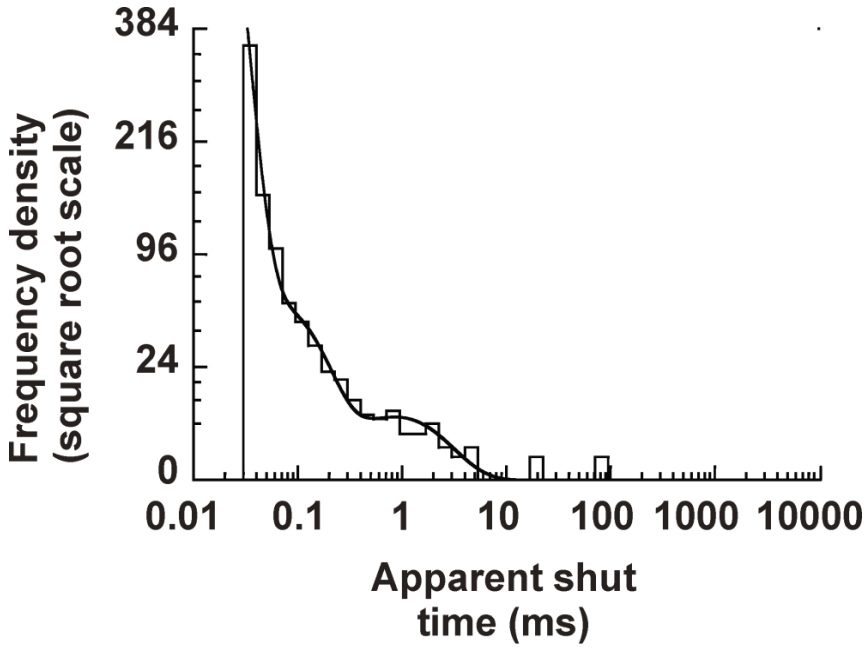

Figure 2.4 Shut time distribution for a recording of α3 GlyR at 1mM glycine.
For this experiment a t_{crit} of 10 ms was chosen, as clearly isolated intercluster shut times longer than the t_{crit} are present.

2.5.7 Experimental single channel P_{open} curve.

The P_{open} or open probability is the probability of a channel to be open. This measurement is useful as an empirical index of the activity in the record. If this measurement is done on a single ion channel molecule, its dependence on agonist concentration is a useful test for the validity of the fit of the postulated mechanism. The P_{open} cannot be calculated for the whole record, because it will be distorted by the long sojourns in the desensitized states and also because the number of channels is unknown. Hence it is important to identify the parts where the channels are desensitized, and exclude them from the measurement of the P_{open}. The remaining sections are clusters, which come from the activation of only one channel

molecule, and include sojourns in all the states of the activation mechanism. Thus they can be used to calculate the probability for a single ion channel to be open when in equilibrium with a given concentration of agonist. The dependence of the cluster P_{open} from the agonist concentration provides the best means of constructing the receptor equilibrium concentration response curve relation. Bursts cannot be used for the calculation of the P_{open} because, even if all events within a burst originate from the same channel as in cluster, the sojourns in the unbound state of the receptor and the fraction of time that receptor spends in this state cannot be estimated.

After open and shut times were measured by the idealisation of the records, the values for the P_{open} curve were obtained as the ratio between the total open times within clusters and the duration of the clusters. The averaged P_{open} values were plotted against concentration and fitted with the Hill equation (weighted least square fit) using the CVFIT program. The EC_{50}, Hill slope and max P_{open} were compared with those predicted by the results of fitting single channel data in HJCFIT. For P_{open} curves calculated from fitted mechanisms, we used the Hill slope at EC_{50} , defined as the tangent to the predicted concentration dependence of P_{open} on concentration and it was found numerically by the equation below, because it is not constant,

$$n_{H50} \equiv \frac{dln\left(\frac{P_{open}}{P_{max}-P_{open}}\right)}{dln(G)} | G = EC_{50} \qquad \text{[eq. 2.3]}$$

where G is the glycine concentration.

Such method for calculating the P_{open} curve has some advantages, it is corrected for the desensitization and it measures the response on an absolute scale, because the maximum possible response is 1.

2.5.8 Correlation between durations of adjacent open and shut times

Single channel activity is a memoryless process. This means that the duration of a sojourn in any individual state does not depend on how that state was reached. Nevertheless, channel activity can show correlations (Fredkin and Rice, 1985) between the duration of one opening and that of the adjacent shutting. This feature is very important, because it can give information about how the states are connected to each other.

The presence and the properties of correlations depend on how states are connected to each other. Correlation can arise only if there are at least two indistinguishable shut states and at

least two indistinguishable open states with the same conductance. Furthermore there must be at least two routes from open states to shut states before correlations are expected. Correlation will be found if there is no single state, deletion of which totally separates the open states from the shut states. The number of states to be deleted to achieve such separation is the connectivity between shut and open states. Correlation is seen if the connectivity is greater than one. The schemes below have three shut states (C) and two open states (O) connected in a different way.

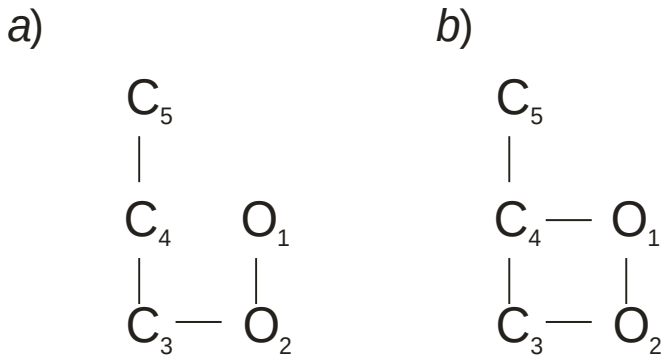

Scheme *a* will not give rise to any correlation, because the connectivity between open and shut states is one (C3 to O2), the deletion of state C_3 or O_2 will separate open and shut states. On the contrary, scheme *b* has connectivity two (C4 to O1 and C3 to O2), so correlation may be seen if the two open states have different mean lifetimes.

To construct the graph, a certain number of contiguous shut time ranges must be defined, each centred around the time constant of a component of the shut-time distribution. For each range, the average of the open times must be calculated for all openings that were adjacent to this shut time, and the average is plotted against the mean of the shut times in the corresponding range on a logarithmic scale.

2.5.9 Maximum likelihood fitting of kinetic mechanisms to single-channel data by the HJCFIT program

Establishing a kinetic mechanism allows detailed understanding of the effect of structure changes in agonists and the effect of mutations on receptors. In order to study the question of interest, a qualitative reaction scheme must be postulated and the value for the rate constants must be found. This can be done by a method which maximises the likelihood of the entire sequence of open and shut times at several concentrations. This provides estimates of the rate

constants directly from the observations, and takes both missed events and correlations into account. The computer program HJCFIT (Colquhoun *et al*., 1996; Colquhoun *et al*., 2003) is available for doing direct maximum likelihood fitting of rate constants for evaluation of kinetic schemes.

The data input into the program consists of the entire sequence of apparent durations of open and shut times, the imposed time-resolution. To this we must add a postulated mechanism and a set of initial guesses of the rate constants. The open and shut time intervals are measured from an experimental recording. The time-resolution (t_{res}) is crucial for making allowance for missed brief events. The t_{res} is defined so that events shorter than t_{res} are omitted and all the longer ones are present in the record.

The HJCFIT program calculates a likelihood value for the experimental sequence of the apparent open and shut times. The t_{res} is taken into account by the program by implementing a combination of the exact and asymptotic solutions for missed event correction by Hawkes, Jalali and Colquhoun (Hawkes *et al*., 1990; Hawkes *et al*., 1992). The rate constants are then adjusted to maximize the likelihood of the experimental data, and the best values are those that maximize this likelihood. For each mechanism the fit can be repeated with different initial guesses, in order to make sure that the rate constants estimated correspond to a global maximum. If the likelihood surface has such a single and well defined maximum, the same values of rate constants should be obtained when the program converges, no matter what initial guesses were used.

To test if a postulated mechanism describes well the behaviour of the receptor, the predictions of the mechanism and the optimised rate constants estimated by HJCFIT are used to calculate the distributions that should be observed and these are then compared with the experimental observations. This is done by inspecting the distribution of observed open and shut time distributions, the conditional mean open time plots, the P_{open} concentration curve and the time course of the macroscopic currents. The estimated rate constants are used to calculate predicted distributions of the dwell times. These predicted distributions then are superimposed to the experimental histograms. If the HJC distribution is close to the experimental histogram, the mechanism and the estimated rate constants describe the data well. Predicted and experimental correlations plots can be compared too.

Another test of how well the mechanism predicts the data is provided by the P_{open} curve. The value of the rate constants for a specific mechanism can be used by HJCFIT program to calculate the P_{open} as follows:

$$P_{open} = \frac{{}^{e}\mu_{open}}{{}^{e}\mu_{open} + {}^{e}\mu_{shut}} \qquad \text{[eq. 2.4]}$$

where $e_{\mu open}$ is the apparent mean open time and $e_{\mu shut}$ is the apparent mean shut time. These quantities are evaluated in the HJCFIT program. The predicted P_{open} curve is superimposed on experimental observed P_{open} points. As the Hill slope of the P_{open} curve is not constant with concentration, it is better to use the Hill slope at EC_{50}, defined as in eq. 2.3.

The quality of the fit was judged by eye and by comparing predicted and observed values for the EC_{50} and for the Hill slope at EC_{50}.

Chapter 3: Results

This Chapter follows from work published as a paper of which I was a first author

3.1 The α3 rat glycine receptor

It is well recognized that the kinetic properties of synaptic channels are the main factor that sets the time course of synaptic currents. Because of that, the same neurotransmitter can give rise to synaptic currents with different decay times at different synapses, depending on the nature of the receptors in the postsynaptic membrane (Verdoorn *et al.*, 1990; Tia *et al.*, 1996; Picton and Fisher, 2007). The composition of receptors for the same transmitter can vary considerably depending on developmental age, CNS area and presynaptic *versus* postsynaptic location and receptors that contain different subunit isoforms can have profoundly different kinetics (Takahashi *et al.*, 1992; Krupp *et al.*, 1994; Singer *et al.*, 1998).

Glycinergic transmission is a good example of this phenomenon. GlyRs are pentameric ligand-gated ion channels that are permeable to Cl^- and presumably to HCO_3^- (Bormann *et al.*, 1987; Ehrlich *et al.*, 1999; Backus *et al.*, 1998). GlyRs mediate much of the fast inhibitory synaptic transmission in the spinal cord and brainstem (Legendre, 2001; Lynch, 2004; Callister and Graham, 2010) and can be either homomeric (only α subunits), or heteromeric, *e.g.* contain both α and β subunits (Langosch *et al.*, 1988) . Four isoforms of the α subunit are known in mammals (α1, α2, α3 and α4) and their expression changes with development and differs across CNS regions.

At birth, rat GlyRs contain mostly α2 subunits (Legendre, 2001), but, during development, α2 expression decreases, whereas the α1 and α3 subunits become more abundant (Kuhse *et al.*, 1990; Malosio *et al.*, 1991b; Harvey *et al.*, 2004). The α2 homomeric channels mediate currents with very slow deactivation kinetics, with a decay time constant of the order of 100 ms, and their properties make them unsuitable to mediate glycinergic inhibitory postsynaptic current (IPSC) in the adult CNS (Mangin *et al.*, 2003; Krashia *et al.*, 2011). The time course of glycine synaptic currents is typically very fast, with decay time constants between 5 and 10 ms (Singer *et al.*, 1998; Burzomato *et al.*, 2004) and matches well the kinetic properties of α1β GlyR heteromers (Burzomato *et al.*, 2004; Pitt *et al.*, 2008) .

It is not clear whether the α3 subunit has a synaptic role in adult CNS. We know that α3 expression increases with age (Kuhse *et al.*, 1990) and that it is concentrated in discrete areas of the CNS (Harvey *et al.*, 2004). For instance, in the spinal cord, α1 is found throughout the grey matter, whereas α3 is confined to the superficial laminae of the dorsal horn (I and II), a

distinctive pattern that strongly suggests that GlyR α3 is specifically involved in nociceptive circuits. This hypothesis was confirmed by the finding that mice genetically deficient in GlyR α3 display less central sensitization in some inflammatory pain models (Harvey *et al*., 2004; Harvey *et al*., 2009).

3.1.1 Aims of the work

Recombinant GlyR containing the α3 subunit have been characterized with respect to their conductance, agonist sensitivity, and desensitization behaviour (Bormann *et al*., 1993; Breitinger *et al*., 2002; Heindl *et al*., 2007; Chen *et al*., 2009). However, nothing is known of their activation and deactivation kinetics, at either macroscopic or single channel level. It is particularly important to determine if the deactivation/burst kinetics of α3 GlyR are distinguishable from those of α1-containing GlyR. As deactivation sets the time course of synaptic currents, differences between the two receptors might allow us to identify synaptic currents mediated by each of the two subtypes, on the basis of their decay time courses.

Another important reason to characterise the kinetic properties of different channel isoforms is to understand how the molecular process of ion channel activation maps to the protein structure in homologous subunits. Mechanistic analysis of single channel records tells us how many agonist molecules are needed for maximum activation and whether the activation trajectory of the channel has to go through intermediate states. Fitting kinetic models to single-channel data from recombinant α1, α2 and α1β GlyRs led to the proposal of a detailed activation mechanism ("flip") that incorporates intermediate shut states between agonist binding and channel opening (Burzomato *et al*., 2004; Krashia *et al*., 2011). Mechanisms that include pre-open shut states, such as flip states or "primed" states (Mukhtasimova *et al*., 2009), are now known to describe well the activation of a variety of wild-type and mutant Cys-loop channels, including glycine, muscle nicotinic, and $GABA_A$ receptors (Burzomato *et al*., 2004; Plested *et al*., 2007; Mukhtasimova *et al*., 2009; Lape *et al*., 2009; Keramidas and Harrison, 2010; Lape *et al*., 2012). Microscopic affinity increases with flipping and this suggests that these intermediate shut states may be the kinetic reflection of conformational changes in the extracellular domain before channel opening.

Here we extend this approach to recombinant α3 GlyRs and their activation mechanism. We found that single-channel and macroscopic data from recombinant α3 homomers are well described by either a flip-type mechanism (Burzomato *et al*., 2004) or a Jones and Westbrook mechanism (Jones and Westbrook, 1995). Notably, α3 channels differ from other GlyRs

isoforms in that their maximal activation requires the agonist glycine to occupy five binding sites. This suggests that all the five agonist binding sites in a homomeric Cys-loop channel can contribute to function.

3.1.2 Features of α3 rat glycine receptor

Single channel experiments were performed in cell-attached configuration at a pipette potential of +100 mV, with no correction for junction potential, as this was calculated to be at most +1 mV (Clampex 10.2; MDS Analytical Technologies). Recordings were done using different concentration of glycine (50 - 10000 μM) dissolved in the extracellular solution. Recordings were idealized (7000 - 10000 transitions per patch) by time-course fitting with the program SCAN. Segments showing seal breakdowns, or multiple channel openings were excluded, and those intervals marked unusable. The aim of this stage of the analysis was to construct distributions of fitted amplitudes, shut times and open periods from the experimental data. The EKDIST program was used to characterize distributions of events, by fitting Gaussian densities to the current amplitude histogram and a mixture of exponential densities to the dwell time histograms. Openings that had not reached their full amplitude (being shorter than twice the rise time of the filter) were excluded from the fitted amplitude histograms. A single Gaussian was sufficient to produce a good fit of the amplitude histogram and the average amplitude of the single-channel currents was 5.8 ± 0.2 pA (S.D. of the mean; n = 21 patches). A time resolution of 30 μs was retrospectively imposed to both open and shut times using EKDIST (Colquhoun, 1995). The initial characterization of the dwell-time distributions was performed to determine a suitable value for the critical time, t_{crit}, to divide recordings into segments that are likely to arise from the activity of only one channel molecule (bursts or clusters; see below). All programs used in our analysis can be downloaded from Onemol (http://www.onemol.org.uk).

3.1.3 Experimental dwell time distributions

The cell-attached recordings in Figure 3.1 (A) clearly show that the pattern of α3 GlyR single-channel activity depends strongly on the glycine concentration. Note that the electrochemical potential drive Cl^- ions from the pipette to the cell, thus is an inward current. When this is low (eg 50 μM glycine, as in the top traces), channel openings occur in bursts, eg as single openings or as groups of few openings separated by long shut times. Each burst is likely to represent the activation of a single molecule (*e.g.* what happens between binding and unbinding of the agonist; (Edmonds *et al*., 1995) and the shut times between bursts are terminated by agonist binding. Thus, at higher glycine concentrations, activations get closer

and closer to each other and at 200 μM glycine and above, we observe clusters, long groups of openings that contain many events and are terminated by desensitized intervals (Sakmann *et al*., 1980; Colquhoun and Ogden, 1988).

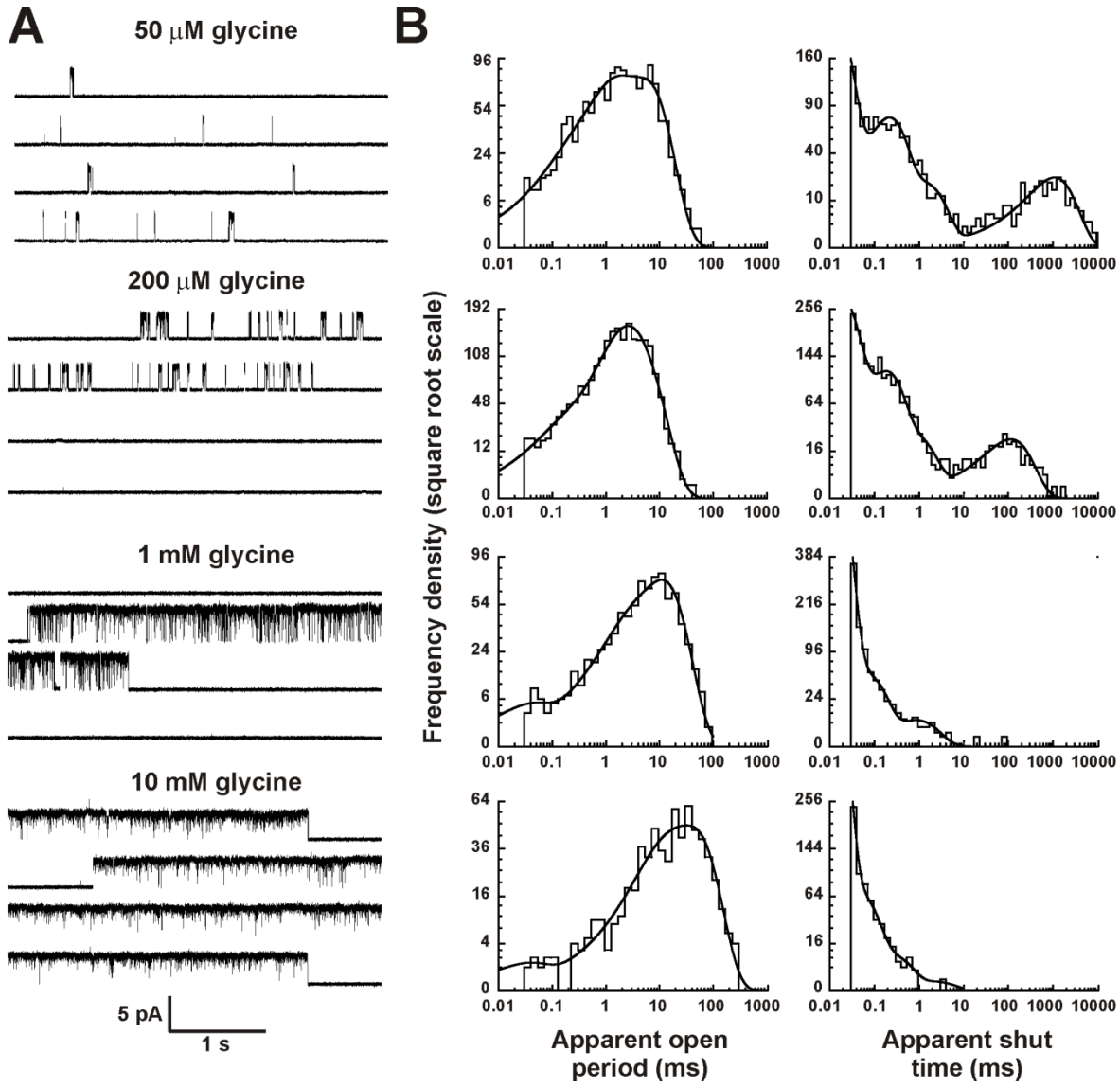

Figure 3.1 Activation of homomeric α3 GlyR by increasing concentrations of glycine
A, The traces are continuous sweeps of cell-attached single channel recordings at 50, 200, 1000 and 10000 μM glycine (3 kHz filter). Isolated bursts of openings are observed at 50 μM, at higher concentrations the bursts group together to form clusters. B, Apparent open (left column) and shut time (right column) dwell-time distributions, for the same patches shown in A. Distributions were fitted with a mixture of exponential probability density functions (Table 3.1).

After idealization of single channel current traces by time-course fitting, the apparent open and shut time distributions were plotted and fitted with a mixture of exponential probability density functions (Figure 3.1 B). The term ‘apparent' indicates that our estimate of the true

duration of an opening or a shutting may be affected by our inability to detect short-lived events (*e.g.* shorter than 30 μs). Ideally the number of exponential components needed to fit the dwell time distributions indicates the minimum number of the shut/open states present in the activation mechanism, as some small components can be undetectable in real data distribution. The results of these empirical fits are used only to obtain an indication about the minimum number of states needed and more importantly to choose the appropriate t_{crit} for the second stage of analysis (see Chapter 2 Methods). Adequate fit of open and shut time distributions required three and four exponential components, respectively (see Table 3.1 for a summary).

Table 3.1 Properties of dwell time distributions

Apparent open periods				
Gly (μM) [*n*]	**τ_1 (ms) [area (%)]**	**τ_2 (ms) [area (%)]**	**τ_3 (ms) [area (%)]**	**Mean open time (ms)**
50 [4]	0.15 ± 0.05 [20 ± 10]	0.9 ± 0.2 [44 ± 4]	4.6 ± 0.6 [40 ± 10]	2.2 ± 0.5
200 [4]	0.09± 0.03 [5 ± 1]	1.5 ± 0.1 [33 ± 4]	5.3 ± 0.8 [61 ± 5]	3.9 ± 0.6
300 [3]	0.07± 0.04 [3 ± 1]	1.7 ± 0.3 [16 ± 3]	5.7 ± 0.3 [81 ± 3]	5.1 ± 0.04
1000 [4]	0.11± 0.09 [8 ± 4]	3.8 ± 2 [30 ± 10]	12 ± 2 [60 ± 20]	8.6 ± 1.1
10000 [2]	0.07 ± 0.04 [2.2 ± 0.4]	5.6 ± 3 [17 ± 9]	30 ± 10 [81 ± 9]	23.9 ± 8.9
Apparent shut times				
Gly (μM) [n]	**τ_1 (ms) [area (%)]**	**τ_2 (ms) [area (%)]**	**τ_3 (ms) [area (%)]**	**τ_4 (ms) [area (%)]**
50 [4]	0.04 ± 0.02 [49 ± 7]	0.33 ± 0.06 [28 ± 4]	2.9 ± 0.8 [5 ± 1]	1700 ± 600 [17 ± 4]
200 [4]	0.03 ± 0.01 [62 ± 1]	0.27± 0.07 [26 ± 2]	30 ± 20 [6 ± 1]	200 ± 60 [5 ± 1]
300 [3]	0.009 ± 0.001 [88 ± 2]	0.3 ± 0.2 [8 ± 1]	0.50 ± 0.05 [3 ± 1]	38 ± 6 [0.9 ± 0.2]
1000 [4]	0.01 ± 0.004 [61 ± 7]	0.05 ± 0.02 [30 ± 6]	0.3 ± 0.1 [9 ± 3]	1.9 ± 0.5 [1 ± 0.3]
10000 [2]	0.010 ± 0.001 [70 ± 30]	0.03 ± 0.02 [30 ± 30]	0.4 ± 0.2 [2 ± 1]	1.2 ± 0.7 [0.2 ± 0.1]

Distributions were fitted with mixtures of exponential probability density functions. *n*, the number of patches for each concentration (indicated in brackets in the first column). The time constant of each component and its relative area (in brackets) are given as mean ± SD of the mean.

Apparent open times (Fig 3.1B, left column) shifted toward longer values at higher glycine concentrations, and the mean open time increased, from 2.2 ± 0.5 ms at 50 μM glycine, to 24

± 9 ms at the highest glycine concentration, 10 mM (*n*= 4 and 2 patches, respectively, see Table 3.1). In the shut time distributions (Fig 3.1B, right column), multiple components were clearly detectable. The longer components were concentration dependent and became shorter at the higher agonist concentrations. In particular, the mean duration of the longest shut times decreased from 1.7 ± 0.6 s at 50 µM glycine to 1.2 ± 0.7 ms at 10 mM glycine. On the other hand, the shortest shuttings remained relatively stable, with a mean duration of 40 ± 20 µs and 10 ± 1 µs at 50 µM and 10 mM glycine, respectively. It is this shortest component that dominates the shut time distribution at the higher agonist concentrations (Table 3.1). Because these shuttings are so short, with an average duration close to or below our experimental resolution, many of the shortest shuttings are likely to be missed in the idealization and will contribute to the apparent lengthening of the open times with increasing glycine concentrations.

3.1.4 P_{open} Curve

The concentration dependence of single channel activity can be displayed and characterized as a P_{open} curve. This is done by identifying clusters, stretches of openings that arise from the activation of just one channel (see Chapter 2 Methods). Examples of clusters at several concentrations of glycine are shown in Figure 3.2 A. The P_{open} values of such clusters were measured and plotted against glycine concentration in Figure 3.2 B (see Table 3.2 for a summary). Fitting these data points with the Hill equation gave a maximum open probability of 0.991 ± 0.003, an EC_{50} of 297 ± 4 µM and a Hill slope of 3.7 ± 0.1.

Table 3.2 P_{open}

Glycine (µM)	Number of clusters	Number of patches	Number of openings	Cluster length (s)	P_{open}
200	19	4	500 ± 100	11 ± 3	0.18 ± 0.01
300	2	2	1600 ± 400	15 ± 3	0.58 ± 0.04
500	11	3	540 ± 90	2.2 ± 0.4	0.87 ± 0.01
1000	8	4	600 ± 200	5 ± 1	0.975 ± 0.004
10000	4	2	230 ± 80	6 ± 3	0.996 ± 0.003

Values are obtained for each patch as ratios of total open time and total cluster duration (calculated from recordings idealized by time-course fitting). Values are means ± SD of the mean.

The Hill equation was fitted simply to obtain an empirical estimate of the steepness of the P_{open} curve that we could use for comparison with the predictions of postulated mechanisms (Burzomato *et al*., 2004), even though it describes no possible physical mechanism. The Hill equation is not a realistic way to represent the combination of *n* ligand molecules with one

receptor, because it implies that *n* ligands collide simultaneously with the receptor and that all combine with it. Such multiple collisions are very unlikely and moreover intermediate receptors where not all the binding sites are occupied exist. Nevertheless a slope greater than one can be interpreted as suggesting that more than one molecule is involved in some way.

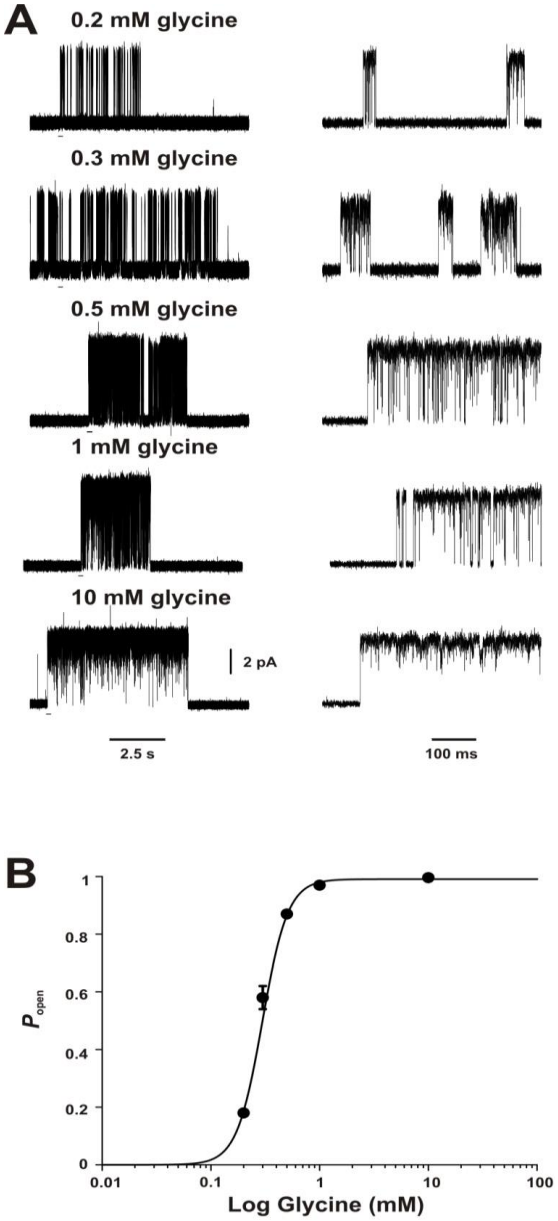

Figure 3.2 Concentration dependence of the open probability of homomeric α3 GlyR clusters A, Examples of clusters recorded at 200, 300, 500, 1000 and 10000 μM glycine. The bars under the traces on the left show the regions expanded in time on the right. B, Cluster open probability, P_{open}, plot versus glycine concentration. The symbols show the mean values (with error bars for the SD of the mean, where this is bigger than the symbol size) for the patches included in the analysis (2-4 at each concentration). P_{open} values were obtained for each patch from the ratio between the total open time and the total clusters duration, from recordings idealized by time-course fitting. The solid line is a fit of the Hill equation, which yielded an EC_{50} of 297 ± 4 μM and a Hill slope of 3.7 ± 0.1.

3.1.5 Fitting mechanisms

The HJCFIT method (Colquhoun *et al*., 2003) was used to fit several putative mechanisms to idealized single channel records. Sets of data from different recordings, each made at a different concentration, were fitted simultaneously. Each set contained four different glycine concentrations, spanning the whole of the P_{open} curve. At the end of fitting, the quality of the fits was assessed by visual inspection of the agreement between the model predictions and the experimental open/shut time distribution and P_{open} curve. We will describe only the models that best describe the data (Fig 3.3) of the approximately thirty models we tested.

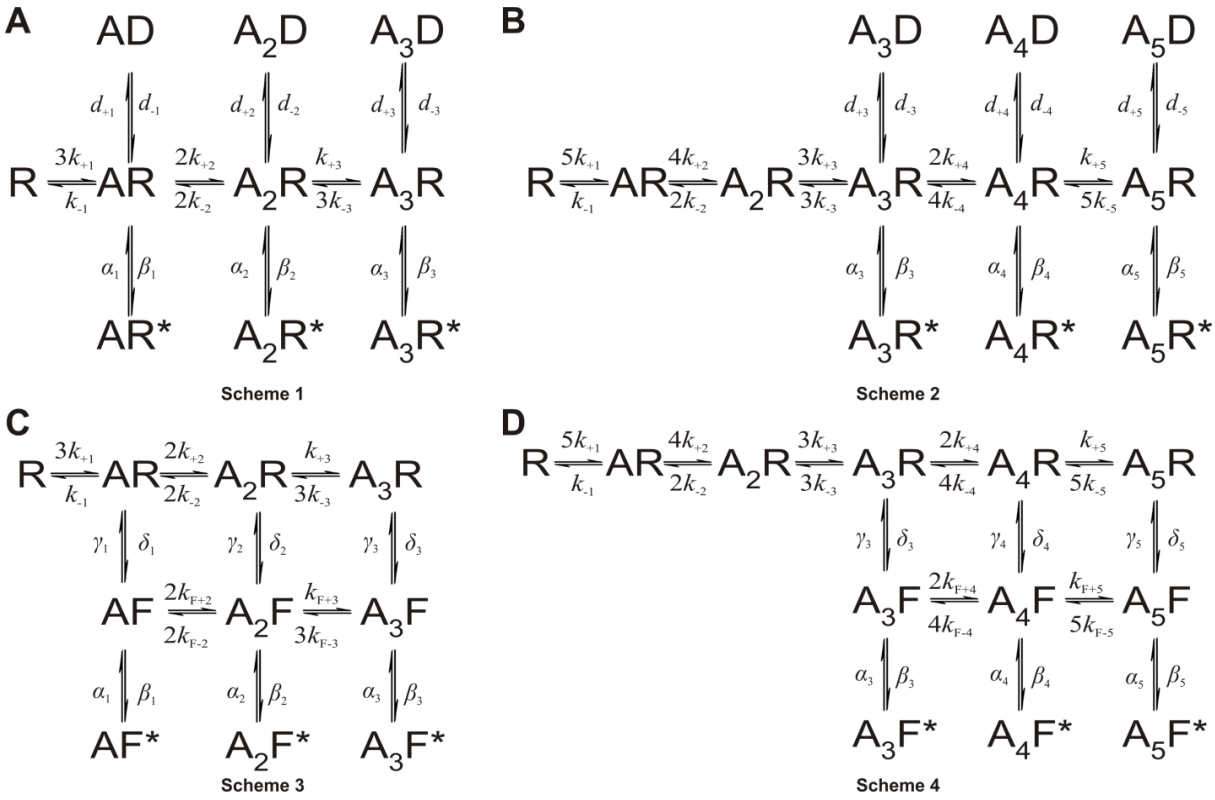

Figure 3.3 Some of the kinetic schemes tested for α3 GlyR
Scheme 1 and Scheme 2 are Jones and Westbrook type mechanisms (Jones and Westbrook, 1995) modified to include three (A) or five (B) binding sites. The letter D indicates distal desensitized states. Scheme 3 (C) is the Flip mechanism proposed for the heteromeric α1β glycine receptor (Burzomato *et al*., 2004). Scheme 4 (D) is a Flip mechanism with five binding sites. In all schemes, the letter A denotes an agonist molecule and its subscript indicates the number of agonist molecules bound to the receptor. The letters R and R* denote resting shut states and open states of the receptor, respectively. The letter F indicates intermediate flipped shut states that connect resting and open states.

Two of the models discussed (*e.g.* the five-binding site versions of the Jones and Westbrook model and of the 'flip' model, Fig 3.3 B and D, respectively) fitted the data well. For comparison, we describe also the results of fitting the same mechanisms in the three-binding

site versions (Fig 3.3 A and C). These are known to describe adequately the behaviour of the related α1 and α1β glycine receptor isoforms (Burzomato *et al*., 2004), but we found that they failed to fit α3 data well. Other mechanisms tested and found inadequate include both simpler schemes (*e.g.* sequential schemes and subsets of the flip and Jones and Westbrook mechanisms) and variants of the 'primed' mechanisms such as those we applied to the startle disease mutant K276E (Lape *et al*., 2012).

3.1.5.1 Jones and Westbrook-type mechanisms

The original form of this mechanism (with two binding steps) was proposed by Jones and Westbrook for the activation of $GABA_A$ receptors (Jones and Westbrook, 1995). From each resting bound state, the channel can either open or enter a short-lived desensitized state. Scheme 1 in Figure 3.3A shows how we adapted this mechanism for α1β heteromeric glycine receptors, to include three agonist binding sites, three short lived "desensitized" states and three open states (Burzomato *et al*., 2004). The main property of Scheme 1 is that the agonist binding sites are allowed to interact with each other, and change their affinity with the level of ligation. In fitting this type of scheme to α3 data, no constraints were imposed on the values of the binding rate constants across the mechanism, so the number of free parameters was 18.

The dwell time distributions calculated from this model and its fitted rate constants (not shown) were in good agreement with the experimental ones. However, the prediction of the P_{open} curve (Fig 3.4A) was not satisfactory, particularly in terms of the Hill slope. The best fit of this model predicted a slope of 2.5 ± 0.2 and therefore could not match the steep slope of the experimental curve (3.7 ± 0.1). The other parameters of the observed curve, such as EC_{50} and maximum P_{open}, were reasonably well described (EC_{50} = 310 ± 30 μM and maximum P_{open} 0.997 ± 0.001). The average values for the rate constants estimated for Scheme 1 (and the other Jones and Westbrook-type schemes) are shown in Table 3.3. Data are the average of estimates obtained from fits to three independent single channel data sets. Equilibrium constant values were calculated for each set from the ratio of the appropriate rate constants and then averaged. The failure of the mechanism with three binding sites to match the observed high slope of the P_{open} curve is a strong indication that α3 receptors may require the binding of more than three agonist molecules in order to achieve maximum open probability. We therefore proceeded to test Scheme 1 variants with four or five binding sites. For instance, Scheme 2 (Fig 3.4B) has five glycine binding sites, three desensitized states and three open states. Here, the channel can access the desensitised and open states only from the

three highest levels of ligation. Scheme 2 incorporates all the features of Scheme 1, but increasing the number of binding sites to five increases also the number of free parameters to 22. Once again, the dwell time distributions predicted by the results of fitting Scheme 2 (Fig 3.4D) were in good agreement with the data, and fits were good across the three sets. The fit of Scheme 2 predicted a Hill slope of 3.7 ± 0.1 for the P_{open} curve. This exactly matches the observed value (Figure 3.4C) and is much better than the prediction of Scheme 1 (three binding sites, Figure 3.4A).

We tested also a Jones and Westbrook variant with four glycine binding steps (Figure 3.4B, top): fitting this scheme gave good descriptions of the dwell-time distributions (data not shown), and predicted a somewhat shallower Hill slope for the P_{open} curve (3.4 ± 0.2; Figure 3.4B, bottom).

The first feature that is apparent from the results of the fits of Scheme 2 shown in Table 3.3 is that, at the highest level of ligation, α3 channels open with a fast opening rate (180000 ± 20,000 s^{-1}) and high efficacy (34 ± 4). These estimates are consistent across the sets, with CVs of about 10%. As the channel binds more glycine molecules, there is a clear increase in efficacy (nearly 100-fold). This is almost entirely due to an increase in the value of the opening rate constant, in a manner similar to that observed for other isoforms of the glycine channel (Burzomato *et al*., 2004). The poor reproducibility across data sets of the estimates of efficacy for the two lower-liganded states makes it hard to say whether each molecule of agonist bound contributes equally to the increase in efficacy with ligation. The values of the equilibrium constants for entry into desensitization also change with level of ligation, but in the opposite direction, favouring desensitization at the lower liganded states (note the high CV of D_3 and D_5). These features are very similar in the fits of the schemes with 3 and 4 molecules bound.

In the best-fitting scheme 2, the affinity of agonist binding increases by more than 50-fold over the five binding steps. This is a consistent feature of this mechanism, despite the relatively high variability of the estimates of the dissociation constants (Table 3.3). In the mechanisms with fewer binding steps, the overall increase in affinity is greater, reaching more than 5000-fold in the mechanism with four binding steps.

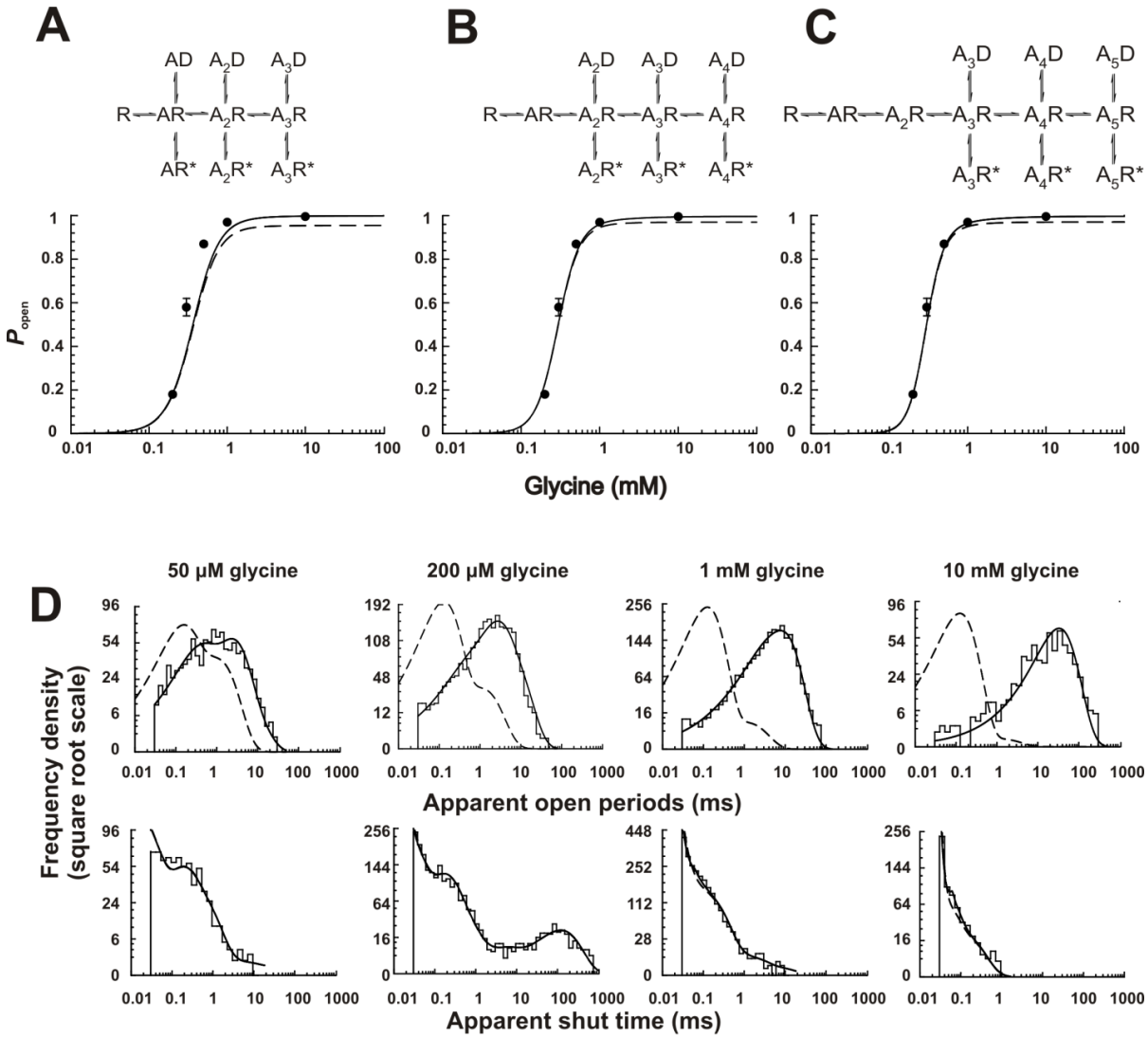

Figure 3.4 Fits of the Jones and Westbrook type mechanisms to α3 GlyR single channel currents

A-C, Open probability curves predicted by rate constant estimates obtained by fits with Jones andWestbrook type mechanisms (shown at top of the panels) with three, four or five binding agonist binding sites. Experimental P_{open} values are plotted as filled circles against the glycine concentration. The solid line is the apparent P_{open} concentration curve predicted by the fitted scheme and rate constants, taking into account the effect of missed events. The dashed line is the ideal curve expected if no events are missed. D, Probability density functions (solid lines) predicted by the fit of Scheme 2 (five binding sites) for apparent opent periods (top plots) and apparent shut times (bottom plots) are superimposed on the experimental histograms at four different glycine concentrations. The dashed lines are the distributions expected if there were no missed events.

Table 3.3 Average rate constants, equilibrium constants and coefficients of variation from the fit of Jones and Westbrook-type schemes

	Unit	J&W, 3 binding sites (Scheme 1)	J&W, 4 binding sites	J&W, 5 binding sites (Scheme 2)
α_1	s^{-1}	2,980 ± 20%		
β_1	s^{-1}	941 ± 65%		
α_2	s^{-1}	825 ± 20%	2,820 ± 16%	
β_2	s^{-1}	20,700 ± 47%	934 ± 54%	
α_3	s^{-1}	6,150 ± 34%	832 ± 21%	2,780 ± 14%
β_3	s^{-1}	180,000 ± 12%	21,200 ± 44%	922± 55%
α_4	s^{-1}		5,830 ± 30%	849 ± 20%
β_4	s^{-1}		180,000 ± 12%	23,800 ± 43%
α_5	s^{-1}			5,530 ± 24%
β_5	s^{-1}			180,500 ± 12%
d_{-1}	s^{-1}	262,000 ± 99%		
d_{+1}	s^{-1}	96,900 ± 98%		
d_{-2}	s^{-1}	6,010 ± 10%	4,060 ± 71%	
d_{+2}	s^{-1}	8,030 ± 6%	51,800 ± 97%	
d_{-3}	s^{-1}	18,400 ± 22%	5,840 ± 11%	124,500 ± 98%
d_{+3}	s^{-1}	1,210 ± 38%	7,800 ± 6%	6,500 ± 72%
d_{-4}	s^{-1}		18,700 ± 25%	6,370 ± 18%
d_{+4}	s^{-1}		1,230 ± 35%	8,290 ± 12%
d_{-5}	s^{-1}			21,100 ± 32%
d_{+5}	s^{-1}			1,250 ± 28%
k_{-1}	s^{-1}	1,260 ± 30%	342,000 ± 73%	2,460 ± 90%
k_{+1}	$M^{-1}\ s^{-1}$	3.50×10^4 ± 23%	1.57×10^6 ± 51%	7.93×10^5 ± 47%
k_{-2}	s^{-1}	2,720 ± 31%	1,636 ± 45%	34,125 ± 97%
k_{+2}	$M^{-1}\ s^{-1}$	6.27×10^6 ± 45%	1.77×10^7 ± 68%	3.96×10^7 ± 98%
k_{-3}	s^{-1}	1,328 ± 27%	1,903 ± 32%	442 ± 38%
k_{+3}	$M^{-1}\ s^{-1}$	7.78×10^6 ± 48%	8.33×10^6 ± 4%	3.38×10^5 ± 28%
k_{-4}	s^{-1}		1,036 ± 26%	1,548 ± 35%
k_{+4}	$M^{-1}\ s^{-1}$		2.33×10^7 ± 48%	6.18×10^6 ± 46%
k_{-5}	s^{-1}			875 ± 26%
k_{+5}	$M^{-1}\ s^{-1}$			2.4×10^7 ± 47%
$E_1 = \beta_1 / \alpha_1$		0.37 ± 77%		
$E_2 = \beta_2 / \alpha_2$		32 ± 58%	0.37 ± 64%	
$E_3 = \beta_3 / \alpha_3$		33 ± 19%	33 ± 54%	0.36 ± 65%
$E_4 = \beta_4 / \alpha_4$			34 ± 16%	35 ± 51%
$E_5 = \beta_5 / \alpha_5$				34 ± 11%
$D_1 = d_{+1} / d_{-1}$		0.97 ± 40%		
$D_2 = d_{+2} / d_{-2}$		1.35 ± 4%	6.02 ± 79%	
$D_3 = d_{+3} / d_{-3}$		0.09 ± 53%	1 ± 5%	0.73 ± 69%
$D_4 = d_{+4} / d_{-4}$			0.09 ± 52%	1 ± 5%
$D_5 = d_{+5} / d_{-5}$				0.08 ± 49%
$K_1 = k_{-1} / k_{+1}$	µM	44,450 ± 40%	461,760 ± 61%	3,240± 48%
$K_2 = k_{-2} / k_{+2}$	µM	820 ± 52%	284 ± 78%	1,200 ± 15%
$K_3 = k_{-3} / k_{+3}$	µM	95 ± 46%	223 ± 30%	1,200 ± 18%
$K_4 = k_{-4} / k_{+4}$	µM		71 ± 42%	502 ± 55%
$K_5 = k_{-5} / k_{+5}$	µM			58 ± 40%
EC_{50}	µM	305 ± 10%	288 ± 6%	284 ± 5%
n_H		2.5 ± 8%	3.4 ± 5%	3.7 ± 3%

All the rate constants were fitted freely in HJCFIT. The values for efficacy at each level of ligation, E, the dissociation equilibrium constants per site, K, the equilibrium constants for the entry into the extra shut states, D_n, the EC_{50} and the Hill slope were calculated from the rate constants for each set and their averages are listed at the bottom of the table. Values are means ± coefficient of variation (i.e. SD of the mean expressed as a % of the mean)

3.1.5.2 Flip mechanisms

Scheme 3 depicted in Figure 3.3 C is the flip mechanism originally proposed by Burzomato *et al.* (2004). This scheme postulates the existence of an additional type of shut state, the flipped state, which represents a concerted conformational change that occurs before the channel opens. In flip-type models, the glycine binding sites are independent and the binding affinity depends only on the state of the receptor (*i.e.* resting or flipped), and not on the level of ligation. Hence the scheme specifies only two equilibrium constants for binding, one for the resting conformation (R) and one for the flipped conformation (F), regardless of how many sites are already occupied. This was done by applying the following constraints to the rate constants: $k_{+1} = k_{+2} = k_{+3} = k_{+}$, $k_{-1} = k_{-2} = k_{-3} = k_{-}$, $k_{F+2} = k_{F+3} = k_{F+}$ and $k_{F-3} = k_{F-2} = k_{F-}$. In addition to that, two rate constants (δ_1 and δ_3, mono- and triliganded unflipping, see Figure 3.3 C) were constrained in order to satisfy the requirement of microscopic reversibility for the two cycles in the flip scheme (Colquhoun *et al.*, 2004). As a result this mechanism had only 14 free parameters.

As we did with the Jones and Westbrook-type mechanisms, we tested additional flip mechanisms, with four or five binding sites. For instance, Scheme 4 depicted in Figure 3.3 D has five binding sites. The main features of the original flip mechanism are conserved and the scheme maintains three open states and three flipped states, which are accessible from the most highly liganded resting states. Binding site independence was satisfied in Scheme 4 by applying the following constraints to the rate constants for binding: $k_{+1} = k_{+2} = k_{+3} = k_{+4} = k_{+5}$, $k_{-1} = k_{-2} = k_{-3} = k_{-4} = k_{-5}$, $k_{F+4} = k_{F+5}$ and $k_{F-5} = k_{F-4}$. Two unflipping rate constants, δ_3 and δ_5, were constrained to satisfy the requirement of microscopic reversibility (Colquhoun *et al.*, 2004). As a result this mechanism had the same number of free parameters as Scheme 3.

After fitting flip mechanisms with three, four or five binding sites, we checked how well the P_{open} curve was described (Fig 3.5 A-C). The EC_{50} predicted was similar for all three mechanism, at around 300 μM (cf observed $EC_{50} = 310 \pm 30$ μM). As expected, the predicted slope of the apparent P_{open} curve became steeper with increasing number of binding sites (2.2 ± 0.1 for Scheme 3 and 3.1 ± 0.1 for Scheme 4), but its maximum value was somewhat lower than the one reached by Scheme 2. The predicted dwell time distributions were in good agreement with the data at all glycine concentrations and the quality of these predictions was similar for flip mechanisms with three, four or five binding sites. Figure 3.5D shows apparent open and shut time distributions predicted by the flip mechanism with five binding sites, superimposed onto experimental data histograms.

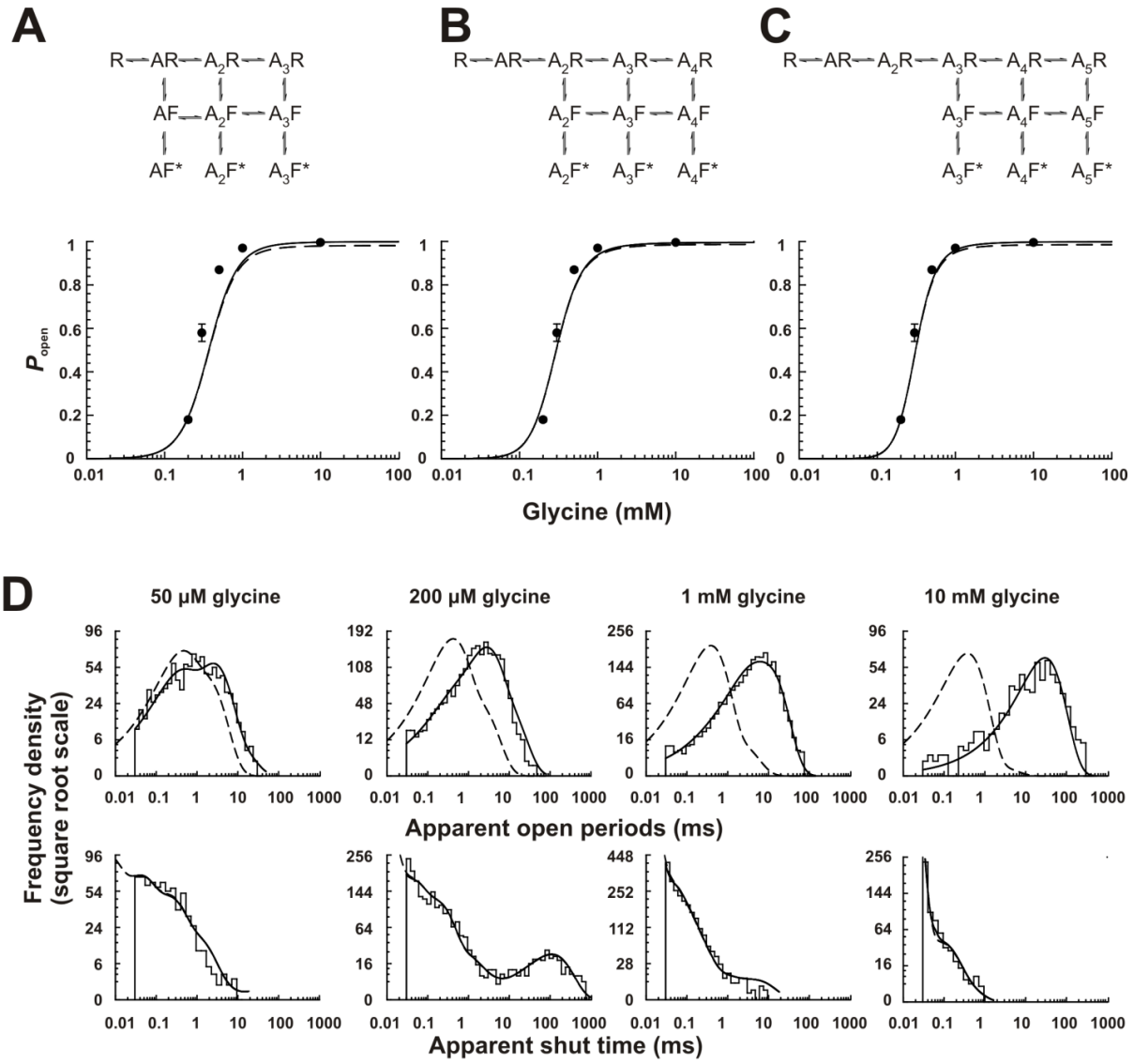

Figure 3.5 Fits of the flip mechanisms to the homomeric α3 GlyR single channel currents
A-C, P_{open} curves predicted by rate constant estimates obtained by fits with flip mechanisms (shown at top of panels) with three, four or five agonist binding sites. Filled circles are experimental data, solid lines- apparent P_{open} curves (corrected for missed events) and dashed lines- the ideal P_{open} curves expected if no events are missed. D, Probability density functions (solid lines) predicted by the fit of Scheme 4 (five binding sites) for apparent opent periods (top plots) and apparent shut times (bottom plots) are superimposed on the experimental histograms at four different glycine concentrations. For more details see Figure 3.3.

As we reported for other glycine receptor isoforms, α3 channel activity displays correlations between open and shut times, and the longer open times are found adjacent to the shortest shut times. The extent of these correlations and their concentration dependence was similar to that we described for α1 receptors and were adequately described by all the variants of the Jones and Westbrook and flip mechanism described here (data not shown).

Table 3.4 Average rate constants, equilibrium constants and coefficients of variation from the fit of flip mechanisms with different number of binding sites

	Unit	Flip, 3 binding sites (Scheme 3)	Flip, 4 binding sites	Flip, 5 binding sites (Scheme 4)
α_1	s^{-1}	2,840 ± 30%		
β_1	s^{-1}	1,230 ± 4%		
α_2	s^{-1}	498 ± 16%	2,690 ± 27%	
β_2	s^{-1}	18,800 ± 14%	1,220 ± 7%	
α_3	s^{-1}	2,370 ± 28%	496 ± 14%	2,520 ± 23%
β_3	s^{-1}	154,000 ± 15%	19,600 ± 13%	1,260 ± 7%
α_4	s^{-1}		2,030 ± 24%	497 ± 13%
β_4	s^{-1}		149,000 ± 16%	20,700 ± 10%
α_5	s^{-1}			1,870 ± 22%
β_5	s^{-1}			147,000 ± 16%
γ_1	s^{-1}	1,830 ± 23%		
δ_1	s^{-1}	91 ± 20%		
γ_2	s^{-1}	6,180 ± 1%	1,950 ± 13%	
δ_2	s^{-1}	4,280 ± 17%	223 ± 23%	
γ_3	s^{-1}	2,120 ± 27%	5,900 ± 5%	2,220 ± 13%
δ_3	s^{-1}	17,500 ± 10%	5,060 ± 18%	419 ± 31%
γ_4	s^{-1}		2,490 ± 26%	5,800 ± 7%
δ_4	s^{-1}		14,500 ± 8%	5,820 ± 22%
γ_5	s^{-1}			2,550 ± 27%
δ_5	s^{-1}			12,700 ± 5%
k_-	s^{-1}	241 ± 1%	236 ± 15%	222 ± 23%
k_+	$M^{-1}\ s^{-1}$	7.32×10^4 ± 9%	1.60×10^5 ± 6%	2.45×10^5 ± 14%
k_{f-}	s^{-1}	4,480 ± 9%	5,270 ± 13%	5,920 ± 16%
k_{f+}	$M^{-1}\ s^{-1}$	9.88×10^6 ± 29%	9.73×10^6 ± 24%	9.73×10^6 ± 21%
$E_1 = \beta_1 / \alpha_1$		0.52 ± 30%		
$E_2 = \beta_2 / \alpha_2$		41 ± 24%	1 ± 28%	
$E_3 = \beta_3 / \alpha_3$		70 ± 14%	42 ± 22%	1 ± 24%
$E_4 = \beta_4 / \alpha_4$			77 ± 11%	44 ± 19%
$E_5 = \beta_5 / \alpha_5$				80 ± 8%
$F_1 = \delta_1 / \gamma_1$		0.05 ± 31%		
$F_2 = \delta_2 / \gamma_2$		0.69 ± 16%	0.11 ± 19%	
$F_3 = \delta_3 / \gamma_3$		11 ± 45%	1 ± 24%	0.18 ± 20%
$F_4 = \delta_4 / \gamma_4$			7 ± 42%	1 ± 29%
$F_5 = \delta_5 / \gamma_5$				6 ± 42%
$K_R = k_- / k_+$	μM	3,350 ± 11%	1,460 ± 10%	885 ± 9%
$K_F = k_{f-} / k_{f+}$	μM	263 ± 25%	196 ± 19%	159 ± 15%
EC_{50}	μM	320 ± 8%	300 ± 5%	275 ± 7%
n_H		2.2 ± 5%	2.7 ± 4%	3.1 ± 3%

The fits constrain the binding and unbinding rates to be the same, regardless of the number of molecules bound, in any conformation. The equilibrium constants, E, F and K, and open probability curve EC_{50} and the Hill slope, n_H, were calculated from the rate constants for each set and then averaged. Values are means ± coefficient of variation (i.e. SD of the mean expressed as a % of the mean).

Rate constants and equilibrium constants from the fits of the flip schemes are shown in Table 3.4 and Figure 3.6. The values estimated for the flip mechanisms were much more consistent across the different sets than those estimated with Jones and Westbrook-type mechanisms, and the highest CV for rate constant values in Scheme 4 was 31% (cf. 98% for Scheme 2).

The results in Table 3.4 have many features that resemble those we described earlier for α1 containing glycine channels. Fully-liganded α3 channels have a high opening rate (150,000 ± 20000 s^{-1}). As more agonist molecules bind, both the pre-opening conformation change to the flipped state and the opening of the channel from the flipped state becomes more favourable. Thus the value of the flipping equilibrium constant, *F*, increased from 0.2 (flipping from A_3R) to 6 (flipping from A_5R) and that of the gating equilibrium constants, *E*, increased from 1 to 80. In the case of *F*, the presence of cycles in the mechanism constrains (by microscopic reversibility) the increase to be similar at each step. This constraint is not present for the estimation of *E* in the model we fitted and most of the increase in *E* was between the two lower liganded open states. Fits of a similar model with connected open states gave poorer results (data not shown), possibly because the interaction between the open channel and permeating chloride ions (Pitt *et al*., 2008; Moroni *et al*., 2011; Houston *et al*., 2009) results in the (apparent) breach of microscopic reversibility. As we reported for α1-containing channels, most of the increase in the value of *E* was due to the increase in the opening rate constant. The increase in glycine affinity with flipping was 6-fold (K_R = 890 μM and K_F = 160 μM), very close to that observed for α1 homomeric channels fitted with the flip model, but much smaller than the 65-fold increase seen in heteromeric α1β GlyR (Burzomato *et al*., 2004).

In the Flip model, overall agonist efficacy depends on the equilibrium constant for flipping (*F)* and the equilibrium constant (*E*) for the open-shut reaction. For the fully liganded receptor, we can define an "effective efficacy", E_{eff}, as

$$E_{eff} = \frac{EF}{F+1} \qquad \text{[eq 3.1]}$$

Both homomeric receptors have a very high maximum P_{open} and their overall efficacy is high (67 for α3 and 35 for α1 homomers).

Our adaptation of the flip mechanism has five binding sites, and the most general version of this mechanism should have five flipped and five open states (as in (Burzomato *et al*., 2004). Mechanisms containing more than three open states gave much worse fits, which failed to describe the shut time distributions and had high coefficients of variation for the estimated rate constants (data not shown).

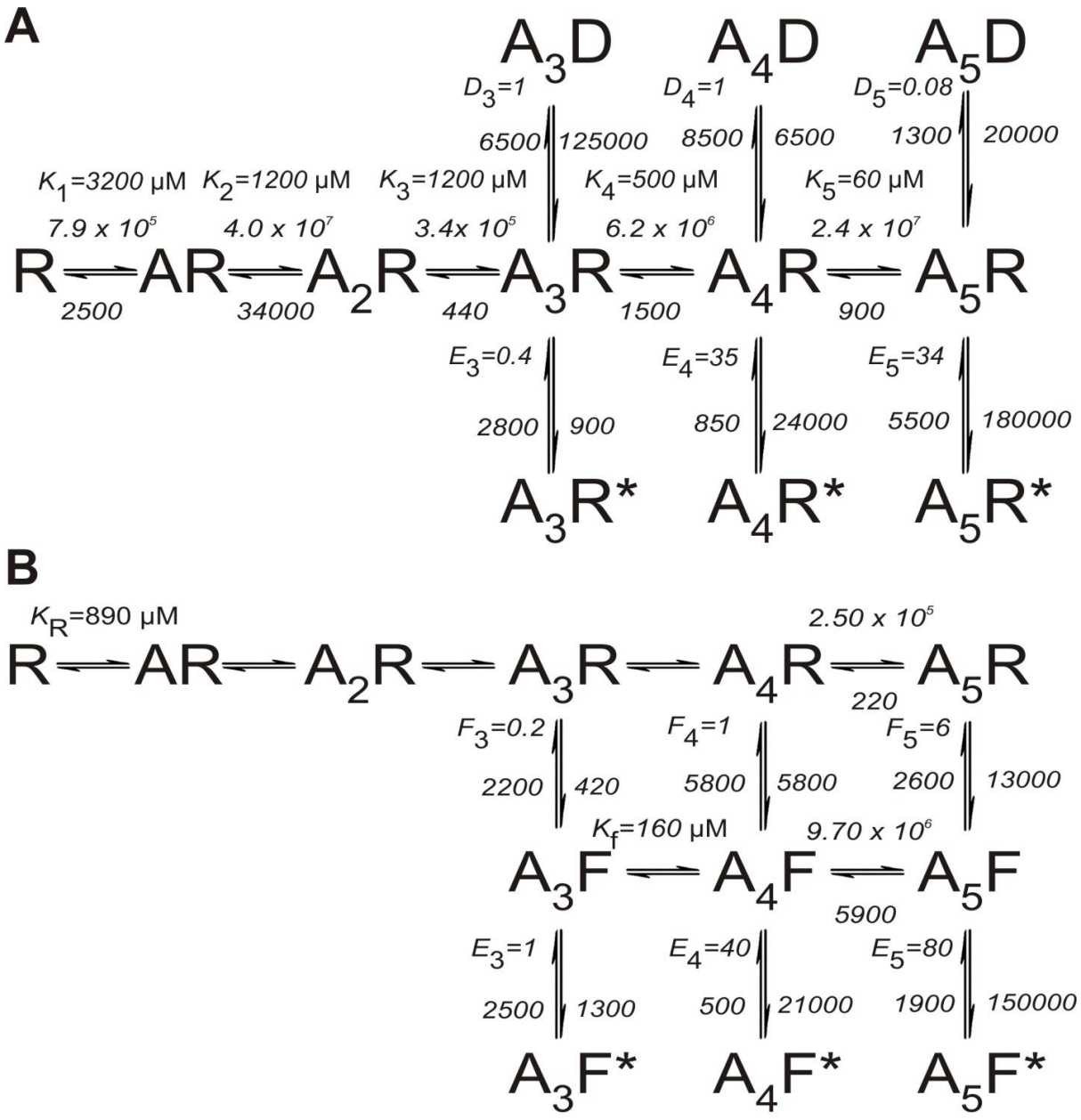

Figure 3.6 Average rate constants for Schemes 2 and 4
The best fitting variants of Jones and Westbrook (A, Scheme 2) and Flip (B, Scheme 4) mechanisms are shown with the averaged rate constants (units and constant names as in Tables 3 and 4) and equilibrium constants from three independent data sets.

It is worth noting that, in the mechanism with five binding sites and three open states (Scheme 4), the lowest liganded open state (triliganded) is visited relatively rarely, with a very low occupancy (< 1%) even at the lowest glycine concentration (50 µM). This suggests that data at this agonist concentration may not contain sufficient information to fit explicitly additional open states with fewer than three agonists bound.

3.1.6 Macroscopic currents

In our final set of experiments, we recorded macroscopic currents elicited by the fast application of brief pulses of glycine to outside-out patches (holding potential -100 mv). The first aim of these recordings was to obtain an estimate of the time course of α3 channel deactivation and therefore an indication of the likely time course of a α3 native synaptic current. This information is not available at present for glycinergic currents mediated by α3 channels. In addition to that, channel behaviour in non-equilibrium conditions is another experimental observation that should be well described by any adequate model of channel activation. Experiments were carried out using a low (20 mM) intracellular chloride concentration, comparable to that likely to be present in the cytoplasm of the cells used in the single channel experiments. This choice was made to ensure that channels were exposed to similar intracellular chloride concentrations in the different patch configurations, and allow us to combine the information from different experiment protocols.

The black trace in Fig 3.7 A is an example of an outside-out current response of α3 homomeric GlyRs to the fast application of a 1- 1.5 ms pulse of 10 mM glycine. These currents were fast, and their time course of decay of these currents between 80-20% of the peak was well fitted with a single exponential with a time constant of 9 ± 0.8 ms (n = 5 patches). The rise time (also fitted between 20 and 80% of peak) was found to be 0.6 ± 0.1 ms (n = 5 patches). Note that the relatively poor expression of this subunit limited the size of the currents we recorded (average peak amplitude 20 ± 10 pA) and consequently the precision with which we could characterize their time course. Using the rate constant values from the fit of each set of single channel data with the different models, we calculated macroscopic currents expected in response to 1.5 ms 10 mM glycine pulses that had a time course similar to that achieved in our experiments (eg 150 μs 20-80% rise and fall). The time course of both rise time and decay of the calculated currents were measured in the same way as for the experimental currents.

The predictions for the decay times are summarized in the graph in Fig 3.7 C, where each symbol represents the time constant predicted from the fit or one of the three independent sets of single channel data and the bars are the average of these three time constant values for each model. The predicted deactivation time course was relatively similar across the schemes that successfully fitted the single channel data and was consistently slower than the decay that we observed experimentally (Figure 3.7 C).

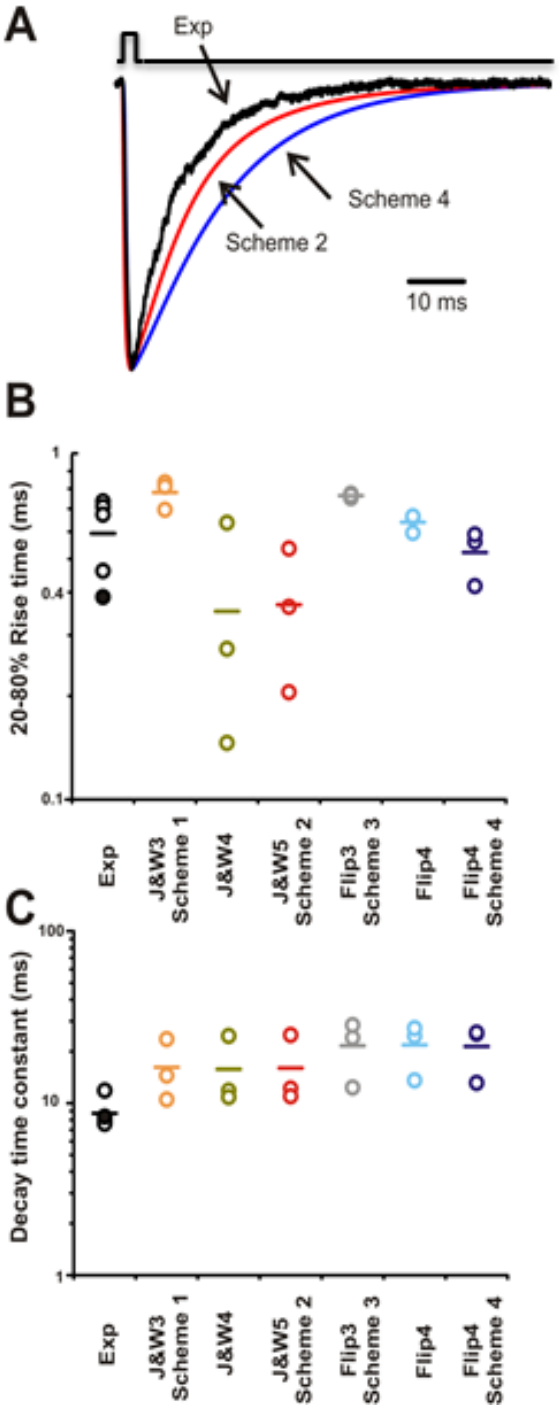

Figure 3.7 Comparison of experimental outside-out currents elicited by concentration pulses with the predictions obtained from the fit to single channel data

A, An experimental current trace recorded in response to a 1.5 ms pulse of 10 mM glycine (Exp) is superimposed on the responses calculated from the results of the fits of Scheme 2 and Scheme 4. The predicted traces are the averages of the responses calculated from each of the three sets of fitted rate constants. Calculated responses were normalized to the peak before averaging. The upper trace shows the solution exchange. B and C, Dot plots summarizing the 20- 80% rise times and the decay time constant for responses calculated from the fitted mechanisms and experimental jumps. The values for each fitted dataset are shown, and the mean is indicated as a bar. Black symbols indicate experimental jumps and the filled circle is the experiment plotted in A.

The two best schemes, *e.g*. the five-binding sites variants of the Jones and Westbrook and the flip mechanisms, predicted decay time constants of 16 ± 4 ms and 21 ± 4 ms, respectively. The picture was somewhat different for the rise-time of the current response (Figure 3.7 B).

The predictions of the five-binding sites variant of the flip scheme (0.5 ± 0.05 ms) were fairly consistent across the fitted sets and matched well our experimental observations (0.6 ms). On the other hand, the predictions of the Jones and Westbrook schemes varied considerably from one fitted set to the other, with an average for the five-site variant of 0.4 ± 0.1 ms. Note that there are unavoidable experimental differences between the cell-attached single channel recordings and the outside-out macroscopic jumps. In particular, the calculations from the fitted mechanism cannot include shifts in the chloride driving force that can take place as a result of the current itself. Such shifts ought to be relatively small, given that the responses we recorded here are small and short, but are expected to speed up the apparent deactivation (Moroni *et al*., 2011, Karlsson *et al*., 2011). It is important to mention that other factors, such as phosphorylation (Gentent and Clements, 2001) and scaffolding proteins (Christie *et al*., 2002) could affect the decay time constant.

In summary, the combination of results from single channel and macroscopic current, suggest that we need more than 3 binding sites, and both J&W and FLIP are good candidate for the kinetic model of α3 Glycine receptor. The two models describe well the single channels open period and shut time distributions, estimate well the P_{open} curve and the macroscopic current.

3.2 ELIC receptor

ELIC is a bacterial ligand-gated ion channel homologous to eukaryotic pLGIC. This channel is found in the enterobacterium *Erwinia chrysanthemi*, an important cause of soft rot in food and ornamental crops, but it is not clear whether ELIC plays a role in the pathogenicity of this prokaryote. ELIC is one of the pLGIC that have been crystallized in their entirety and as such is an important source of structural information: high resolution crystal structures have been obtained for ELIC in an apo state (Hilf and Dutzler, 2008), or with ligands bound in the canonical agonist site, including the agonist GABA (Spurny *et al*., 2012) and the competitive antagonist acetylcholine (Pan *et al*., 2012). Structures have also been solved also for ELIC bound to ligands that are known to modulate the activity of pLGIC, such as benzodiazepines and chloroform (Spurny *et al*., 2013; Spurny *et al*., 2012; Sieghart, 1995; Ernst *et al*., 2003), and divalent ions (Zimmermann *et al*., 2012). The consensus is that these structures all show the pore of ELIC in a nonconducting state (Hilf and Dutzler, 2009; Hilf and Dutzler, 2008; Song and Corry, 2010), but it remains unclear whether they represent resting or desensitised states (Gonzalez-Gutierrez *et al*., 2012).

Most of the published functional data from ELIC or from the other structural model channels GLIC and GluCl are macroscopic characterisations, and no kinetic model is available for any of these channels. ELIC appears to be the best candidate for a single channel kinetic analysis because it is reported to have high single channel conductance (84-96 pS) and show only occasional subconductance transitions (Zimmermann and Dutzler, 2011), suggesting ideal signal-to-noise ratio for this technique. In contrast to that, the conductance of GLIC is low, only 8 pS in wild type (Bocquet *et al*., 2007), and to our knowledge there are no measurements of conductance for the form of GluCl whose crystal structure has been solved.

In addition to that, ELIC is the only one of these three channels that resembles vertebrate Cys-loop channels in being activated by the binding of a small molecule agonist to the canonical agonist binding site in the extracellular domain (Zimmermann and Dutzler, 2011). Other structural model channels are different: GluCl is unusual, in that the form whose structure was solved (the α homomer) opens only if bound both to an orthosteric agonist, glutamate, and to ivermectin, an allosteric modulator that binds in the transmembrane domain. On the other hand, GLIC is not activated by a ligand, but by low pH, and therefore by the protonation of amino acid side chains. The number and location of the residues that have to be protonated to elicit activation in GLIC is not known, but at least one is in the transmembrane domain, well away from the canonical agonist binding site of the superfamily

(Wang *et al*., 2012). This would suggest that ELIC should offer the best model for a study aimed at understanding agonist efficacy in the context of channel structure.

3.2.1 Aims of the work

The ultimate aim of channel kinetics is to identify and measure each step in the activation of a channel and map these steps to specific changes in the structure of the protein. Progress towards this goal requires combining the information that comes from detailed mechanistic modelling (from functional data such as single channel recordings and fast agonist or voltage relaxations) together with information about the channel structure and the conformational states it can access.

In the nicotinic superfamily, decades of recording single channel data and of refining their analysis techniques have produced detailed reaction schemes that describe the activation of several of the major synaptic channels. For muscle nicotinic receptors and glycine receptors, we know that two or three molecules of transmitter must bind to open the channel with maximum efficacy and in those circumstances open probability is very high, above 95%. Synaptic channels open very quickly when the neurotransmitter binds, but the refinement in model fitting techniques has allowed us to detect one or more intermediate states between agonist binding and channel opening. In these states the channel is still closed, but its affinity for the agonist has already increased from its resting value (Burzomato *et al*., 2004; Jadey and Auerbach, 2012). Some of the evidence from the systematic analysis of muscle nicotinic receptor mutants suggests that the perturbation introduced by agonist binding spreads in several discrete steps from the extracellular domain to the channel gate (Grosman *et al*., 2000b; Purohit *et al*., 2007).

Making structural sense of these findings is not straightforward, and we still do not know the exact nature and sequence of the channel conformational changes upon activation or the structural correlates of the intermediate states detected by single channel analysis, despite the clues provided by linear free energy analysis of mutations in the nicotinic receptor and the first solution of both shut and open structures for the same channel, recently obtained for GLIC (Sauguet *et al*., 2014).

One of the problems may be that some of the best structural data come from channels for which we have no single channel kinetics, such as the prokaryotic channels GLIC and ELIC

(Hilf and Dutzler, 2009; Bocquet *et al*.; 2009; Hilf and Dutzler, 2008) and the nematode channel GluCl (Hibbs and Gouaux, 2011). Obtaining a detailed understanding of the activation mechanism of one of these channels might help with the task of mapping structure to function. The present work is the first single channel kinetic characterisation of ELIC.

3.2.2 Features of single channel current

All single channel recordings were performed in outside-out configuration. The agonist (0.3-100 mM propylamine) was applied via perfusion. The bath level was kept as low as possible to reduce noise. Currents were recorded at a pipette potential of -60 mV. For off-line analysis, data were filtered digitally (low pass Gaussian filter) using the program Clampfit 10.2 to achieve a final cut-off frequency of 3– 6 kHz.

Recordings were idealized (6000- 24000 transitions per patch) by time-course fitting with the program SCAN. Segments showing seal breakdowns, or dubious channel openings were excluded, and those intervals marked unusable. Afterwards, we imposed a temporal resolution between 25-40 μs depending on the signal-to-noise level obtained during the recording. The temporal resolution is the duration of the shortest events that can be reliably detected, and its value is taken into account in implementing the exact solution for missed events correction by (Hawkes *et al*., 1992; Hawkes *et al*., 1990). Given that we observed a marked rundown in outside-out macroscopic currents, we checked particularly carefully the stability of the single channel activity over time and found that average open/shut periods remained stable for up to 20- 30 minutes. Patches were analysed further only if the amplitudes of channel openings and the open and shut dwell times were stable through the recording.

The idealized open/shut period interval histograms were empirically fitted by exponential probability density functions (EKDIST program). This allowed us to check that distributions were consistent across patches at the same agonist concentration and to proceed to the next stage of the analysis and determine a suitable value for the critical time, t_{crit}. This value is chosen to divide recordings into segments that are likely to arise from the activity of only one channel molecule (bursts or clusters). Briefly, shut times that are longer than the t_{crit} are deemed to be between bursts (or clusters).

In order to evaluate kinetic schemes and obtain the rate constants associated with them, maximum likelihood fitting was performed with the HJCFIT program (Colquhoun *et al*., 2003; Colquhoun *et al*., 1996). Idealised single channel records were grouped into 3 sets. Each set consisted of 4 patches at different propylamine concentrations (0.5, 1, 5 and 10 mM) and the four patches in the set were fitted simultaneously. Openings in each idealised record were divided into groups using a t_{crit} value for shut times, and only shut times shorter than t_{crit} were used for fitting. The longer shut times cannot provide information about the rate constants in the mechanism because they are distorted by the number of channels in the patch. For lower concentrations of agonist (0.5mM to 5mM), where groups of openings can be treated as 'bursts', some of that information was recovered by using CHS vectors, and exploiting the fact that having more than one channel in the patch can only shorten the apparent shut time. Thus, the "real" shut time (between two openings of the same channel molecule) has got to be at least as long as the observed shut time (Colquhoun *et al*., 1996).

The maximum likelihood fits were performed using the HJCFIT program. This optimises a likelihood function for the data sets of idealized sequences of events, given the postulated model and the initial guesses for the rate constant values, and taking into account the imposed resolution. Fits were repeated using several different sets of initial guesses to check the consistency of the maximum value of the likelihood. In order to test the quality of the fits, we calculated the dwell-time distributions, open/shut correlation plots and macroscopic current time course expected from the fitted mechanism and compared them with the experimental observations.

The rate constant values from the fit of each set of single channel data were used to calculate the relations between the agonist concentration and mean burst length (DC-PyPs program: https://code.google.com/p/dc-pyps/). The results were averaged and displayed in Figure 3.18A. We also used the results of the fits to simulate realizations of single-channel activity (SCSIM program) shown in Figure 3.18

All data are expressed as mean ± S.D. of the mean. For the values of the estimated rate constants, we report the mean of estimates obtained from different sets and the coefficient of variation (CV) of the mean. The SCAN, EKDIST and HJCFIT programs can be downloaded from Onemol (http://www.onemol.org.uk).

3.2.3 Results

3.2.3.1 Whole-cell concentration-response curve

The traces in Figure 3.8A are whole-cell currents elicited by the U-tube application of the agonist propylamine to ELIC channels expressed in a HEK293 cell (holding voltage -30 mV). ELIC current responses activated relatively slowly and decayed quickly upon agonist removal.

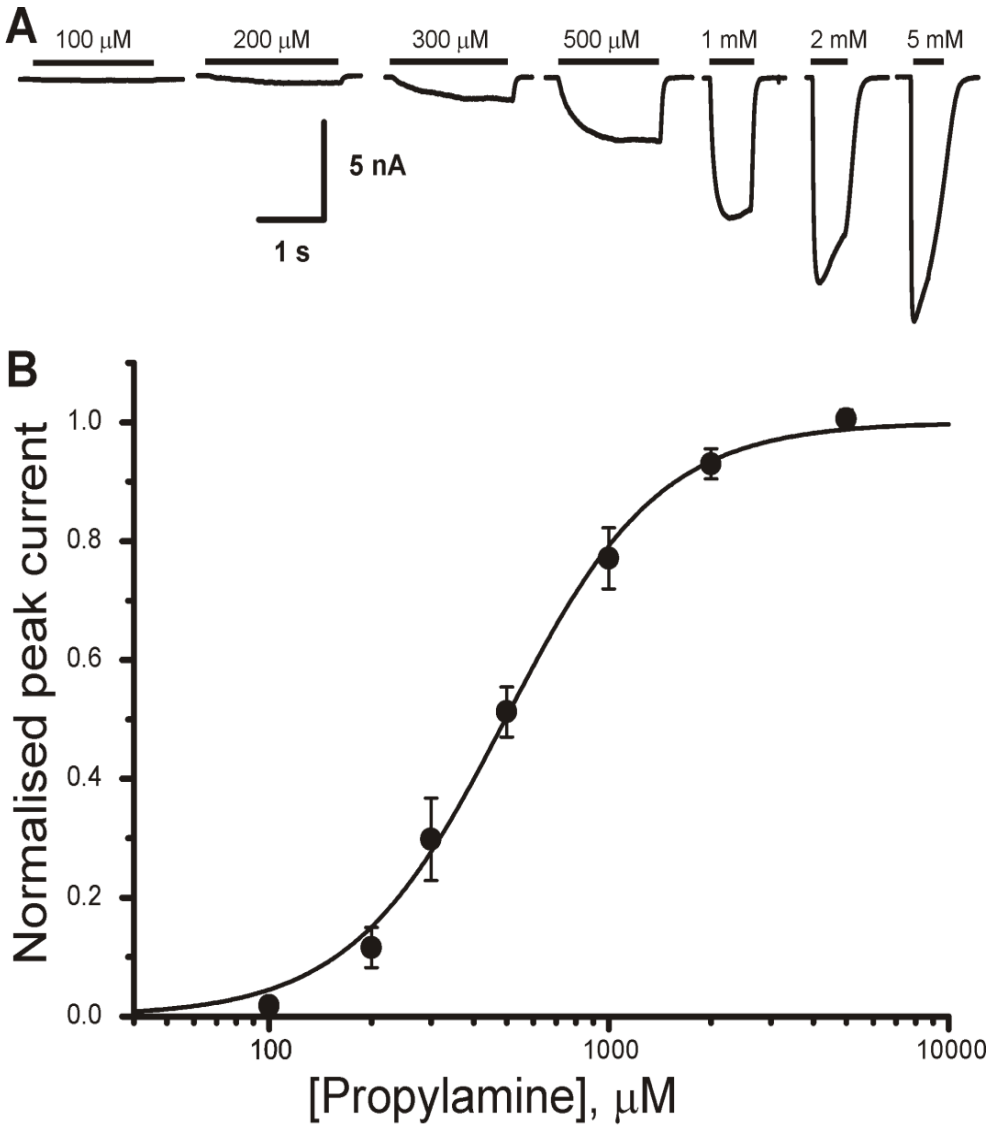

Figure 3.8 The whole cell concentration-response curve for the ELIC agonist propylamine
A) Representative macroscopic whole cell currents elicited by U-tube application (horizontal bars above the traces) of propylamine to ELIC-expressing HEK293 cells held at –30 mV. B) Average concentration-response curve for propylamine (n = 4 cells). Individual dose-response curves were obtained in each cell, measuring responses at their peak and normalising them to the fitted maximum. Normalised curves were averaged and fitted withthe Hill equation (EC_{50} = 500 ± 100 μM; n_H = 2.2 ± 0.1; maximum current = 9 ± 2 nA).

At propylamine concentrations higher than 0.5 mM, currents clearly decreased after an initial peak, and this suggested that ELIC desensitises with sustained agonist application. The graph in Fig 3.8B is the concentration-response plot for propylamine, fitted with the Hill equation (n = 4). The average EC_{50} was 500 ± 100 μM and the Hill slope = 2.2 ± 0.1. The maximum current (9 ± 2 nA) was reached at 5 mM propylamine. These values are very similar to those reported for ELIC receptors expressed in oocytes (EC_{50} = 446 μM and Hill slope = 3.0; (Zimmermann and Dutzler, 2011).

3.2.3.2 Outside-out macroscopic currents

We recorded also macroscopic currents elicited by fast, theta-tube application of propylamine onto outside-out patches, in order to obtain a better characterization of the macroscopic time course of ELIC activation, desensitization and deactivation. It was not possible to obtain a full dose-response curve from this set of experiments, because relatively few agonist responses could be recorded from each patch. These outside-out recordings typically lasted about 5- 10 minutes and we often observed marked rundown in the amplitude of responses. Only about a quarter of patches lasted long enough to provide 10 to 20 agonist responses that were sufficiently stable in amplitude (< 30 % change) to be analysed and only five patches were stable enough for us to apply two different agonist concentrations.

The traces in Figure 3.9A are typical current responses to long applications of propylamine (1, 10 and 50 mM; around 500 ms; holding voltage -100 mV). The appearance of these responses at different agonist concentrations is very similar to that of whole cell responses. The lowest agonist concentration at which outside-out responses could be obtained was 1 mM, where currents were quite small (90 ± 50 pA; n = 4).

In Figure 3.9B, the same responses are scaled to their peak, in order to show how their onset accelerated as the agonist concentration was increased. Current rise times were well fitted by a single exponential component, with time constants of 280 ± 30 ms at 1 mM (n = 3), 19 ± 3 ms at 10 mM (n = 6) and 7 ± 1 ms at 50 mM propylamine (n = 7; see the plot in Figure 3.9C; closed circles).

Just as in the whole-cell experiments, responses desensitised in the continuous presence of propylamine concentrations equal to or greater than 10 mM, and a clear sag of the current after the peak was observed in about half of the patches. At higher agonist concentrations

this decay was somewhat faster (700 ± 300 ms and 380 ± 40 ms, *n*= 6 and 7, at 10 and 50 mM, respectively) and the extent of the apparent desensitisation greater (residual current at 500 ms of 63±7% and 34±3% of peak, at 10 and 50 mM propylamine, respectively).

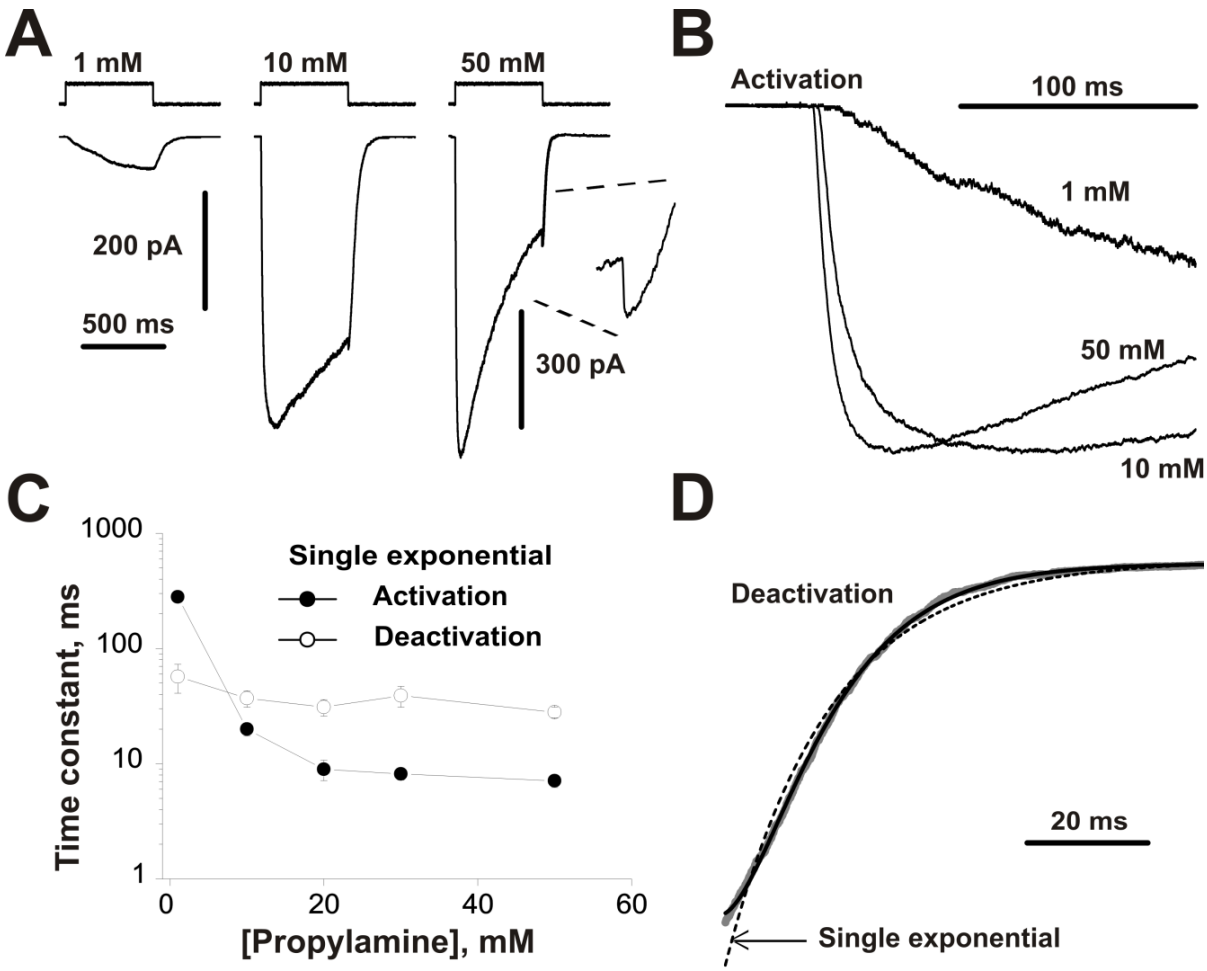

Figure 3.9 Macroscopic ELIC currents evoked by fast propylamine applications to outside-out patches

A) ELIC current traces recorded in response to 500 ms steps of propylamine (the 1 and 10 mM traces are from the same patch). The enlarged inset shows the rebound current seen after the end of the propylamine pulse for concentrations greater than 1 mM. Top traces show the solution exchange measured at the open tip at the end of each experiment. B) The responses from panel A are scaled to their peak, to show that the activation gets faster at higher agonist concentrations. C) Plot of the time constants for activation and deactivation of agonist currents as a function of propylamine concentration (from fits of a single exponential, see text, n =3-7). D) This example of the deactivation phase of a response to 50 mM propylamine (grey trace) shows that the sigmoidal time course of current decay requires two exponential components for a satisfactory fit (solid black line). A single exponential fit is shown for comparison.

The response deactivation that followed the end of the application was complex, irrespective of agonist concentration. Figure 3.9A and its inset show that at the end of the 10 and 50 mM agonist applications there was a rapid surge of current. The amplitude of this rebound current (relative to the agonist current at the end of the step) increased with agonist concentration, and was 4.5 ± 0.3% (n = 5 out of 6 patches) and 13 ± 1% (n = 6 out of 7 patches) after 10 mM and 50 mM propylamine, respectively. This rebound resembles the muscle nicotinic 'off'-current, which is known to arise from the relief of low-affinity open channel block produced by positively charged agonists binding in the channel (Maconochie and Steinbach, 1995; Lape *et al*., 2009; Legendre *et al*., 2000).

After the rebound peak, the ELIC current decreased with a sigmoidal time course (thick gray trace in Figure 3.9D), and two exponential components of opposite amplitudes were required for a good fit (Fig 3.9D, black solid line) at all agonist concentrations (including 1 mM, where the rebound current was absent). Nevertheless, we fitted the deactivation phase of the averaged currents from 90% of the current at the end of the pulse to baseline with a single exponential (black dashed curve) in order to obtain a crude overall description of experimental deactivation and be able to compare it with the deactivation calculated from the mechanisms estimated from single channel data (see below). The deactivation time constant (open circles, Figure 3.9C) did not change much with agonist concentration, but was somewhat slower after 1 mM than after 10 mM propylamine (60 ± 20 ms *vs* 30 ± 6 ms; $n = 3$ and 6, respectively; two-tail unpaired Student's *t*-test $P = 0.002$)

3.2.3.3 The single-channel activity of ELIC

General observations. The lowest propylamine concentration that elicited ELIC channel activity in the outside-out patch configuration was 0.3 mM. At this concentration, openings could be detected in approximately one third of the patches.

Example traces of ELIC single-channel currents recorded in the presence of 0.5, 5 and 50 mM propylamine are shown in Figure 3.10A. As reported by (Zimmermann and Dutzler, 2011), ELIC does open to more than one conductance level. Conductance varied both within groups of openings, and across different groups of openings, but differences in conductances did not occur in a clear-cut pattern. There was no obvious pattern to the occurrence of subconductances, and in particular no relation to agonist concentration. Because of that, in the kinetic analysis we treated all conductance levels as open. In each patch that showed more

than one conductance, levels were close to each other, making it hard to measure them unambiguously (by fitting gaussians to the amplitude distribution). It was not possible to be sure that the different levels represented distinct conductance states that occurred consistently in each recording. The mean open amplitude was 8.8 ± 0.40 pA in the 9 patches at 0.3-1 mM propylamine (range 7.0 to 11.3 pA).

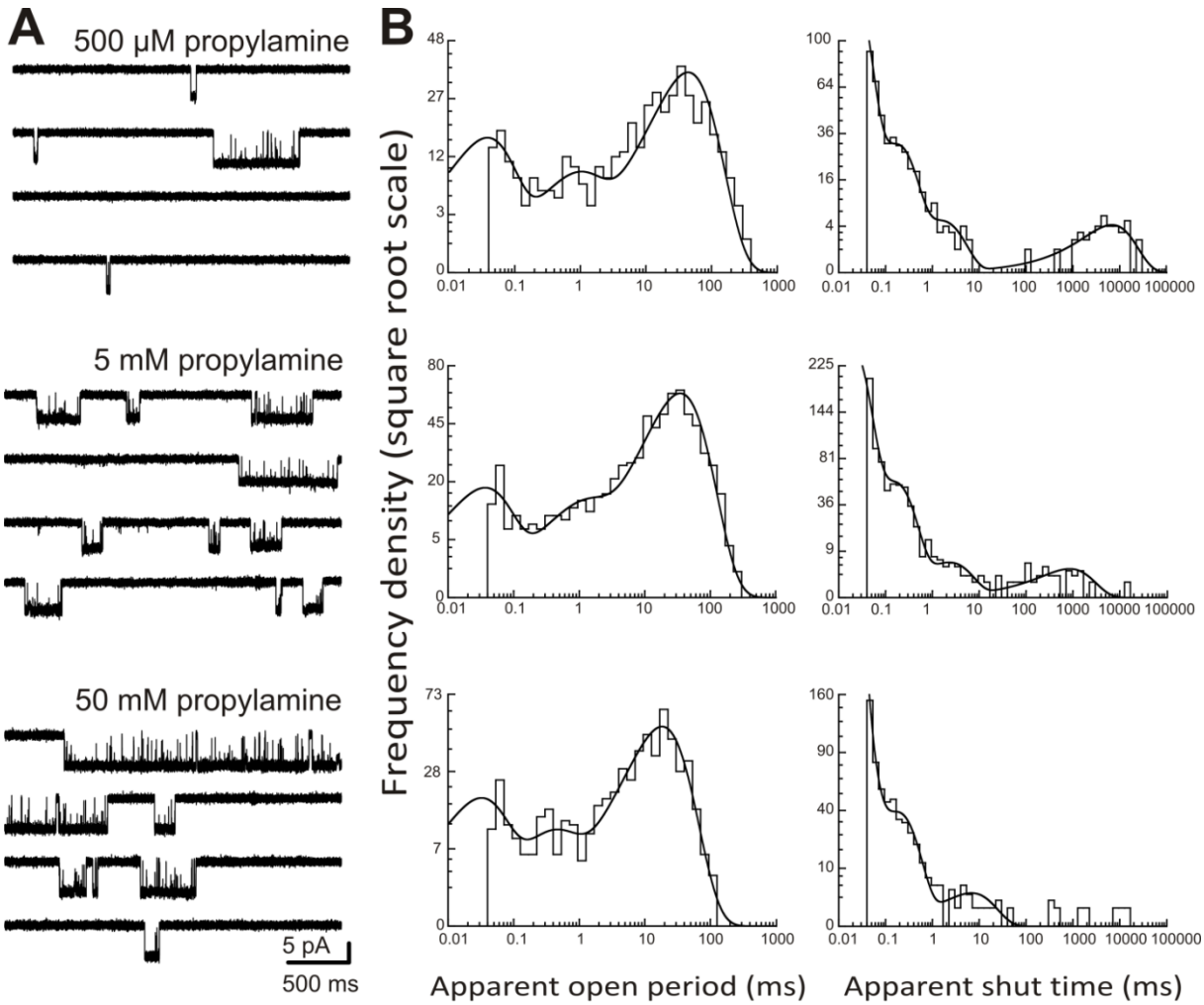

Figure 3.10 ELIC single activity evoked by propylamine.
A) Single channel currents in the presence of 0.5, 5 and 50 mM propylamine is shown as continuous recordings from outside-out patches held at -60 mV (filtered at 3 kHz low-pass filter for display). B) Dwell-time distributions for the patches shown in panel A, fitted with a mixture of exponential probability density functions (apparent open periods in the left column, apparent shut times in the right column).

Thus, in our conditions (symmetrical K^+, 0.5 mM Ba^{2+}) the chord conductance of the ELIC pore was 147 pS, much higher than the values previously reported, which were measured using sodium as the permeant ion (84-96 pS, (Zimmermann and Dutzler, 2011)).

The off-currents observed in our macroscopic agonist responses suggest that propylamine can block the channel with low affinity. This sort of block produces shuttings that are too short to be detectable as such, but should reduce the apparent amplitude of the channel openings. If present, this effect was too small to be unambiguously detected, given the observed variability in current amplitude: the average amplitude of the openings was 9.0 ± 0.75 pA and 8.2 ± 0.43 pA at 0.5 mM and 50 mM propylamine, respectively (n = 3 patches each, cf. the 13% increase in current with unblock at the end of 50 mM agonist pulses).

At first glance, ELIC resembles other ligand-gated ion channels, in that it activates in groups of openings. At 0.5 mM propylamine, the mean length of these groups of openings is 290 ± 60 ms (110 groups from 3 patches; critical time interval, t_{crit} 10 ms). As the concentration increases, these groups become, on average, longer (eg at 5 mM propylamine, mean group length is 900 ± 300 ms; 56 bursts from 3 patches; t_{crit} 10 ms), but medium-short groups did not entirely disappear (see the example in the bottom sweep, at 50 mM). Most other channels in the nicotinic family, except for α2 homomeric glycine receptors and 5-HT3A channels (Krashia *et al*., 2011; Corradi *et al*., 2009) respond to increases in agonist concentration with much more marked changes in burst behaviour.

Figure 3.10B shows also the dwell time distributions for apparent open (left column) and shut times (right), fitted with a mixture of exponential probability density functions. It is of note that adequate fit of open period distributions required three exponential components at all concentrations (see Table 3.5). It is very unusual for a channel in the nicotinic superfamily to have more than one open state at saturating agonist concentrations. The values of the time constants and areas of all three open period components remained relatively stable in the range of propylamine concentrations tested (0.5 to 50 mM), except for a decline in the average duration of the longer components at 50 mM. For instance, the longest component decreased from 33 ± 2 ms at 10 mM to 15 ± 2 ms at 50 mM. Except at the highest agonist concentration, the shut time distributions were best fitted with four exponential components (Table 3.5). The time constant of the slowest (fourth) component of the shut time distribution became shorter as the agonist concentration increased, and could no longer be unambiguously detected in all patches at 50 mM propylamine.

Table 3.5 Time constants and areas of the components of open and shut time distributions at different propylamine concentrations

Apparent open periods				
Propylamine (mM) [*n*]	**τ_1 (ms) [area (%)]**	**τ_2 (ms) [area (%)]**	**τ_3 (ms) [area (%)]**	**Mean open time (ms)**
0.5 [3]	0.043 ± 0.008 [26 ± 2]	1.5 ± 0.4 [12 ± 0.5]	34 ± 6 [62 ± 3]	25 ± 5
1 [3]	0.07 ± 0.02 [20 ± 5]	5 ± 4 [13 ± 2]	39 ± 9 [68 ± 3]	30 ± 7
5 [3]	0.05± 0.02 [16 ± 2]	2 ± 1 [9 ± 1]	39 ± 5 [75 ± 3]	33 ± 5
10 [3]	0.04 ± 0.02 [20 ± 2]	2 ± 2 [12 ± 1]	33 ± 2 [68 ± 1]	27 ± 2
50 [3]	0.08 ± 0.03 [14 ± 5]	0.9 ± 0.3 [5 ± 3]	15 ± 2 [80 ± 9]	13 ± 2

Apparent shut times				
Propylamine (mM) [*n*]	**τ_1 (ms) [area (%)]**	**τ_2 (ms) [area (%)]**	**τ_3 (ms) [area (%)]**	**τ_4 (ms) [area (%)]**
0.5 [3]	0.010 ± 0.004 [92 ± 6]	0.11 ± 0.03 [6 ± 5]	1.1 ± 0.3 [5 ± 1]	4000 ± 2000 [1 ± 1]
1 [3]	0.011 ± 0.003 [89 ± 9]	0.14± 0.03 [7 ± 6]	1.3 ± 0.3 [2 ± 2]	1300 ± 300 [2 ± 2]
5 [3]	0.014 ± 0.004 [80 ± 12]	0.14 ± 0.02 [18 ± 10]	2.2 ± 0.2 [2 ± 1]	1100 ± 400 [0.8 ± 0.4]
10 [3]	0.012 ± 0.002 [80 ± 8]	0.14 ± 0.02 [18 ± 7]	1.3 ± 0.4 [1.8 ± 0.4]	56 ± 4 [0.5 ± 0.3]
50 [3]	0.06 ± 0.04 [91 ± 2]	0.15 ± 0.02 [8 ± 2]	3 ± 2 [1.1 ± 0.5]	

Distributions were fitted with mixtures of exponential probability density functions. n, the number of patches for each concentration(indicated in parentheses in the first column). The time constant of each component and its relative area (in parentheses) are given as mean ± SD of the mean.

Open probability. At concentrations greater than 5 mM, an additional component of very long shut intervals appeared (Fig 3.10A and B). These intervals were too few to be fitted by an exponential component, but they were clearly distinct from the next slowest shut time component (which is concentration dependent) and were longer, ranging from 100 ms to about 10 s. By analogy with observations in other channels (Sakmann *et al*., 1980), they are likely to be sojourns in long-lived desensitized states (cf. the macroscopic desensitisation time constant of 0.38 ± 0.04 s at 50 mM).

The presence of these intervals can often be exploited in single channel analysis to establish the concentration dependence of the open probability of a ligand-gated ion channel, because they divide the record into clusters of openings. If the open probability of these clusters is sufficiently high, clusters that show no double or multiple openings can be safely attributed to the activity of a single channel molecule (Colquhoun and Hawkes, 1990). We attempted to carry out this process in ELIC records, and identified stretches of openings that were terminated by long shut intervals and were without double openings. Typically, we had very few of these long shut intervals in each patch and very few possible clusters (3 to 11). The choice of what to classify as an intercluster shut time was largely arbitrary, because we could not use any formal criteria to identify them (i.e. calculate a critical time interval between two exponential components to minimize misclassified shut interval number). We chose an arbitrary critical time interval, t_{crit}, so that the longest well defined exponential component in the shut time distributions was interpreted as arising within the cluster (as suggested by its dependence on concentration). By this criterion, gaps were classified as between clusters if longer than 100 ms at 10 mM, 50 ms at 50 mM and 10 ms at 100 mM). Cluster P_{open} values were calculated for all of these concentrations, and were found to be similar and above 96%. Note that the macroscopic dose-response curve of Fig.3.8 indicates that concentrations equal to or above 5mM should elicit a maximum receptor response. At concentrations lower than 10 mM, we could not identify desensitised gaps, and therefore we were unable to define clusters to construct a P_{open} curve.

3.2.3.4 Fitting activation mechanisms to single channel data

We investigated the activation process of the ELIC receptor by fitting a range of mechanisms directly to the single channel data, using the HJCFIT program. Candidate activation mechanisms were fitted to three independent sets of single channel data. Each set contained four records obtained at different propylamine concentrations (0.5,1,5 and 10 mM) spanning the whole of the dose response curve, to obtain sufficient information on the different steps of the mechanism. Each single channel record was appropriately divided into bursts or clusters (Colquhoun *et al*., 2003).

The adequacy of the models fitted was judged by comparing their predictions with the experimental observations. The rate constant values estimated in the fits were used to calculate the expected appearance of several types of single channel data displays (i.e. apparent open and shut time distributions and open and shut time correlations) and the time course of macroscopic current responses to fast concentration jumps.

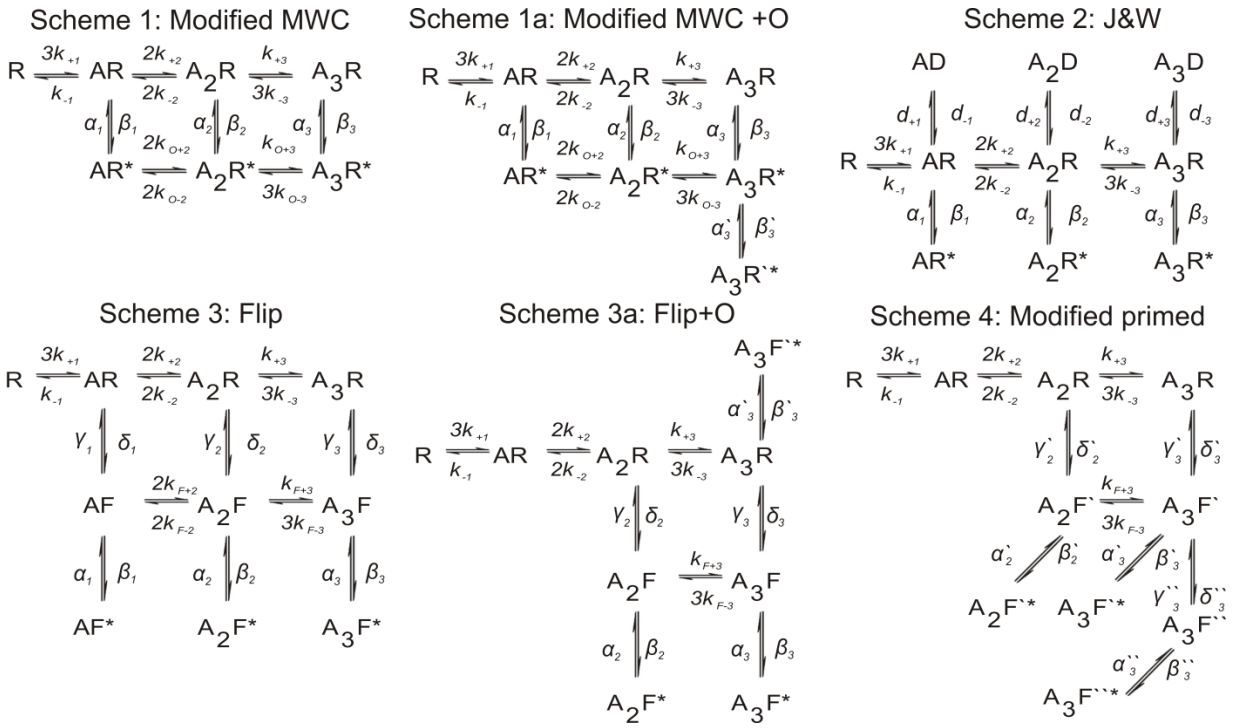

Figure 3.11 The main activation mechanisms tested by global fitting to ELIC single channel data

Schemes 1-4 show the Monod, Wyman and Changeux mechanism (MWC), the Jones and Westbrook mechanism (J&W), the Flip mechanism and a variant of the Primed mechanism as fitted, with the names of the rate constants for reference (see Tables). Schemes were modified to include three binding sites and exclude unliganded openings. Schemes 1a and 3a are variants of the MWC and Flip mechanisms, modified to make an additional open state accessible to the fully liganded receptor. For the MWC mechanism, we tested also a variant where the additional open state was entered from the resting fully liganded state (not shown). The letter A denotes an agonist molecule and its subscript indicates the number of agonist molecules bound to the receptor. The letters R and R* denote resting shut states and open states of the receptor, respectively. The letter F and F` indicates intermediate flipped and primed shut states that connect resting and open states. The letter D indicates distal desensitized states.

We tested several kinetic mechanisms belonging to four major classes of models (Figure 3.11) that have been successfully employed to investigate the activity of channels in the nicotinic superfamily, namely, "modified Monod-Wyman-Changeux" (modified MWC; Scheme 1), "Jones and Westbrook" (J&W; Scheme 2), "flip" (Scheme 3) and "modified primed" (Scheme 4). Note that the open probability of unliganded wild-type ELIC is too low for us to obtain information on unliganded openings, and therefore unliganded open states are neither shown in the mechanisms in Figure 3.11 nor fitted.

*Scheme 1: "Modified Monod-Wyman-Changeux" model (Fig 3.11A).*The modified MWC is an adaptation of the model proposed by Monod, Wyman and Changeux in 1965 for the

binding of oxygen to haemoglobin (Monod *et al*., 1965). The MWC mechanism has been widely used to describe the activation of many ion channels. In particular, it has been employed to calculate energy paths in another member of the Cys-loop family, the muscle nicotinic acetylcholine receptor (Auerbach, 2012). The MWC mechanism postulates that the channel can reversibly adopt two global conformational states, open or closed, and that these two conformations have different affinities for the ligand. This implies that the agonist binding sites are independent, and that the binding affinity depends on the state of the receptor (eg open or closed), but not on the level of ligation. When fitting a mechanism to data, this means imposing the constraint that the microscopic binding rate constants should be the same at each level of ligation, $k_{+1} = k_{+2} = k_{+3} = k_{+}$, $k_{-1} = k_{-2} = k_{-3} = k_{-}$. In the MWC variant used here, three molecules of agonist can bind, there are three cycles and eight free parameters (plus three rate constants calculated from microscopic reversibility).

Examples of open and shut dwell time distributions and correlation plots for one of the fitted sets are shown in Figure 3.12. Top and middle rows are the predictions from the fit (solid smooth line) superimposed on the open and shut time experimental histograms. Even a cursory inspection of the apparent open and shut time distributions is sufficient to see that the predictions of this scheme were very poor at all concentrations.

Of course it is not surprising that a scheme such as modified MWC, with a single fully liganded open state, should fail to describe an open time distribution that has more than one open component at high agonist concentration. The simplest explanation of this behaviour is that the fully bound channel can open to more than one open state. In an effort to improve fits, we tried variants of the MWC mechanism with extra open states connected either to A3R* (eg Scheme 1a in Figure 3.11; fit results summarized in Table 3.6) or to A3R (not shown). These variants were better at predicting open, but not shut times distributions (data not shown). In order to improve the prediction of shut times, we ran also fits of the two variants of MWC without the constraint of microscopic reversibility, but this did not produce any improvement (data not shown). Thus, we proceeded to test mechanisms with more shut states, from different mechanism classes (Figure 3.11).

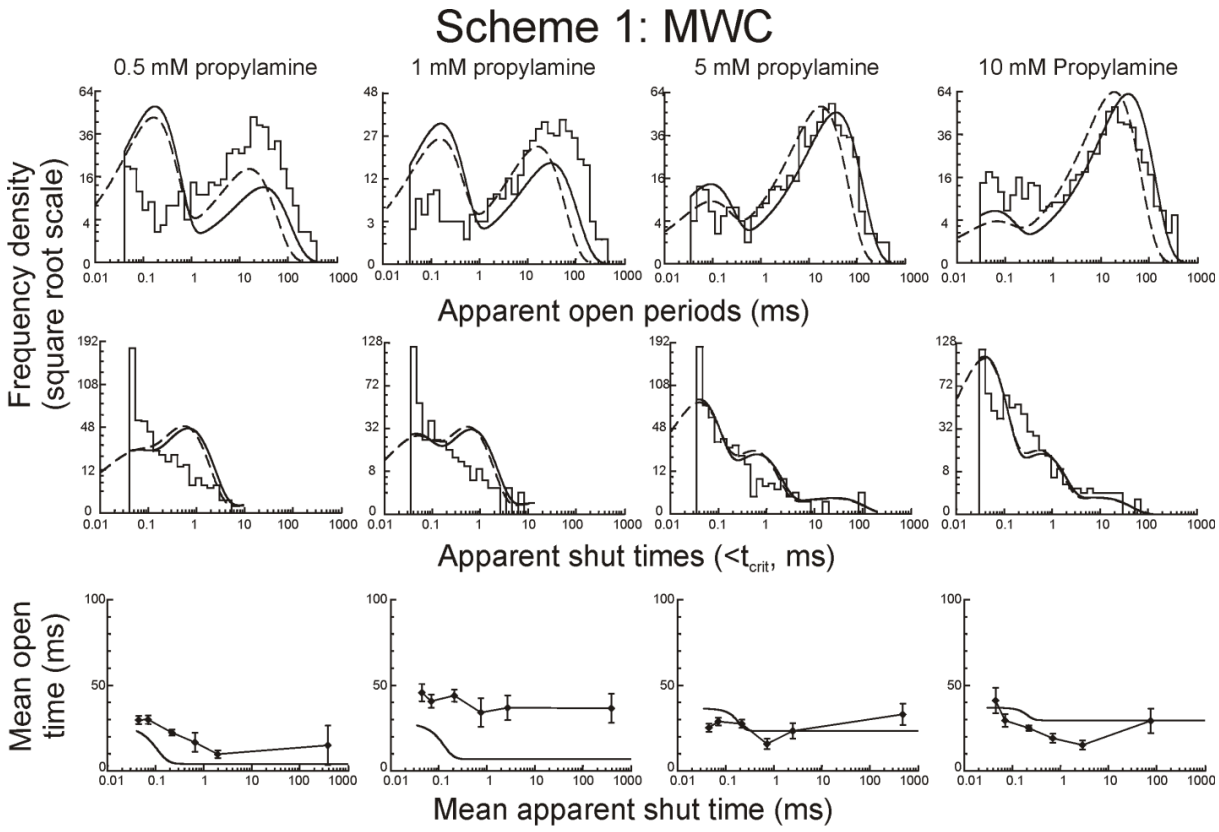

Figure 3.12 Testing the adequacy of the MWC mechanism fitted to ELIC single channel data
Scheme 1 was fitted directly to a dataset of four idealised single channel records obtained at 0.5,1, 5 and 10 mM propylamine. The results of the fit were used to calculate the probability density functions predicted by the Scheme. These are shown as solid lines in the top two rows of plots (the dashed lines are the distributions expected if there were no missed events), for apparent open periods (top) and apparent shut times (middle row). Superimposing these predicted dwell time distributions on the experimental histograms for the same records shows that the best fit of MWC does not adequately describe ELIC single channel kinetics. The bottom row plots compare the experimental open-shut time correlations in the records of this set (circles and error bars and connecting lines) and the MWC scheme predictions of these correlations, calculated from the fitted rate constants (solid lines).

Table 3.6 Rate and equilibrium constant values obtained from the global fits of MWC and MWC+Open models to single channel data sets

	Unit	MWC (Scheme 1)	MWC + Open(Scheme 1a)
α_3`	s^{-1}		167 ± 9%
β_3`	s^{-1}		6,450 ± 14%
α_1	s^{-1}	60 ± 63%	86,300 ± 100%
β_1	s^{-1}	0.147 ± 71%	7 ± 100%
α_2	s^{-1}	3,150 ± 27%	101,200 ± 49%
β_2	s^{-1}	2,730 ± 10%	5,480 ± 68%
α_3	s^{-1}	46 ± 7%	2,100 ± 16%
β_3	s^{-1}	31,400 ± 5%	15,300 ± 32%
k_+	$M^{-1} s^{-1}$	2.54×10^4 ± 10%	2.15×10^4 ± 67%
k_-	s^{-1}	163 ± 7%	58 ± 63%
k_{o+}	$M^{-1} s^{-1}$	1.40×10^6 ± 24%	9.97×10^7 ± 96%
k_{o-}	s^{-1}	13.3 ± 41%	93 ± 51%
$E_1 = \beta_1 / \alpha_1$		0.0016 ± 42%	0.0002 ± 82%
$E_2 = \beta_2 / \alpha_2$		1.0 ± 29%	0.04 ± 69%
$E_3 = \beta_3 / \alpha_3$		700 ± 11%	7.9 ± 35%
E_3` $= \beta_3$` $/ \alpha_3$`			38.6 ± 11%
$K_R = k_- / k_+$	mM	6.4 ± 5%	6.3 ± 11%
$K_o = k_{o-} / k_{o+}$	mM	0.0092 ± 24%	22.9 ± 64%
EC_{50}	mM	0.81 ± 3%	1.14 ± 6%
n_H		2.6 ± 1%	2.5 ± 2%

The fits constrain the binding and unbinding rates to be the same, regardless of the number of molecules bound and conformation. Those constraints were implemented by the following equations: $k_{+1} = k_{+2} = k_{+3} = k_+$; $k_{-1} = k_{-2} = k_{-3} = k_-$ and $k_{o+2} = k_{o+3} = k_{o+}$; $k_{o-2} = k_{o-3} = k_{o-}$. In addition, one rate constant in each cycle was fixed by the constraint of microscopic reversibility (Colquhoun et al., 2004). The equilibrium constants, E and K, and open probability curve EC50 and the Hill slope, nH, were calculated from the rate constants for each set and then averaged. Values are means ± coefficient of variation (i.e. SD of the mean expressed as a percentage of the mean).

Scheme 2: "Jones and Westbrook" mechanism. One such scheme is the Jones-Westbrook mechanism (J&W; Scheme 2 in Figure 3.11; Jones and Westbrook 1995), which postulates that when the receptor is in one of the resting bound states, it can either open or enter a short-lived desensitized state. The J&W scheme was fitted to ELIC data without constraints on the binding rate constants, because in other channels in this superfamily J&W-type schemes fit well only if the agonist binding sites are allowed to interact with each other, and change their affinity with the level of ligation. The number of free parameters was 18.

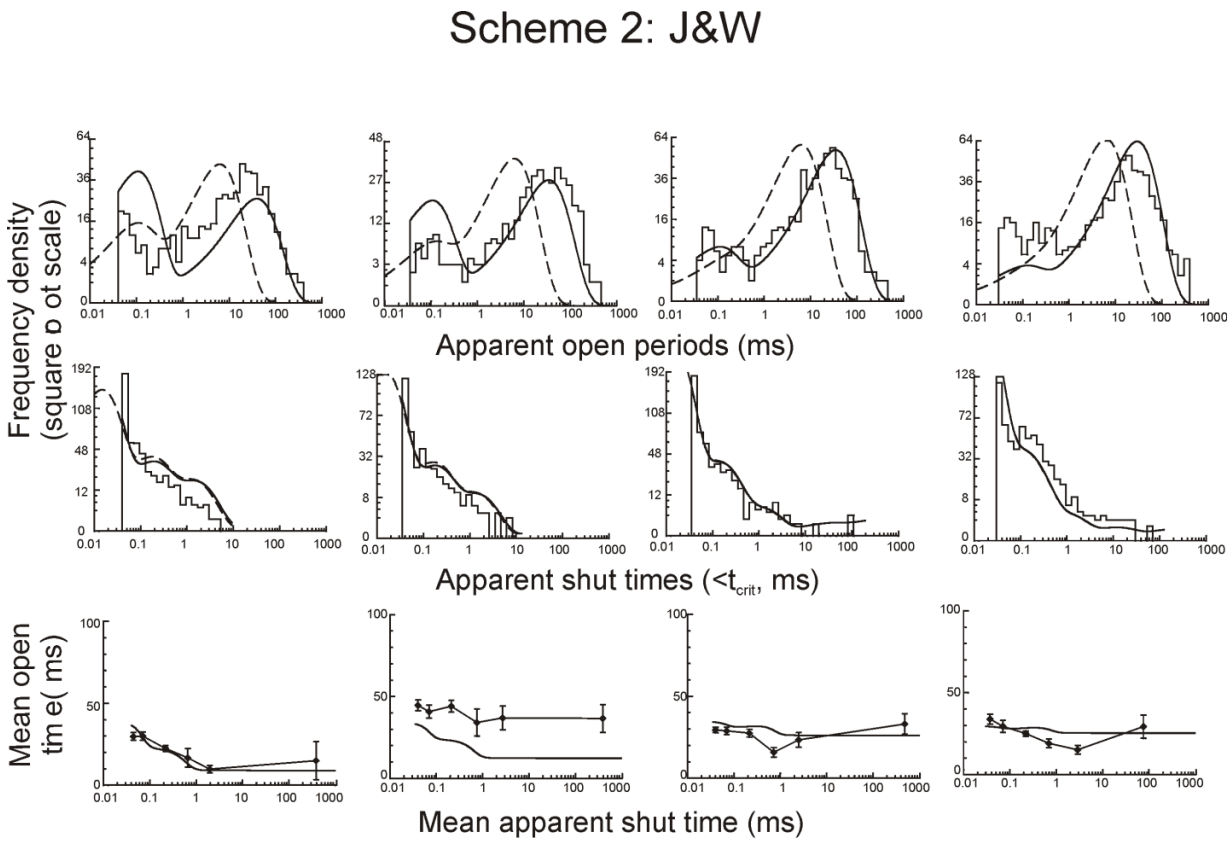

Figure 3.13 Testing the J&W mechanism fitted to ELIC single channel data
The plots compare the experimental results (dwell time distributions and open-shut correlations, see details in the legend of Figure 3.12) with the predictions of the fit of scheme 2, J&W, fitted to the same dataset as in Figure 3.12. The J&W mechanism was no better than MWC at describing open period distributions, but its prediction of the apparent shut time distribution was better.

The prediction of shut time distributions was slightly better with J&W than with MWC, probably because the J&W mechanism has more shut states and more free parameters. As with MWC, this form of J&W has only one fully liganded open state, and its prediction of

open time distributions was very poor (Figure 3.13). This was substantially improved by adding extra open states to the fully liganded branch (eg connected to the A3R* state, data not shown). Even so, the rate constant estimates from J&W were very variable across the three independent data sets analysed (table 3.7).

Table 3.7 Rate and equilibrium constant values obtained from the global fits of the J&W model to three independent single channel data sets

	Unit	J&W
α_1	s^{-1}	86,300 ± 100%
β_1	s^{-1}	16 ± 64%
α_2	s^{-1}	14,900 ± 41%
β_2	s^{-1}	37,400 ± 93%
α_3	s^{-1}	127 ± 13%
β_3	s^{-1}	56,600 ± 6%
d_{-1}	s^{-1}	12,400 ± 100%
d_{+1}	s^{-1}	336,000 ± 99%
d_{-2}	s^{-1}	4,680 ± 75%
d_{+2}	s^{-1}	1,730 ± 19%
d_{-3}	s^{-1}	5,460 ± 18%
d_{+3}	s^{-1}	6,010 ± 20%
k_{-1}	s^{-1}	378,000 ± 83%
k_{+1}	$M^{-1}\ s^{-1}$	6.88×10^5 ± 52%
k_{-2}	s^{-1}	476 ± 7%
k_{+2}	$M^{-1}\ s^{-1}$	3.78×10^5 ± 5%
k_{-3}	s^{-1}	112,000 ± 99%
k_{+3}	$M^{-1}\ s^{-1}$	1.08×10^8 ± 99%
$E_1 = \beta_1 / \alpha_1$		0.37 ± 99%
$E_2 = \beta_2 / \alpha_2$		1.5 ± 81%

$E_3 = \beta_3 / \alpha_3$		450 ± 8%
$K_1 = k_{-1} / k_{+1}$	mM	1,500 ± 62%
$K_2 = k_{-2} / k_{+2}$	mM	1.3 ± 8%
$K_3 = k_{-3} / k_{+3}$	mM	1.3 ± 12%
$D_1 = d_{+1} / d_{-1}$		210 ± 74%
$D_2 = d_{+2} / d_{-2}$		0.99 ± 45%
$D_3 = d_{+3} / d_{-3}$		1.3 ± 41%
EC_{50}	mM	1.9 ± 43%
n_H		2.3 ± 10%

All the rate constants were fitted freely in HJCFIT. The values for efficacy at each level of ligation, E, the dissociation equilibrium constants per site, K, the equilibrium constants for the entry into the extra shut states, D_n,the EC50 and the Hill slope were calculated from the rate constants for each set and their means are listed at the bottom of the table. Values are means ± coefficient of variation (i.e. SD of the mean expressed as a percentage of the mean).

Scheme 3: "Flip" mechanism. The Flip mechanism (Scheme 3 in Figure 3.11) describes well the single channel activity of several glycine receptor isoforms (Lape *et al*., 2008; Marabelli *et al*., 2013; Krashia *et al*., 2011; Burzomato *et al*., 2004). This scheme postulates the existence of an additional set of shut ('flipped') states, that represent a concerted conformational change that occurs before the channel opens (Burzomato *et al*., 2004). Scheme 3 has three open states and three flipped states, one at each level of ligation. In flip-type models, the agonist binding sites are independent and, as in MWC, the binding affinity depends only on the state of the receptor (i.e. resting or flipped), and not on the level of ligation. Hence the scheme estimates only two equilibrium constants for binding, one for the resting conformation (R) and one for the flipped conformation (F), regardless of how many sites are already occupied. This is done by applying the following constraints to the binding rate constants: $k_{+1} = k_{+2} = k_{+3} = k_+$, $k_{-1} = k_{-2} = k_{-3} = k_-$, $k_{F+2} = k_{F+3} = k_{F+}$ and $k_{F-2} = k_{F-3} = k_{F-}$. In addition to that, two rate constants (δ_1 and δ_3, mono- and triliganded unflipping) are constrained by the requirement of microscopic reversibility for the two cycles (Colquhoun *et al*., 2004) and therefore this mechanism had only 14 free parameters.

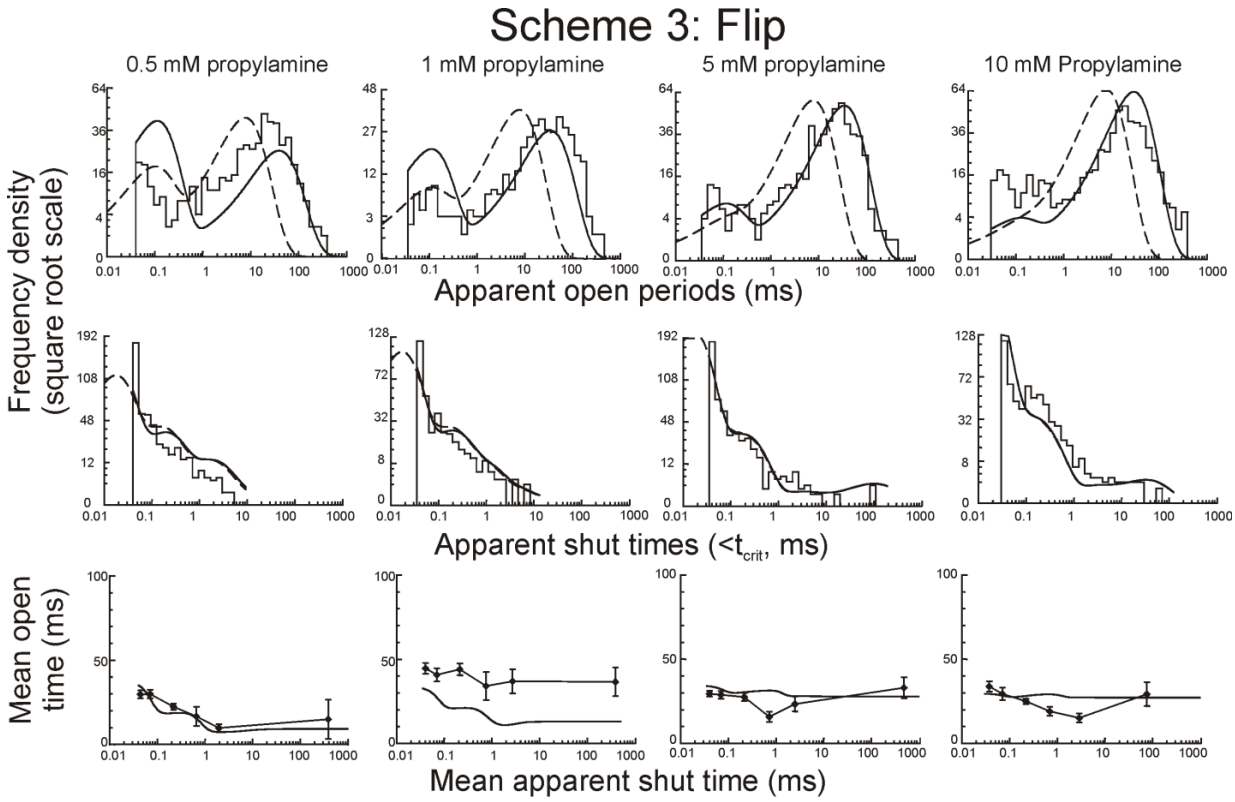

Figure 3.14 Testing the Flip mechanism fitted to ELIC single channel data
The plots compare the experimental results (dwell time distributions and open-shut correlations, see details in the legend of Figure 3.12) with the predictions of the fit of scheme 3, Flip, fitted to the same dataset as in Figure 3.12. The Flip mechanism was no better than MWC at describing open period distributions, but its prediction of the apparent shut time distribution was better.

Open/shut time distributions and correlation plots for the example set fitted with Scheme 3 are shown in Figure 3.14. The average values for the rate constants estimated for all three sets are shown in Table 3.8. Just as we found for the MWC and the J&W models, Flip, with a single fully-liganded open state, could not describe ELIC open time distributions. The shut time distributions and the correlation plots predicted by fits of the Flip and J&W mechanisms were almost indistinguishable.

Again, we tested also Flip scheme variants, with an extra open state connected to the fully liganded resting state, A3R. The best of these was Scheme 3a (Figure 3.11; results in Figure 3.15 and Table 3.8). This was the first mechanism to provide an adequate description of the data, as shown by the open and shut time distributions in Figure 3.15. The 'flipped' intermediate states are reached more easily as more binding sites are occupied and the flipping equilibrium constant, *F*, increases from 0.1 (flipping from A2R) to 0.4 (flipping from

A_3R; cf. values of 1 and 8 for the same steps in the α1 homomeric glycine receptor (Burzomato *et al.*, 2004). The ELIC values are low, suggesting that the initial conformational change is relatively unfavourable in ELIC, compared with other nicotinic-type channels. Note also that for ELIC we could not get consistent estimates for the monoliganded flipping and opening steps (probably because transition do not occur often enough) and thus Scheme 3a does not attempt to include such states in the fit. The main open state for fully liganded ELIC is reached with high efficacy (E_3 = 510), which is largely due to a low closing rate constant (120 s^{-1}). Doubly-liganded channels that have flipped can also open, with fairly high efficacy (E_2 = 21). The increase in propylamine affinity with flipping was about 5-fold (K_R = 6.9 mM and K_F = 1.3 mM), in line with the relatively modest value estimated for α1 homomeric glycine receptors.

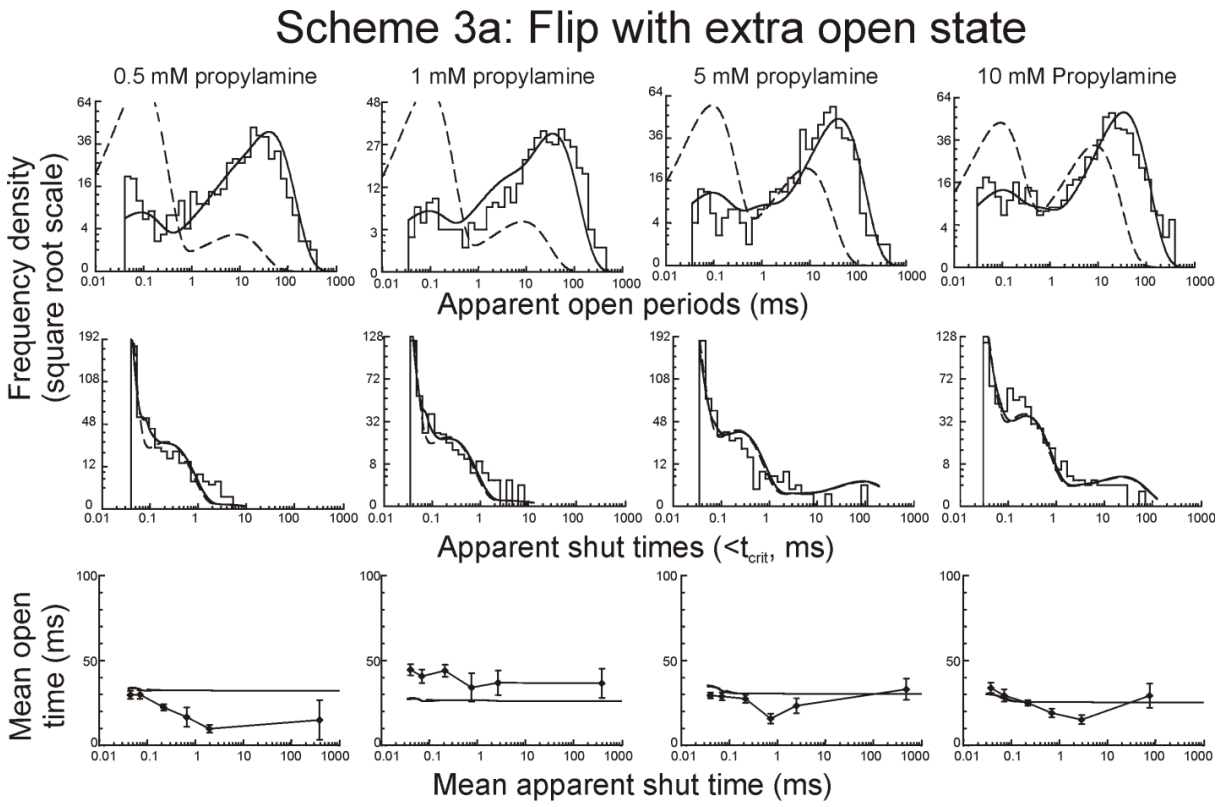

Figure 3.15 Testing Flip+O, a variant of the Flip mechanism with an added open state, fitted to ELIC single channel currents

As in Figure 3.12, the plots compare the experimental dwell time distributions and correlations with those calculated from the results of fitting Flip+O (scheme 3a in Figure 3.11) to the same dataset as in Figure 3.12. Note that open period distributions were predicted well when an extra open state was added to the fully liganded end of Flip.

Table 3.8 Rate and equilibrium constant values obtained from the global fits of the Flip and Flip + Open to three independent single channel data sets

	Unit	Flip(Scheme 3)	Flip + Open(Scheme 3a)
α'_3	s^{-1}		19,200 ± 21%
β'_3	s^{-1}		1,590 ± 16 %
α_1	s^{-1}	21,000 ± 99%	
β_1	s^{-1}	24,000 ± 67%	
α_2	s^{-1}	31,000 ± 62%	12,000 ± 48%
β_2	s^{-1}	124,000 ± 55%	125,000 ± 5%
α_3	s^{-1}	88 ± 24%	120 ± 18%
β_3	s^{-1}	37,600 ± 23%	61,600 ± 22%
γ_1	s^{-1}	0.0491 ± 81%	
δ_1	s^{-1}	0.00014 ± 90%	
γ_2	s^{-1}	3,260 ± 46%	758 ± 48%
δ_2	s^{-1}	421 ± 84%	87 ± 81%
γ_3	s^{-1}	5,920 ± 31%	10,900 ± 10%
δ_3	s^{-1}	6,820 ± 28%	4,580 ± 18%
k_-	s^{-1}	156 ± 26%	158 ± 9%
k_+	$M^{-1}\ s^{-1}$	1.14×10^4 ± 14%	2.97×10^4 ± 38%
k_{f-}	s^{-1}	175,000 ± 93%	44,400 ± 9%
k_{f+}	$M^{-1}\ s^{-1}$	5.23×10^8 ± 98%	7.35×10^7 ± 72%
$E_{3R} = \beta_{3R} / \alpha_{3R}$			0.085 ± 5%
$E_1 = \beta_1 / \alpha_1$		130 ± 54%	
$E_2 = \beta_2 / \alpha_2$		4.7 ± 62%	21 ± 58%
$E_3 = \beta_3 / \alpha_3$		430 ± 4%	507 ± 4%
$F_1 = \delta_1 / \gamma_1$		0.0048 ± 55%	
$F_2 = \delta_2 / \gamma_2$		0.088 ± 55%	0.10 ± 60%

$F_3 = \delta_3 / \gamma_3$		1.6 ± 55%	0.41 ± 8%
$K_R = k_- / k_+$	mM	15 ± 31%	6.9 ± 36%
$K_f = k_{f-} / k_{f+}$	mM	0.81 ± 31%	1.3 ± 36%
EC_{50}	mM	1.37 ± 15%	1.40 ± 39%
n_H		2.43 ± 1%	2.35 ± 5%

The fits constrain the binding and unbinding rates to be the same, regardless of the number of molecules bound, in any conformation. The two schemes in this table were constrained by the assumption that the binding sites are equivalent and independent. This constraint was implemented by the following equations: $k_{+1}=k_{+2}=k_{+3}=k_+$; $k_{-1}=k_{-2}=k_{-3}=k_-$ and $k_{f+1}=k_{f+2}=k_{f+3}=k_{f+}$; $k_{f-2}=k_{f-3}=k_{f-}$. In addition, one rate constant in each cycle was fixed by the constraint of microscopic reversibility (Colquhoun et al., 2004).The equilibrium constants, E, F and K, and open probability curve EC50 and the Hill slope, nH, were calculated from the rate constants for each set and then averaged. Values are means ± coefficient of variation (i.e. SD of the mean expressed as a percentage of the mean).

Scheme 4: Primed mechanism. Fully liganded opening to more than one open state is an intrinsic property of the primed class of mechanisms (Mukhtasimova *et al*., 2009). These postulate that channel subunits or binding sites change conformation independently of each other, rather than in a concerted fashion (as in flip), and that the channel can open from any (of several) pre-opening intermediates. Lape and colleagues (2012)showed that this feature is necessary to describe the behaviour of a startle disease mutant form of the glycine receptor, α1K276Eβ (Lape et al., 2012).

The general form of the primed mechanism with three binding sites has too many free parameters for robust estimation, but we obtained a good fit with the reduced primed mechanism shown as Scheme 4 in Figure 3.11. The scheme has three open states and two primed states, which are accessible from the di- and triliganded resting states. This mechanism has 15 free parameters, the agonist binding sites are independent, and binding affinity depends only on the state of the receptor (i.e. resting, R or primed, F'), regardless of how many sites are already occupied.. In addition, one rate constant (δ_2) was constrained by microscopic reversibility (Colquhoun *et al*., 2004).

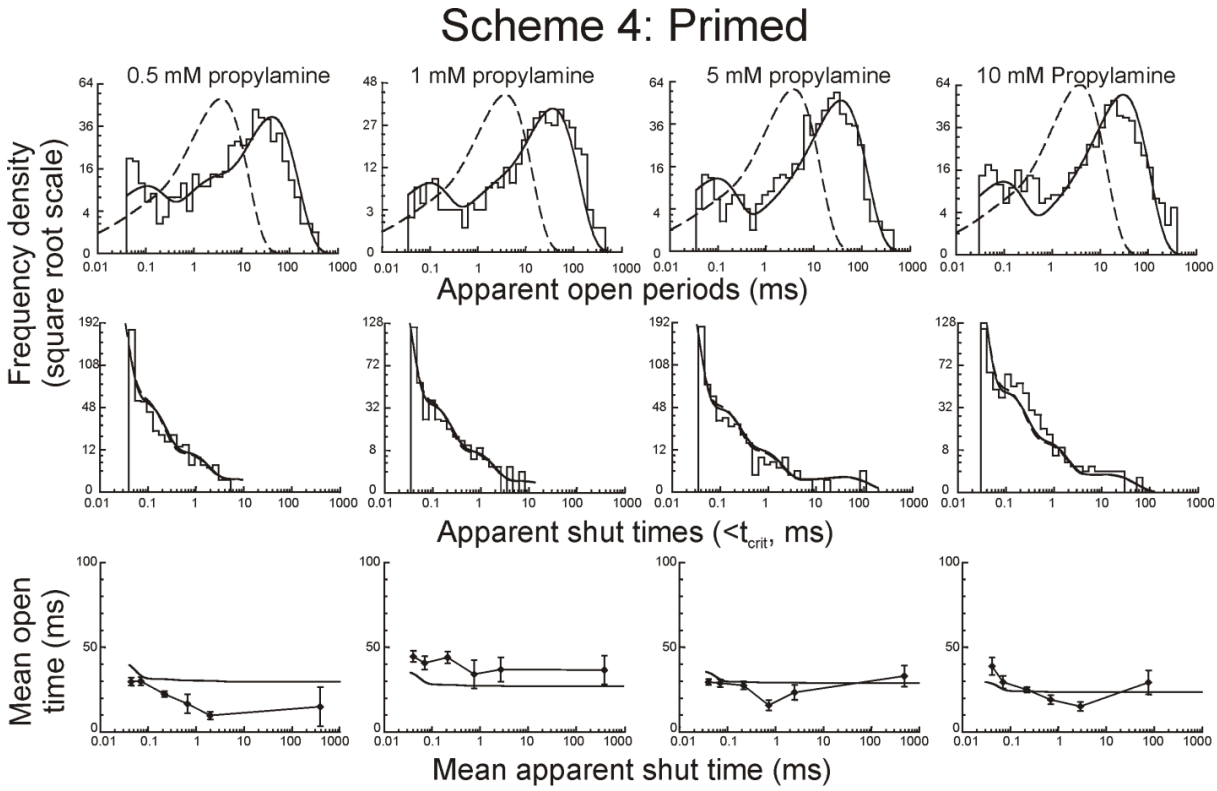

Figure 3.16 Fits of a Primed type mechanisms to ELIC single channel currents
The results of fitting scheme 4 (see Figure 4) are shown by the plots, as comparisons of the scheme predictions with the experimental dwell-time distributions and open-shut correlations. Same dataset and details as in Figure 3.12. The primed mechanism allows the channel to enter more than one "layer" of intermediate states before opening and provided a good description for all the single channel observables.

The results of fitting this scheme are summarized in Figure 3.16 and Table 3.9. The prediction of both dwell time distributions and open-shut correlations was good at all agonist concentrations. In addition to that, the values estimated for the primed mechanism were much more consistent across the different sets than those estimated with other mechanisms.

As more agonist molecules bind, activated states become more accessible. This is largely an effect of easier priming, as the value of the priming equilibrium constant, *F*, increased from 0.013 (A_2R priming to A_2F') to 0.76 and 0.72 (A_3R priming to A_3F' and A_3F' priming to A_3F'', respectively). The most effective opening occurs from the highest primed fully bound state (A_3F''), with a very high opening equilibrium constant (E_3'') of 450, an opening rate constant of 72,000 s^{-1} and a closing rate constant of 180 s^{-1}. As in the modified flip mechanism, partially bound (diliganded) channels open with relatively high efficacy once they have

reached the primed state, as E_2" is 97. The increase in propylamine affinity with priming was 50-fold (K_R = 7.1 mM and K_F = 0.14 mM).

Table 3.9 Rate and equilibrium constant values obtained from the global fits of the primed model to three independent single channel data sets

	Unit	Primed
α''_3	s^{-1}	176 ± 26%
β''_3	s^{-1}	72,200 ± 11%
α'_3	s^{-1}	12,700 ± 3%
β'_3	s^{-1}	3,430 ± 28%
α'_2	s^{-1}	656 ± 43%
β'_2	s^{-1}	57,300 ± 91%
γ''_3	s^{-1}	12,000 ± 31%
δ''_3	s^{-1}	8,330 ± 27%
γ'_3	s^{-1}	2,530 ± 35%
δ'_3	s^{-1}	1,830 ± 27%
γ'_2	s^{-1}	29,300 ± 91%
δ'_2	s^{-1}	33 ± 34%
k_-	s^{-1}	83 ± 12%
k_+	$M^{-1}\ s^{-1}$	1.20×10^4 ± 12%
k_{f-}	s^{-1}	207,000 ± 46%
k_{f+}	$M^{-1}\ s^{-1}$	5.36×10^9 ± 49%
$E''_3 = \beta''_3 / \alpha''_3$		450 ± 17%
$E'_3 = \beta'_3 / \alpha'_3$		0.27 ± 26%
$E'_2 = \beta'_2 / \alpha'_2$		97 ± 85%
$F''_3 = \delta''_3 / \gamma''_3$		0.72± 15%

$F'_3 = \delta'_3 / \gamma'_3$		0.76 ± 8%
$F'_2 = \delta'_2 / \gamma'_2$		0.013 ± 80%
$K_R = k_- / k_+$	mM	7.1 ± 11%
$K_f = k_{f-} / k_{f+}$	mM	0.14 ± 82%
EC_{50}	mM	1.4 ± 15%
n_H		2.5 ± 1%

The fit were constrained by the assumption that the binding sites are equivalent and independent. This constraint was implemented by the following equations: $k_{+1}=k_{+2}=k_{+3}=k_+$ and $k_{-1}=k_{-2}=k_{-3}=k_-$. In addition, one rate constant in each cycle was fixed by the constraint of microscopic reversibility (Colquhoun et al., 2004).The equilibrium constants, E, F and K, and open probability curve EC50 and the Hill slope, nH, were calculated from the rate constants for each set and then averaged. Values are means ± coefficient of variation (i.e. SD of the mean expressed as a percentage of the mean).

3.2.3.5 Mechanism prediction of P_{open} and macroscopic channel behaviour

We found that only the modified flip and the primed mechanisms could describe the ELIC single channel dwell distributions. Can these schemes account also for the other experimental observations we obtained?

Maximum open probability is given by

$$Max\ P_{open} = \frac{E_{eff}}{E_{eff}+1}\ , \qquad \text{[eq 3.2]}$$

where E_{eff} is the overall agonist efficacy.

In the Flip + Open scheme, E_{eff} depends on the equilibrium constant for flipping (F_3) and the equilibrium constants for opening (E_{3R} and E_3) for the fully liganded receptor

$$E_{eff} = \frac{E_{3R}+E_3F_3}{F_3+1} \qquad \text{[eq 3.3]}$$

In the primed scheme, E_{eff} depends on the equilibrium constant for primed (F' and F'') and the equilibrium constant (E' and E'') for the open-shut reaction for the fully liganded receptor:

$$E_{eff} = \frac{E3`F3`+E3``F3``F3`}{F3`F3``+F3`+1} \qquad \text{[eq 3.4]}$$

The effective efficacy for propylamine on ELIC was very high in both schemes, 196 in Flip +Open and 126 in Primed.

Both schemes correctly predicted a maximum open probability greater than 99%, in agreement with our observations of cluster P_{open} values between 96 and 99% at 10-100 mM propylamine.

Because we could not obtain a single channel concentration-P_{open} curve, we can compare mechanism predictions only with our whole-cell dose-response curves. Both single-channel schemes predicted a propylamine EC_{50} value of 1.4 mM, somewhat higher than the observed value of 0.5 mM and Hill slope values of 2.35-2.50 (Tables 3.8 and 3.9, cf. the observed value of 2.2). Note the value of this comparison is limited, because the single-channel mechanisms are estimated from data from which desensitised intervals are excluded, whereas desensitisation may well distort whole-cell dose-response curves because of the relative slowness of agonist applications in these experiments. In principle, partial equilibration with desensitised states (which are by definition high affinity) at the response peak should increase the apparent agonist potency and account for some of this discrepancy.

We calculated also the predictions of the two schemes for the time course of agonist outside-out currents (figure 3.17). A recorded macroscopic current response to a 500 ms 10 mM propylamine pulse is shown in Figure 3.17A and the equivalent response calculated, for a realistic agonist pulse, with the primed mechanism (Scheme 4) is shown in Figure 3.17B. This first calculated response does not decline during the application, because the single-channel analysis does not attempt to estimate desensitisation, but desensitized states can be added empirically to the mechanism, to give Scheme 5 in Figure 3.17C. We chose a value of 1 s^{-1} for the forward rate constant (into desensitization), to match the reciprocals of the approximate cluster length and of the macroscopic desensitization τ, and a value of 0.5 s^{-1} for the backward rate constant (out of desensitization), to reproduce the observed extent of desensitization at the end of this pulse.

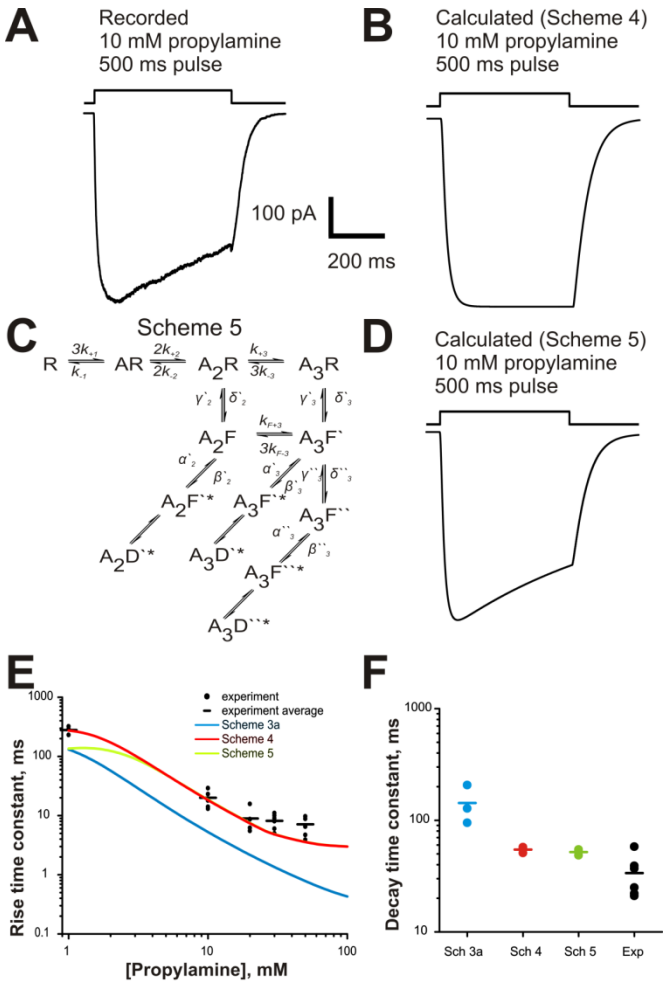

Figure 3.17 Primed activation schemes fitted to single channel data predict the time course of macroscopic agonist responses

A) ELIC inward current recorded in response to a 500 ms step of 10 mM propylamine applied to an outside-out patch (square pulse above is the open tip solution exchange measured at the end of the experiment). B) Average macroscopic current calculated from the rate constants of the fit of the Primed mechanism (Scheme 4) to the 3 sets of single channel data in response to a 10 mM propylamine concentration jump (time constant of the solution exchange, 200 µs, upper trace). C) Scheme 5 shows the Primed mechanism modified by the empirical addition of desensitised states (D*) connected to the open states. D) Average macroscopic current calculated from Scheme 5, where the rate constants for entry and exit into desensitised states are empirically estimated from macroscopic data (see text) E) Experimental rise times for currents evoked by different agonist concentrations compared with the predictions of the best schemes fitted to single channel data. Points are the experimental values, with the mean shown as a dash, and the coloured curves are the average activation time constants calculated from the scheme fits to the single channel data. The predictions of the Flip+O mechanism (Scheme 3a) are consistently faster than the observed values, which are well predicted through the agonist concentration range by Schemes 4 and 5 (Primed and Primed+ desensitisation, red and green, respectively). F) Dot plots showing the 20-80% decay time constant of the off-current values measured in experimental responses to concentration jumps 50mM propylamine (black) and in calculated responses from the mechanism fits (color coding as in E, dash shows the mean values). Both variants of the primed mechanism gave an acceptable description of the experimental observations.

The macroscopic current calculated from Scheme 5 for the same agonist pulse (Figure 3.17D) reproduces well the time course of the experimental current.

Figure 3.17E shows a comparison of the observed values of the current rise τ as a function of agonist concentration (black circles, one per patch, and short dash for the average) with the predictions of the best Schemes (3a, 4 and 5; averages for the three fits). Scheme 3a (blue; and mechanisms 1 and 2, data not shown) predicted rise τ values that were consistently much faster than the ones we measured. The predictions of the two variants of the primed scheme (Schemes 4 and 5, red and green, respectively) were good across all propylamine concentrations. There was a small discrepancy at concentrations higher than 20 mM, where predicted currents had a faster rise than observed ones, possibly because of the effect of propylamine block.

Figure 3.17F shows a comparison of the observed and predicted values for the deactivation τ calculated from Schemes 3a, 4 and 5 (each point is calculated from the fit to an independent data set). Predictions by both Scheme 4 and 5 were very good, whereas those of Scheme 3a were much slower than the experimental values.

3.2.3.6 Mechanism prediction of burst length

One last set of experimental observations that should be accounted for by an adequate mechanism is the single channel mean burst length. This is a useful additional comparison, because reliable burst length measurements can be obtained from recordings that contain too few events to be incorporated into the global mechanism fits, such as patches at 0.3 mM propylamine (trace in Figure 3.18B), where mean burst length is 140 ± 30 ms (213 bursts from 3 patches).

The Primed mechanism (Scheme 4) predicts that mean burst length should monotonically increase with agonist concentration (dashed line in Fig 3.18A). At low concentrations, the Scheme 4 predictions are very close to our observations (data are shown as closed circles in Fig 3.18A). Figure 3.18C depicts a simulation from Scheme 4 of single channel currents at 0.3 mM propylamine, and shows a mixture of short and long bursts similar to that observed in the experimental recording above (Figure 3.18B). However, at higher propylamine concentrations, the experimental mean burst length was much shorter than predicted by the Primed mechanism.

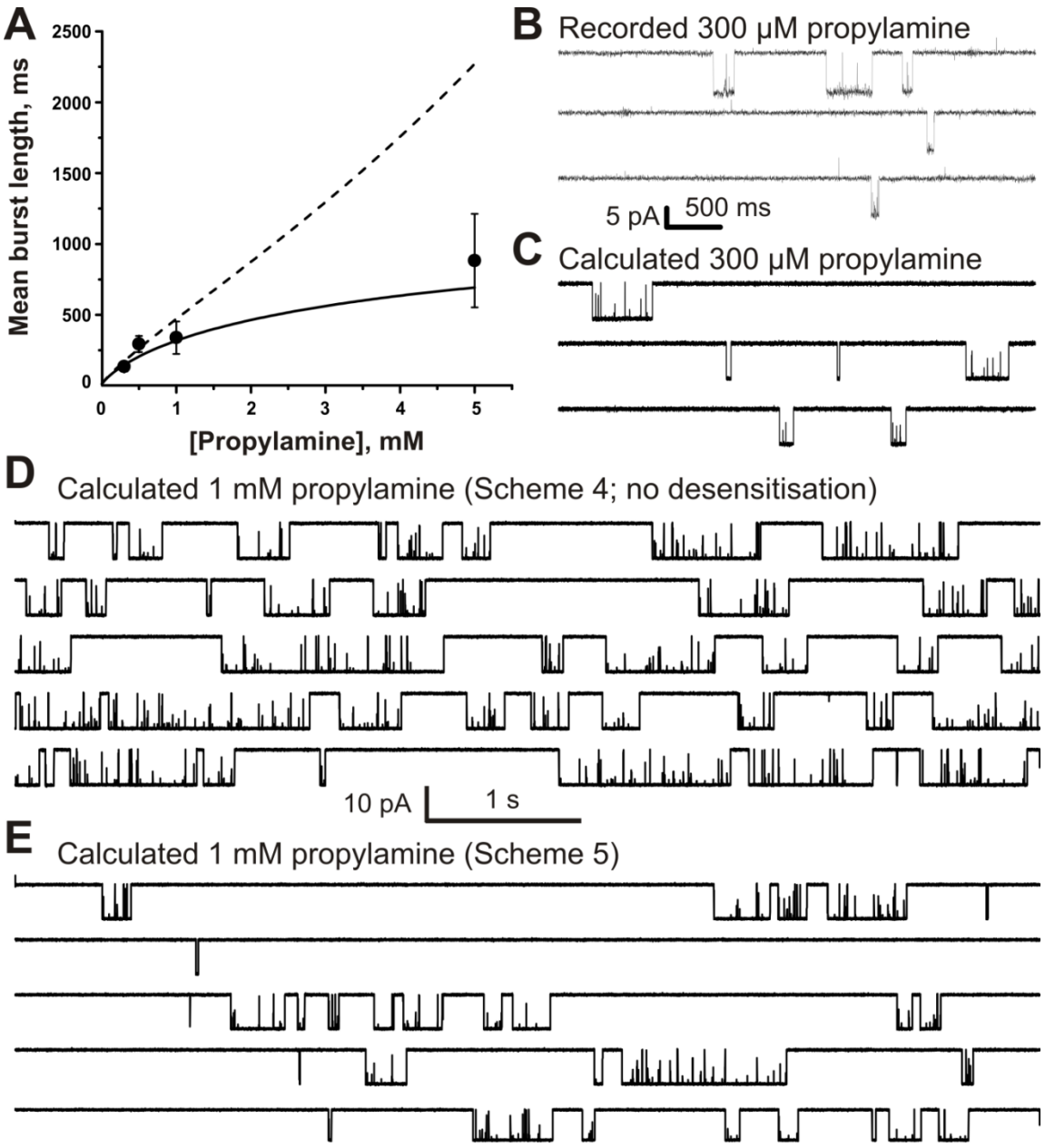

Figure 3.18 ELIC bursts can be ended by desensitization.
A) Observed values of ELIC mean burst length (filled circles) are not well described at high propylamine concentrations by Scheme 4 (Primed), which predicts a linear increase in burst length with agonist concentration (dashed line). Scheme 5 (primed with the addition of desensitised states) gives a better prediction of burst length (continuous curve), suggesting that desensitization can terminate bursts. B) Traces are continuous sweeps of single channel recordings at 0.3 mM propylamine (filtered at 3 kHz for display) from outside-out patches held at -60 mV. C) Traces are continuous sweeps of single channel activity calculated from Scheme 4 at 0.3 mM propylamine (3 kHz low-pass filter, 1 channel in the patch). Note the qualitative similarity between the experimental and the simulated trace at low concentration (cf. the 0.3 mM point in A). D) and E) Traces are continuous sweeps of single channel activity simulated at 1 mM propylamine from the two variants of the Primed mechanism, without desensitisation (Scheme 4) and with desensitisation (Scheme 5; 3 kHz low-pass filter, 1 channel in the patch).

For example, the predicted burst length at 5 mM propylamine would be about 2.5 s, but the measured average burst length was 0.9 ± 0.3 s (t_{crit} = 10 ms; 56 bursts from 3 patches). Scheme 5 (Primed adjusted by the addition of macroscopic desensitisation) predicted very well the mean burst length at all propylamine concentrations (Figure 3.17A, solid line). This suggests that at higher concentrations, bursts can end not only by deactivation (eg agonist unbinding) but also by other ways that are not included in Scheme 4, for instance by desensitisation, as clusters do. An interesting observation is that the average experimental burst length at 5 mM (ca. 1 s) approaches the length of clusters at the higher concentrations, where clusters could be defined (eg at 10 mM, 2.2 ± 0.8 s, t_{crit} = 100 ms, 26 clusters from 3 patches; 50 mM 1.0 ± 03 s, t_{crit} = 60 ms, 29 clusters from 3 patches).

This observation suggests that the number of bursts in each cluster must be very small, indeed that many clusters may contain a single burst. Measuring single channel P_{open} relies on correctly identifying clusters vs. bursts and on obtaining clusters that contain a sufficient number of bursts. This could explain our difficulties in obtaining an open probability curve for ELIC. We explored the plausibility of this hypothesis by simulating single channel activity with and without desensitisation. The current traces in Figure 3.18D and 3.18E show 50 s of the activity of a single channel molecule simulated for Schemes 4 and 5 in 1 mM propylamine (close to EC50). When there is no desensitization (Fig 3.18D), the channel is open for approximately 50% of the time and produces bursts that are on average much longer than at 300 μM propylamine. When desensitization is added (Scheme 5), the bursts clearly shorten and clusters start appearing (Fig 3.18E). However, most of the apparent clusters (defined by the longest shut intervals) do not contain a sufficient number of bursts to give a good estimate of the channel open probability. Many apparent clusters contain just a single burst and have nearly 100% P_{open} and even clusters that do contain several bursts have open probability much higher than 50%. This qualitative example clearly shows that desensitization can terminate both bursts and clusters of bursts in ELIC, that it introduces ambiguity in choosing appropriate t_{crit} values for cluster separation and consequently leads to strong overestimation of the channel open probability.

Chapter 4: Discussion

4.1 Aims

The main aim of my thesis was to characterize the activation mechanism of homomeric α3 GlyRs and ELIC receptor, and to estimate their rate constants.

Knowledge of the kinetics of ligand gated ion channels is important both for understanding their structure-function properties and for obtaining accurate quantitative models of the events at a realistic model of the synapse. Knowing the kinetic mechanism allows us to identify which reaction steps are involved in the difference in efficacy of different agonist and in the effect of mutations. In order to investigate the kinetic mechanisms we used single channel recording and direct model fitting to these data by maximum likelihood.

4.2 Maximum likelihood fitting of single channel data

The traditional way of using single channel data to extract kinetic information consisted of fitting a mixture of exponential components to histograms of channel dwell times such as open period duration, shut time duration and burst length duration. Some feature of the mechanism that governs the receptor behaviour can be extracted using these empirical fits. For example, the number of exponential components required to fit open and shut time distributions represent the minimum number of open and shut states to incorporate in the mechanism. Other inferences can be made from the presence and extent of concentration dependence of the time constants and the areas of the exponential components. However, observed time constants are not related in any simple way to the transition rates of each reaction steps or to the mean lifetime of the states. The rate constants in the mechanism can be only approximately estimated, assuming a relationship to the fit parameters. Moreover, the interpretation of the rate constants from the empirically fitted parameters of single channel data must be developed *ad hoc* for each new mechanism. Thus, the method is not general for every mechanism. Last but not least, this method is not exact, because only approximate corrections for missed events are possible and these are satisfactory only in few cases (i.e. if mostly open or closed times are missed). In addition to that, the information contained in the order of the events is lost, because only the dwell times distributions are analysed.

The analysis done in this work, maximum likelihood fitting of the mechanism to the data, is different (Figure 4.1).

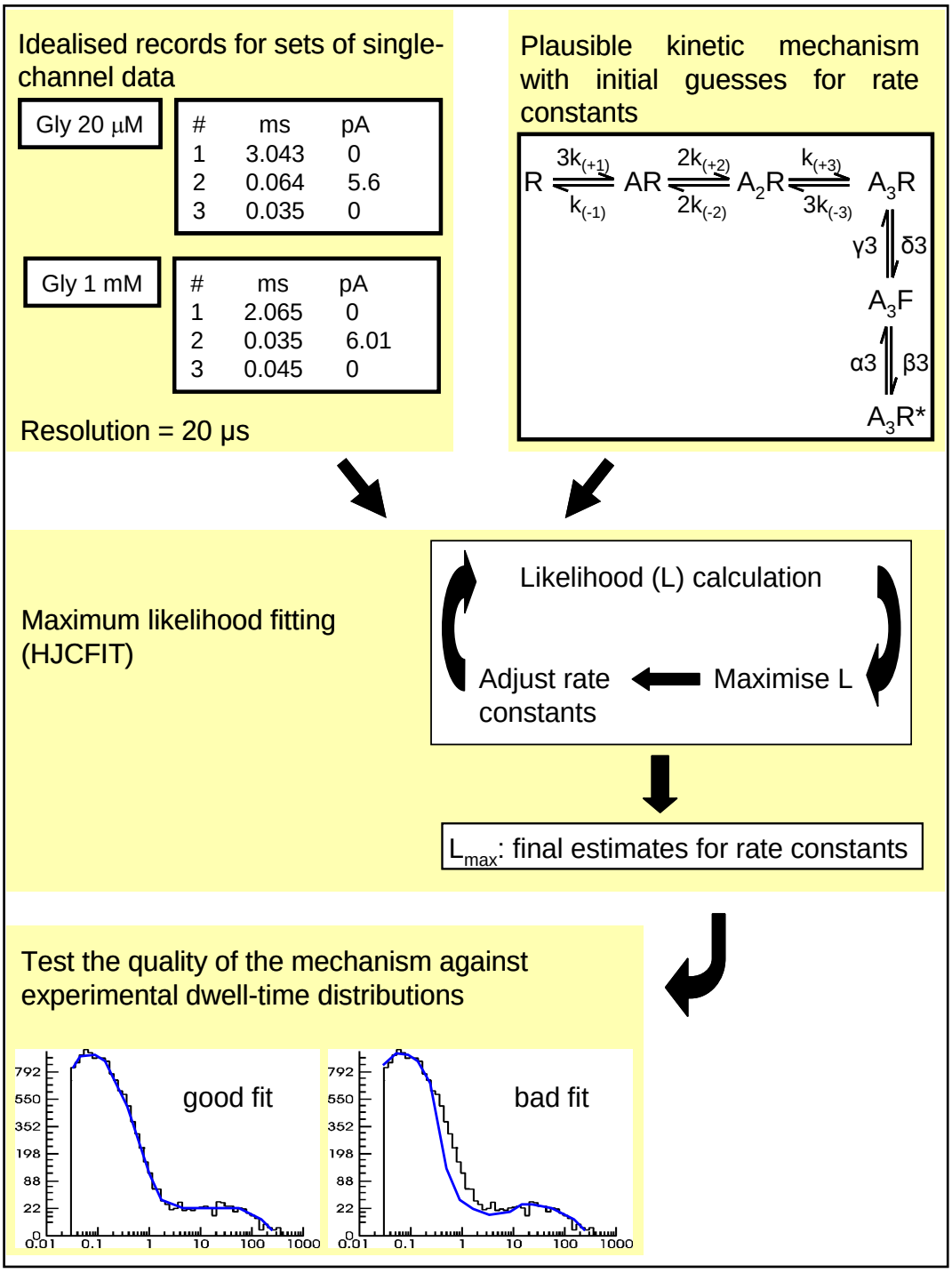

Figure 4.1 Direct maximum likelihood fitting to idealised single-channel data

The rate constants of a postulated mechanism are adjusted until the likelihood of the whole sequence of events in the experimental single channel records is maximised. The validity of the final calculated rate constants is tested against the experimental observations, usually these being the shut times (as in the figure), the open times (or open periods) and the P_{open} curve. The scheme is considered satisfactory if the predicted distributions are in agreement with the experimental ones.

The whole idealized record, which is the ordered sequence of events with their duration, is analysed, rather than the dwell time distributions. The input of the fitting program HJCFIT consists of one or more idealised records with their resolution, the agonist concentration and an *a priori* mechanism hypothesis. Initial guesses for the rate constants of the mechanism are provided and subsequently optimised by HJCFIT to maximise the likelihood of the experimental sequence of events in the data. This method takes into account all the information contained in the record, both duration of the events and the order in which events occur. The parameters fitted to the data are the physical rate constants. Defining a mechanism and its **Q** matrix, allow the evaluation of all the rate constants at once. Moreover it is possible to use different data obtained at different concentrations of agonist and fit them simultaneously. Furthermore, because a mechanism is specified a priori, full and exact missed events correction is possible (Hawkes *et al*., 1992). The putative mechanism being tested and the rate constant estimated for this mechanism allow us to calculate the different types of distributions that we can obtain from the data. These predictions can be compared with the experimental distributions, to assess how well the mechanism agrees with the data. This makes it possible to compare different mechanisms by evaluating which one better predicts the experimental distributions.

Obviously maximum likelihood fitting has drawbacks. These are mainly due to the difficulty of identifying mechanisms, because a good fitting mechanism is not necessarily unique. If more than one mechanism fits the data equally well, it is not possible to choose between them on the basis of the quality of the fit. In this case the plausibility of each mechanism has to be considered, taking into account the physical interpretation of each scheme (i.e. number of agonists to fully activate the receptor and the presence of intermediate states). It must be always borne in mind that we obtain the simplest mechanism that can account for the observation.

4.3 The activation mechanism of α3 glycine receptor

4.3.1 Features of single channel activity and *P*open-concentration curve

Single channel experiments were performed in the cell-attached configuration at different glycine concentrations (50, 200, 300, 500, 1000 and 10000 μM). This range encompasses the saturating concentration and the lowest concentration at which it was possible to collect a sufficient number of events in a single experiment.

4.3.1.1 Amplitude distribution

Recombinant α3 GlyR expressed in HEK 293 cells have been reported to show several different conductances, of 102 pS, 85 pS and 58 pS in outside-out recordings (Bormann *et al*., 1993). In our cell-attached recordings we found that the distributions of current amplitudes were well fitted with a single Gaussian in all patches, with a consistent value of 5.8 ± 0.2 pA (S.D. of the mean; n = 21 patches) and without clear subconductance levels. This situation is similar to our findings for other homomeric glycine channels in cell-attached recordings, where sublevels were absent or rare (1-2% of events; α1 and α2, respectively; (Beato *et al*., 2004; Krashia *et al*., 2011). Glycine channel subconductances are commonly observed in outside-out recordings, but are rarer in the cell-attached configuration. This phenomenon could be due to phosphorylation, which can modulate the synaptic efficacy by controlling channel conductance (Van Hooft and Vijverberg, 1995). The α1β channels open to two levels in outside-out patches from HEK cells (Pitt *e al*., 2008), but do not show sublevels in cell-attached recordings from the same heterologous system (Burzomato *et al*., 2004). A similar pattern is seen in patches from motoneurones (probably heteromeric GlyRs, three conductances in outside-out and one in cell-attached, (Beato and Sivilotti, 2007).

4.3.1.2 Dwell-times distributions and P_{open} curve

Apparent open period and apparent shut times distributions for α3 were fitted with a mixture of probability density functions after imposing a resolution of 30 μs to all patches. An open period is defined as the duration between two adjacent resolvable shut times, it is the opposite for a shut period. At ideal resolution, the number of exponential components needed to fit an open period, or a shut time distribution would represent the exact number of open and shut states that the channel can access. However, in real experiments one or more components could be missed because of limited bandwidth, thus the distributions provide only the *minimum* number of states, open or shut, that might be present in the kinetic scheme. From the analysis of the distributions, other types of descriptive information can be extracted, such as concentration dependence and the areas of the different exponential components. The

apparent open period distributions were well fitted with a maximum of three exponential components. The first (fastest) component was stable across all the concentrations, whereas the third (slowest) component became longer as the concentration of glycine increased (i.e. 4.6 ms at 50μM to 30 ms at 10,000 μM). The mean open time also became longer in high glycine, and increased from 2.2 ms at 50 μM to 30ms at 10,000 μM. Those fits indicate that the activation mechanism of the α3 GlyR must contain at least 3 open states. Their concentration dependence suggests that they have a different number of bound glycine molecules and that the short openings correspond to a lower liganded open state, whereas the long openings are produced by a fully liganded open state.

It is important to include in the analysis only stretches of data that are likely to come from one single channel molecule (bursts at low concentrations and clusters at high concentrations), and for this purpose, a critical shut time (t_{crit}) must be chosen. Shut times longer than t_{crit} are classified as between bursts/clusters, whereas shut times shorter than t_{crit} are classified as within bursts/clusters. At the lowest concentration (50 μM glycine), there are single openings or groups of few openings divided by long shut times. These groups are activations, or bursts and are terminated by the unbinding of the glycine. At concentrations greater than 50 μM glycine, glycine quickly rebinds and activations become closely spaced to form clusters. Clusters are separated by long sojourns in desensitized states. Analysis of shut time distributions is used to choose the appropriate t_{crit} at each concentration. Shut time distributions were fitted with a maximum of four exponential components. The time constants of the first three components were the most consistent across the different patches and concentrations, and the majority of the events belonged to the shortest component (areas from 50% to 70%). The longer component became shorter as glycine concentration was increased, indicating that this is an intra-cluster component.

The concentration dependence of single channel activity can be displayed and characterised as a P_{open} curve. This is done by using the t_{crit} to identify clusters, stretches of opening that arise from the activation of only one channel. Gaps were classed as between clusters if longer than t_{crit} of 1000 ms for 200 μM, 1000 ms for 300 μM, 10 ms for 1,000 μM and 1 ms for 10,000 μM. The P_{open} for each cluster was calculated as the ratio between the cluster open time and cluster total duration, obtained from the idealised traces. This procedure weighs the contribution of each cluster to the P_{open} value according to its duration, because P_{open} estimates derived from longer clusters are more precise. These values were averaged and their relation with agonist concentration fitted empirically with the Hill equation (weighted

least square fit) using the CVFIT program. This gave a maximum P_{open} of 0.99, and EC_{50} of 300 μM and a Hill slope of 3.7. The Hill equation was fitted simply to obtain an empirical estimate of the steepness of the P_{open} curve that we could use for comparison with the predictions of the postulated mechanisms.

4.3.2 The kinetic mechanism of α3 GlyR using maximum likelihood fitting

Three independent sets, each containing four recordings at different concentrations of glycine, were assembled. Putative mechanisms were fitted simultaneously to all the concentrations in a set by maximum likelihood with missed events correction (taking into account the experimental resolution of 30 μs). Adequacy of the mechanism was judged by assessing the agreement of its prediction with the single channel data plotted as dwell-time distribution and P_{open} curve and the experimental observations of macroscopic current time course. We attempted to fit 30 different reaction schemes to the steady-state single-channel activity evoked by glycine concentrations from 50 μM to 10 mM and we described two schemes that gave good results. General features that were required for a mechanism to prove adequate included the presence of as many as five agonist binding sites, and the possibility of channel opening at the three highest levels of ligation, with opening efficacy increasing as more ligand molecules bind.

4.3.3 Both the Jones and Westbrook and the flip mechanism with five binding steps provide an adequate description of the data.

Two schemes, Jones and Westbrook and flip, described well the experimental data, provided they were adapted to incorporate five binding steps. Predictions of dwell time distributions were almost indistinguishable in quality for these mechanisms, independently of the number of binding sites. The two forms of Jones and Westbrook schemes we tested (Schemes 1 with three binding sites and 2 with five binding sites) are effectively variants of a sequential mechanism and all their parameters were allowed to vary freely, including the microscopic affinity of the successive binding steps.

Recent work from our lab has proposed a different mechanism to account for the activation of Cys-loop channels, namely, the flip mechanism (Scheme 3; Burzomato *et al.*, 2004). This scheme incorporates the idea of the Monod-Wyman-Changeux mechanism (Wyman & Allen, 1951; Monod *et al.*, 1965), where ligand binding stabilizes the protein conformations that have higher ligand affinity. In the flip mechanism, these are the flipped shut states to which glycine binds with higher affinity (*cf.* resting state affinity, K_R, *versus* the 'flipped' state affinity, K_F). In mechanisms of this type, there is no interaction between binding sites, but

there is an increase in the overall affinity, after all subunits change their conformation in a concerted fashion. In our schemes, this behaviour is imposed by ligand binding constraints, which mean that the flip mechanisms have only two equilibrium constants for binding, and therefore only 14 free parameters (for any number of binding sites).

If we consider exclusively the present data and analysis, both mechanisms describe well the α3 data, and it is not possible to judge which one is the best. The Jones and Westbrook mechanism with five binding sites gave a better prediction of the slope of the P_{open} curve (3.7 *cf.* 3.1 for flip), but it has many more free parameters than the flip mechanism with the same number of binding sites. Furthermore we found the parameter estimates for the Jones and Westbrook type schemes to be highly variable across sets (Table 3.3, section 3.1.5.1).

Nevertheless, there are also other considerations that must be made. The most important is that the flipped closed states in the flip mechanism, but not in the Jones and Westbrook mechanism, have a plausible physical interpretation, in that they may correspond to intermediate states in the receptor's trajectory to activation. Other lines of evidence, such as the results of Φ analysis (Auerbach, 2005), suggest that multiple such states may indeed exist. Finally, variants of the flip mechanism describe well the activity of many Cys-loop receptors (Burzomato *et al.*, 2004; Plested *et al.*, 2007; Keramidas & Harrison, 2010; Lape *et al.*, 2012). We tested also variants of the 'primed' mechanism proposed by Sine and co-workers (Mukhtasimova *et al.*, 2009). This mechanism hypothesizes that the activation intermediates arise from changes that are not concerted across the binding sites, but occur at each individual site in isolation. We could not obtain satisfactory fits of variants of this mechanism to α3 channel activity (data not shown). It was found that this mechanism performs poorly (essentially because it has many free parameters) when fitted to wild-type heteromeric glycine receptor data, but is necessary to describe well the data from a loss of function mutant that is slower in activating and can open from intermediate levels of priming (α1K276Eβ; Lape *et al.*, 2012). This suggests that α3 channels resemble α1β receptors, also in that the increase in affinity that occurs early after binding is so fast as to appear concerted (with the sensitivity of our method).

4.3.4 How many agonist molecules bind to activate α3 GlyR?

Homomeric receptors in the Cys-loop family are made of five identical subunits and, thus, have five potential binding sites at which an agonist could possibly bind. An early work on

the activation of homomeric α1 and heteromeric α1β GlyRs strongly indicated that these channels open to three open states (Beato *et al.*, 2002; Beato *et al.*, 2004; Burzomato *et al.*, 2004) in agreement with other data from native or recombinant receptors (Twyman & Macdonald, 1991; Lewis *et al.*, 2003). In addition to that, the maximum P_{open} is reached when three (out of the possible five) binding sites in homomeric α1 channels are occupied by the agonist. This is in close agreement with the results of the elegant work by Sine, Bouzat and co-workers on chimeric nicotinic α7/5-HT_{3A} channels (Rayes *et al.*, 2009).

The situation is quite different for α3 channels, where the much steeper Hill slope of the P_{open} curve cannot be accounted for, if only three binding sites are included in the mechanism. Increasing the number of binding sites to five raises the slope values predicted by the mechanisms to 3.7 and 3.1 for the Jones and Westbrook and flip schemes, respectively, approaching the experimental value of 3.7. It is not clear why α3 homomers require all five binding sites to be occupied in order to open at maximum efficacy. Of course, even in homomeric α1 receptors, we could not exclude that all five binding sites can bind the agonist, even though maximum P_{open} is reached with three glycine bound. Structural data from ELIC and GluCl strongly suggests that all the binding sites can be occupied in channels in this super-family, but cannot give us information on the efficacy of each state of ligation (Hilf & Dutzler, 2008; Hibbs & Gouaux, 2011).

The main indication for the number of bound glycine molecules needed for maximum efficacy is the steep slope of the P_{open}. This observation appears to be quite robustly reproducible, irrespective of choices made in the analysis, such as the value of t_{crit} chosen (at both high and low concentrations of agonist; data not shown). The slope of the P_{open} curve is so well determined that even removing either of the data points at the lowest concentrations of glycine (200 μM or 300 μM) leaves it effectively unchanged. An interesting parallel with our data is the observation that glycine is less potent and that partial agonists are less efficacious on α3 receptors than on α1(Chen *et al.*, 2009). The characterization of chimeric constructs in the same study suggested that the M4 transmembrane domain controlled much of the observed differences in agonist efficacy.

4.3.5 A specific synaptic role for a3 glycine receptors

Last but not least, our work shows that α3-containing GlyR are fast channels that are suitable for synaptic activity. They resemble α1 containing GlyR in their kinetics and may well mediate glycinergic synaptic currents in the adult. Comparison of our glycine concentration jump data across the two subunits indicates that synaptic currents mediated by α3 homomeric channels, if they exist, would have a decay time course (9 ms time constant; 20 mM intracellular chloride) slightly slower than that of α1-containing channels (4 and 6 ms time constants for α1 and α1β, respectively; 30 mM intracellular chloride, Pitt *et al.*, 2008; Moroni *et al.*, 2011). While this difference is consistent and easily detectable in our experimental protocols, it may well be too small to make identification of α3-mediated currents in neurons unambiguous.

Given that the decay of α3 currents is not particularly distinctive, could other properties of these receptors give them a synaptic role distinct from that of α1? We calculated the peak open probability predicted for α3 currents by the results of our best fitting mechanisms in response to a synaptic-like concentration pulse of glycine. Beato and colleagues (2008) estimated that, at synapses onto rat lumbar motoneurons, glycine concentration peaks at 2.2-3.5 mM and decays with a time constant of 0.6-0.9 ms. If we take the concentration of glycine to peak at 3.5 mM and decay with a time constant of 0.9 μs, the peak P_{open} values predicted were strongly mechanism dependent, with values of 15±1%, 40±10%, 9±1% and 15±3% for schemes 1, 2, 3 and 4, respectively (*cf.* 46% for the α1 glycine receptor, from the rate constants of Burzomato *et al.*, 2004).

Our present data suffer from the limitation that we could not express α3 heteromers, which are the form of channel that one would expect to be present at synapses because of the interaction between the β subunit and gephyrin. It is interesting to note that recent work by Callister and Graham on A52S homozygous mice (Graham *et al.*, 2011) suggests that pure α3 synapses are unlikely to be the majority, even in superficial dorsal horn neurons, where α3 expression is highest. Their hypothesis is that α3 often forms receptors together with α1 (and probably β), and it could be that α3β channels form efficiently only if they incorporate also α1. Thus the poor expression of the α3 subunit in our expression system (as a homomer and

especially as an α/β heteromer) would not preclude its physiological function. The difficulty in expressing defined composition mixed receptors makes it impossible to test this hypothesis experimentally. It is hard to speculate what the properties of such a mixed α1/α3 receptor would be and why they would be appropriate to inhibition in nociceptive pathways. It is possible that such a receptor would have properties intermediate between α1 and α3 channels, and that the presence of α3 would reduce the open probability (especially at lower levels of ligation).

Our conclusion is that α3 GlyR activation can be well described by both "Flip" and "Jones and Westbrook" mechanisms in a manner similar to that we reported for α1β heteromeric GlyR. Inspection of the features revealed by the fits showed both intriguing differences and similarities between α3 and α1 homomers. The high sequence homology of these isoforms may allow us to investigate the structural basis of the differences by mutating the channels.

4.4 Activation mechanism of ELIC receptor

4.4.1 Functional properties of ELIC

Our observations confirm and extend the description of the properties of ELIC from other labs, particularly with respect to slow activation and to the presence of slow but detectable desensitisation (Laha *et al*., 2013).

For a channel in the nicotinic superfamily, ELIC activates remarkably slowly in response to agonists, with a limiting on-relaxation time constant of about 10 ms to high concentrations of propylamine. ELIC is known to activate slowly in response to other agonists, such as cysteamine, for which values reported for the limiting time constant of activation range from 20 to 85 ms, in experimental conditions comparable to ours (eg rapid agonist application to outside-out patches) (Zimmermann and Dutzler, 2011; Zimmermann *et al*., 2012; Gonzalez-Gutierrez *et al*., 2012; Laha *et al*., 2013). Activation is known to be slow also for the other prokaryotic model channel, GLIC, with limiting time constants between 10 and 150 ms (Gonzalez-Gutierrez *et al*., 2012; Laha *et al*., 2013; Velisetty and Chakrapani, 2012). Some of the variability may be due to differences in the divalent ions in the recording medium (Spurny *et al*.,2012; Zimmermann *et al*., 2012).

ELIC deactivation has a clearly sigmoidal time course. Detectably sigmoidal off-relaxations of agonist currents are reported for other channels in this superfamily, such as 5-HT3A receptors and indeed GLIC (Corradi *et al*., 2009; Velisetty and Chakrapani, 2012), suggesting that these channels can re-open with good efficacy once the agonist pulse is over when they have lost one or more of the full complement of agonist molecules bound. In contrast to that, muscle nicotinic channels have a very low probability of opening when partially liganded (eg monoliganded) and do not have a sigmoidal deactivation (Maconochie and Steinbach, 1998). Interestingly, at saturating propylamine, the ELIC current risetime is monoexponential. This suggests that the paths followed by the channel through activation and deactivation by saturating propylamine are different.

The initial phase of the off-relaxation of ELIC agonist currents is notable for the presence of a rebound current: this is likely to be due to the dissociation of agonist molecule from binding sites in the pore. The size of this current at 10 and 50 mM and the speed of its onset suggest a very low affinity, of the order of 200-300 mM. The expected decrease in the amplitude of single channel currents at the highest agonist concentrations is likely to be too small to be unambiguously detected in a channel like ELIC.

4.4.2 Single channel properties of ELIC

4.4.2.1 Amplitude of the ELIC single channel currents

Our single channel recordings confirm the report (Zimmermann and Dutzler, 2011) that ELIC channels open to a high main conductance. In our conditions (symmetrical K^+, 0.5 mM $Ba2^+$) the chord conductance of openings elicited by low propylamine concentrations was 147 pS, much higher than the values previously reported, which were measured using sodium as the permeant ion (84-96 pS, (Zimmermann and Dutzler, 2011)). However, the distributions of amplitudes for ELIC were complex and were well fitted using two Gaussian distributions for all patches. In each patch there was more than one conductance, with amplitude levels close to each other, making it hard to measure them unambiguously (by fitting Gaussians to the amplitude distribution). Hence, it was not possible to be sure that the different amplitude levels represented distinct conductance states that occurred reproducibly in the recordings. The mean open amplitude was 8.8 ± 0.40 pA in the 9 patches at 0.3-1 mM propylamine (range 7.0 to 11.3 pA). There was no obvious pattern to the occurrence of subconductances, and in particular no relation to agonist concentration.

4.4.2.2 Dwell-times distributions and P_{open} curve

ELIC receptor records, at first, were obtained in the cell-attached configuration, which showed ELIC single channel openings occurring in long groups and separated by long shuttings, irrespectively of the concentration of agonist used. Thus, for ELIC receptor recordings in cell attached configuration, was not possible to distinguish between clusters and bursts as channel activity presented a very similar appearance at all concentrations. All the putative clusters at any concentration have a high P_{open} (i.e. greater than 95%) and contain few short shuttings, in a manner similar to that of α2 GlyR (Krashia *et al*., 2011). Thus single channel recordings, in cell attached configuration, revealed no clear concentration dependence. We had also experimented with outside-out recordings, in an attempt to improve our success rate in obtaining recordings with channel activity and we serendipitously realised that a more pronounced concentration-dependence was detectable in these records. ELIC receptor in outside-out configuration showed bursts like activity at low agonist concentrations, while clusters were visible at high concentrations. We can speculate that the different single channel activity in the two configurations could be due to phosphorylation

which modulates desensitisation (Lohse, 1993), deactivation (Gentet and Clements, 2002) and open probability (Song and Huang, 1990).

Single channel experiments were performed in outside-out configuration at different concentration of propylamine (from 0.3 to 50mM) spanning the range from saturating propylamine to the lowest concentration at which was possible to collect a sufficient number of single channel events.

Apparent open period and apparent shut time distributions for ELIC were fitted with a mixture of probability density functions after imposing a resolution of 20-40 μs. The apparent open period distributions were well fitted with a maximum of three exponential components. The values of the time constants and areas of all three components remained relatively stable in the range of the agonist concentration tested (0.5 to 50mM, see table 3.5, section 3.2.2.3).

The mean open time was stable from 0.5 mM up to 10 mM propylamine (25 ms) and decreased to 13ms at 50mM propylamine. This analysis indicates that the activation mechanism of the ELIC must contain at least 3 open states. Their concentration dependence suggests that they have a different number of bound ELIC molecules and that the short openings correspond to a lower liganded open state, while the long openings come from fully liganded open state. Note that we need more than one open state at saturating agonist concentrations, which is unusual for channels in the nicotinic superfamily.

Burst activity was detected from 0.3mM to 5mM propylamine (but relatively few events were collected at 0.3 mM) and clusters at concentrations greater than 5 mM. Shut time distributions were fitted with a maximum of four exponential components. The time constants of the first three components were the most consistent across the different patches and concentrations, and the majority of the events belong to the shortest component (areas from 80% to 90%). The longer component become shorter as propylamine concentration is increased, suggesting that this is an intra-cluster component.

At concentrations greater than 5mM, an additional component of long shut intervals appears, and ranged from 100 ms to 10 s. Those intervals are likely to be sojourns in long lived desensitized states. The presence of those intervals can be exploited to establish the concentration dependence of the open probability of a ligand gated ion channel, because they divided the record into clusters of openings. We attempted to carry out this process in ELIC records, and identified stretches of openings that were terminated by long shut intervals and

were without double openings. Typically, we had very few of these long shut intervals in each patch and very few possible clusters (3 to 11). The choice of what to classify as an intercluster shut time was largely arbitrary, because we could not use any formal criteria to identify them (i.e. calculate a critical time interval between two exponential components to minimize misclassified shut interval number). We chose an arbitrary t_{crit}, so that the longest well defined exponential component in the shut time distributions was interpreted as arising within the cluster (as suggested by its dependence on concentration). The t_{crit} values for different concentrations were chosen so that gaps were classified as between clusters if longer than 100 ms at 10 mM, 50 ms at 50 mM and 10 ms at 100 mM. Cluster P_{open} values were calculated for all these three concentrations, and were found to be similar and above 96%. Despite considerable effort, we failed to obtain numbers of events usable in global fits at agonist concentrations lower than the macroscopic EC_{50} (0.5 mM). At EC_{50}, one would expect to be able to identify desensitised clusters, groups of openings where a single channel molecule opens at 50% open probability before entering a prolonged desensitised state. This proved impossible (cf. Fig.3.10A) and we failed to construct a concentration – P_{open} curve.

The other most striking features of ELIC single channel activity was the presence of more than one open state, persisting at a high agonist concentration. ELIC shares both this property and a relatively weak dependence of pattern of openings upon agonist concentration, with the homomeric α2 glycine receptor (Krashia *et al*., 2011).

At first sight, there are some similarities between the ELIC and α2 glycine receptor. The decay recorded from a short pulse of agonist, which should correspond to the mean burst length (at very low agonist concentration) is long, 40 ms for ELIC and 120 ms for α2 glycine receptor (Krashia *et al.*, 2011). Moreover the mean open time is high, (i.e. 25 ms at 0.5mM propylamine for ELIC and 13ms at 0.02 mM of glycine for the α2 glycine receptor (Krashia *et al*., 2011), cf 1 ms at 0.01 mM glycine for α1 GlyRs and 2 ms at 0.05 mM glycine for α3 GlyRs, respectively; (Marabelli *et al*., 2013; Beato *et al*., 2004). The long burst length and the long mean open time make it hard to reliably define a t_{crit} to classify activity as intercluster.

4.4.3 The fitted models

We attempted to fit ELIC single channel data with four types of models that are in general use to describe the behaviour of Cys-loop channels. The classical form of the simpler schemes, such as MWC, J&W and Flip, failed to describe the main properties of the

equilibrium single channel data that they were fitted to. Because of the presence of more than one component in the ELIC open time distributions at high propylamine, we modified these schemes by allowing fully liganded states to open to more than one state. This improved the quality of the dwell-time description only for J&W and Flip: in the case of Flip + Open (Scheme 3a), the improvement was substantial and the resulting fits were robust and consistent in their results across the three data sets, with a quality similar to that obtained by fitting the reduced primed scheme (Scheme 4). We then checked whether the results of the single channel analysis could predict the macroscopic current on and off relaxations obtained from independent experiments. Only the Primed and the Flip + Open schemes were found to give predictions that approached the observed macroscopic rise and decay times. However, the Flip +Open scheme was worse than the Primed scheme, in that its predicted onset was consistently too fast and its predicted deactivation too slow. The main difference between the primed and the Flip + Open mechanisms is that primed contains an additional fully-bound pre-opening intermediate (A_3F''). The connectivity of the primed scheme may accommodate the features of ELIC better by allowing a greater difference between the activation and deactivation paths than the simpler flip schemes.

The Primed scheme was originally introduced to represent independent movement in the two binding sites of muscle nicotinic receptor and allows different stability of the open states that stem from one or the other or both binding sites being primed (Mukhtasimova *et al*., 2009). On the other hand, the Flip scheme (Burzomato *et al.*, 2004) resembles MWC (Monod *et al.*, 1965), and depicts initial activation spreading as a concerted step (i.e., all the subunits move together) that simultaneously increases binding affinity at all sites. Reality may fall somewhere between these extremes of total independence (i.e., Primed) and infinite cooperativity (i.e., Flip), with some degree of site-to-site interaction, which may depend on the channel type and on whether the sites are adjacent (Rayes *et al.*, 2009). If the spread of activation across the sites is fast, the primed process may not be distinguishable from a concerted step, and Flip schemes may be sufficient to describe channel activation, because the recordings do not contain sufficient information to fit the Primed mechanism. Moreover, the Primed scheme can easily accommodate a different structural hypothesis compare to Flip, that of a series of conformational changes in the binding site that are made more likely by agonist binding. It is interesting to note that another relatively slowly activating channel, the startle disease mutant of the glycine channel α1K276Eβ, also requires fitting with a primed scheme, in this case an even more extreme form of the mechanism, with three fully bound

intermediates (Lape *et al*., 2012). Again, the difference in the mechanisms fitted to the different channels may be only superficial. It is not inconceivable that the more detailed primed mechanism with several layers of activation intermediates applies also to muscle nicotinic and glycine channels, but that these fast synaptic channels go through the independent priming steps so quickly that only concerted flip intermediates can be resolved. A more difficult question is whether we can identify a structural reason for the slowness of ELIC. It has been suggested that the Cys-loop vertebrate channels activate so quickly (most activate maximally in less than a millisecond), compared with GLIC, because their extracellular domain is more loosely packed, thanks to a polar fault in the hydrophobic core (Dellisanti *et al*., 2011). ELIC resembles GLIC in lacking the two polar residues that are present in the most of the fast channels (the exception are the α glycine subunits, which have hydrophobic residues in the homologous positions).

Our results highlight several features of ELIC activity: the channel opens slowly, visiting at least two pre-opening intermediates before reaching a high maximum P_{open}. Evidence for the number of agonist molecules bound at maximum P_{open} comes from the mechanism prediction of the slope of the whole-cell dose-response curve. In its high maximum P_{open}, ELIC resembles other homomeric nicotinic-type channels, such as all the glycine receptors (Beato *et al*., 2004; Burzomato *et al*., 2004; Krashia *et al*., 2011; Marabelli *et al*., 2013). Full ELIC activation is reached when at least three out of the five possible binding sites in the homomer are occupied by the agonist, a property of ELIC activation that is similar to the activation of α1 glycine receptors (Beato *et al*., 2004; Burzomato *et al*., 2004) and α7 nicotinic (Rayes *et al*., 2009).

Quantitative comparisons between the energy landscape of ELIC activation and those of other nicotinic type channels have to be done with caution, because the necessity of comparing fits of similar models obliges us to use flip model variants, as primed fits are no good for GlyR. The main interesting feature that emerges is a clear resemblance between ELIC and α2 GlyR, in that both channels have relatively poor flipping even when fully bound compared with α1, α3 or α1β, with maximum flipping equilibrium constants of 0.4 and 1 (for ELIC and α2, respectively) cf values of 8-11 for α1 and α3. Despite this disadvantaged flipping step (which resembles that seen with partial agonists on synaptic glycine receptors, cf taurine, (Lape *et al*., 2008), both ELIC and α2 open with maximum P_{open}, because of the high equilibrium constant for the most efficacious opening step (500 and 350, respectively).

In both cases this is largely due to a slow closing rate (120 and 370 s^{-1}, respectively, cf. 700 and 2400 for α1 and α3).

The overall agonist efficacy of the fully liganded receptor depends on the equilibrium constant for primed (*F'* and *F'')* and the equilibrium constant (*E'* and *E''*) for the open-shut reaction:

$$E_{eff} = \frac{E3`F3`+E3``F3``F3`}{F3`F3``+F3`+1} \qquad \text{[eq4.1]}$$

The effective efficacy of ELIC with propylamine as agonist was 107.

Channels that are well-behaved for kinetic analysis provide a concentration- P_{open} curve whose EC50 and slope are key in testing the adequacy of the fitted mechanisms, particularly in terms of the number of agonist molecules needed for full activation, the values of the binding rate constants and their dependence on the state of ligation. Because this was not possible for ELIC, we further tested the primed mechanism by examining its predictions of the results of independent experiments where we measured the time course of macroscopic currents and the mean burst length at low concentrations. This allowed us not only to validate the model fitted and its estimates, but also to gain insight into the cause of the difficulties that we encountered in our single channel analysis. The main problem was that ELIC bursts can terminate by desensitisation, a phenomenon described for other slow, high efficacy channels such as gain of function mutants of muscle nicotinics (Elenes *et al*., 2006). This leads to ambiguity in the classification of groups of openings as bursts or clusters. ELIC clusters are likely to contain few bursts and this leads to problems in measuring P_{open} for non-desensitised states, as shown in Figure 3.18. In addition to that, only the clusters that contain more than one burst will provide information on the interburst shut time duration, which is the observable counterpart of the association rate constant. It was therefore important to check that the rate constant values obtained from single channel fitting provided a good description of the on-relaxation of agonist currents at a range of concentrations. This is reassuring in terms of the accuracy of the results of our fits, and their robustness to ambiguities in classifying bursts and clusters.

How does the primed scheme account for the most distinctive properties of ELIC, such as the concentration dependence of burst length and the time course of the on-and off- relaxation? A useful way of making sense of results of the fits is shown in Figure 4.2B, where the

numbers near the arrows are transition probabilities calculated from the primed rate constants at 0.1 and 10 mM propylamine (10 mM values in bold).

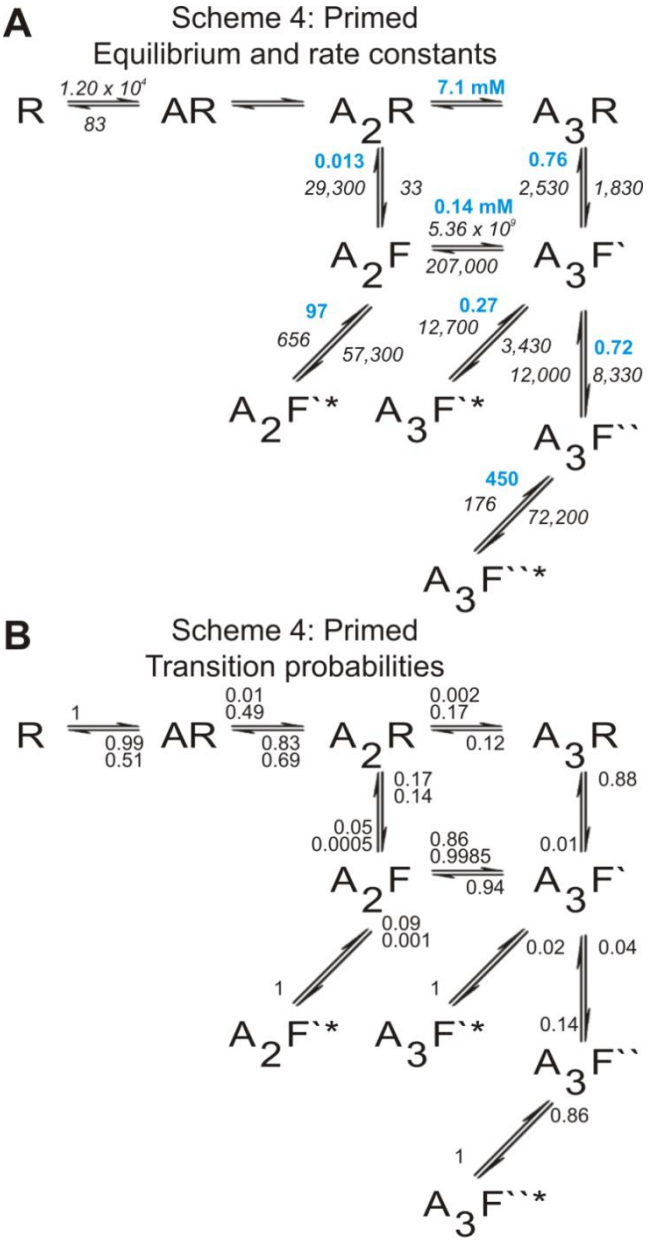

Figure 4.2 Summary of the Primed mechanism fitting results

A) Rate constants are in italic and equilibrium constants are in blue colour. Values of rates constants are means of three estimates and values of equilibrium constants are ratios of mean values (see also Table 3.9). The cycle in this mechanism obeyed microscopic reversibility in each separate fit but due to the averaging effect might not obey with the presented mean values. B) The transition arrows are marked with the transition probability between states. The probability values are shown for two concentrations- 0.1 and 10 mM (where the probability at 10 mM is in bold when different from that at 0.1 mM). The transition probabilities are calculated using the mean rate constants in panel A. The sum of probabilities of transitions leading out of each state is 1.

The concentration dependence of ELIC burst length at equilibrium arises mainly from the concentration dependence of the agonist binding to the primed state A2F' (in manner similar to that we described for α2 glycine receptors, (Krashia *et al*., 2011). Access to the main open state is via state $A_3F'^*$ and this is reached by a different route at low vs high concentrations. At the lower concentrations, route $A_2R \rightarrow A_2F' \rightarrow A_3F'$ is favoured over the alternative route $A_2R \rightarrow A_3R \rightarrow A_3F'$ (probabilities of 0.14 vs 0.0017, respectively at 100 μM propylamine). At 10 mM both routes have similar probabilities, 0.15 and 0.14, respectively.

The receptor exits state A_3F' almost exclusively by unbinding an agonist molecule to reach state A_2F' (probability 0.94). The probability of rebinding to this state is concentration dependent and the increasing number of oscillations between states A_2F' and A_3F' accounts for the burst length increase with rising agonist concentrations.

Wyllie et al. (1998) have shown that the time constants of macroscopic off-relaxations to zero agonist are the same of those of the single-channel equilibrium burst length distribution at low concentration. We have an apparent discrepancy for ELIC, given its overall deactivation time constant is 10-60 ms, and its mean burst length is 140 ms at the lowest agonist concentration that we could record. In this aspect, once again, ELIC closely resembles the α2 glycine receptor (Krashia *et al*., 2011). The primed model results allow us to estimate that it would be necessary to record ELIC activations at around 10 μM propylamine, in order to observe a mean burst length that matches the deactivation time constant.

At the end of the agonist concentration pulse, deactivation occurs almost exclusively via the return route $A_3F' \rightarrow A_2F' \rightarrow A_2R$ which has a probability of 0.32, 200-fold higher than the probability of the alternative route through the state A_3R. Because of that, although there can be no rebinding at zero agonist concentration, the receptor can open again. This is because the channel leaves state A_3F' through state A_2F', which can reopen to $A_2F'^*$ with probability 0.66 (at 0 mM). Because of the high efficacy (E_2' = 97) of this opening and the prolonged oscillations between states A_2F' and $A_2F'^*$, there can be significant opening at these partially bound states. The temporal accumulation of receptors in states A_2F' and $A_2F'^*$ on the deactivation path may accounts for the sigmoidal shape of the ELIC macroscopic response decay.

4.4.4 Conclusions

We have shown that it is possible to describe ELIC macroscopic and single channel activity with mechanistic schemes that are similar to those that are well-established for other channels in the superfamily. ELIC opens in response to the binding of at least three propylamine molecules with high maximum open probability. Activation is relatively slow, mainly because the channel is slow in undergoing the initial pre-opening conformational changes and the fully bound channel can open to two open states.

ELIC presents some useful features for experimental kinetics (high single channel conductance, activation slower than the technical limit of agonist solution exchange), but these are balanced by technical disadvantages. One clear difficulty arises from the long duration of activation bursts with respect to the duration of desensitised clusters. Consequently, each cluster contains at best few bursts and interburst intervals and that limits the information available on the binding steps in the reaction to single channel fitting. This made it especially important for us to validate the single channel model estimates against a wide range of data, including macroscopic current on-relaxations. This once again shows that obtaining full detailed activation mechanisms can be challenging when the channel is not in a fairly narrow ideal window for the values of the rate constants within the fitted scheme vs the desensitisation rates. Conceivably, the usefulness and accessibility of ELIC as a testing ground for work on the structure-function relation in nicotinic type channels would be increased by appropriate mutational engineering to shorten the burst length and obtain a channel that lends itself better to analysis.

Bibliography

Adams DJ, Dwyer TM, Hille B (1980) The permeability of endplate channels to monovalent and divalent metal cations. J Gen Physiol 75:493-510.

Akabas MH, Karlin A (1995) Identification of acetylcholine receptor channel-lining residues in the M1 segment of the alpha-subunit. Biochemistry-Us 34:12496-12500.

Akagi H, Hirai K, Hishinuma F (1991) Cloning of a glycine receptor subtype expressed in rat brain and spinal cord during a specific period of neuronal development. FEBS letters 281:160-166.

Akk G, Steinbach JH (2000) Structural elements near the C-terminus are responsible for changes in nicotinic receptor gating kinetics following patch excision. The Journal of physiology 527 Pt 3:405-417.

Aprison MH, Werman R (1965) The distribution of glycine in cat spinal cord and roots. Life sciences 4:2075-2083.

Araki T, Yamano M, Murakami T, Wanaka A, Betz H, Tohyama M (1988) Localization of glycine receptors in the rat central nervous system: an immunocytochemical analysis using monoclonal antibody. Neuroscience 25:613-624.

Auerbach A (2012) Thinking in cycles: MWC is a good model for acetylcholine receptor-channels. The Journal of physiology 590:93-98.

Baptista-Hon DT, Deeb TZ, Lambert JJ, Peters JA, Hales TG (2013) The minimum M3-M4 loop length of neurotransmitter-activated pentameric receptors is critical for the structural integrity of cytoplasmic portals. J Biol Chem 288:21558-21568.

Barberis A, Petrini EM, and Mozrzymas JW (2011). Impact of synaptic neurotransmitter concentration time course on the kinetics and pharmacological modulation of inhibitory synaptic currents. Frontiers in Cellular Neuroscience, vol. 5, article 6.

Beato M, Sivilotti LG (2007) Single-channel properties of glycine receptors of juvenile rat spinal motoneurones in vitro. J Physiol-London 580:497-506.

Beato M, Groot-Kormelink PJ, Colquhoun D, Sivilotti LG (2002) Openings of the rat recombinant alpha 1 homomeric glycine receptor as a function of the number of agonist molecules bound. J Gen Physiol 119:443-466.

Beato M, Groot-Kormelink PJ, Colquhoun D, Sivilotti LG (2004) The activation mechanism of alpha1 homomeric glycine receptors. J Neurosci 24:895-906.

Beene DL, Brandt GS, Zhong WG, Zacharias NM, Lester HA, Dougherty DA (2002) Cation-pi interactions in ligand recognition by serotonergic (5-HT3A) and nicotinic acetylcholine receptors: The anomalous binding properties of nicotine. Biochemistry-Us 41:10262-10269.

Betz H, Gomeza J, Armsen W, Scholze P, Eulenburg V (2006) Glycine transporters: essential regulators of synaptic transmission. Biochemical Society transactions 34:55-58.

Bocquet N, Nury H, Baaden M, Le Poupon C, Changeux JP, Delarue M, Corringer PJ (2009) X-ray structure of a pentameric ligand-gated ion channel in an apparently open conformation. Nature 457:111-114.

Bocquet N, de Carvalho LP, Cartaud J, Neyton J, Le Poupon C, Taly A, Grutter T, Changeux JP, Corringer PJ (2007) A prokaryotic proton-gated ion channel from the nicotinic acetylcholine receptor family. Nature 445:116-119.

Bondarenko V, Mowrey DD, Tillman TS, Seyoum E, Xu Y, Tang P (2013) NMR structures of the human alpha7 nAChR transmembrane domain and associated anesthetic binding sites. Biochimica et biophysica acta.

Bondarenko V, Mowrey D, Tillman T, Cui T, Liu LT, Xu Y, Tang P (2012) NMR structures of the transmembrane domains of the alpha4beta2 nAChR. Biochimica et biophysica acta 1818:1261-1268.

Bormann J (1986) Electrophysiology of single GABA receptor chloride channels. Clinical neuropharmacology 9 Suppl 4:386-388.

Bormann J, Hamill OP, Sakmann B (1987) Mechanism of anion permeation through channels gated by glycine and gamma-aminobutyric acid in mouse cultured spinal neurones. The Journal of physiology 385:243-286.

Bormann J, Rundstrom N, Betz H, Langosch D (1993) Residues within transmembrane segment M2 determine chloride conductance of glycine receptor homo- and hetero-oligomers. Embo J 12:3729-3737.

Bouzat C, Bren N, Sine SM (1994) Structural basis of the different gating kinetics of fetal and adult acetylcholine receptors. Neuron 13:1395-1402.

Bouzat C, Barrantes F, Sine S (2000) Nicotinic receptor fourth transmembrane domain: hydrogen bonding by conserved threonine contributes to channel gating kinetics. J Gen Physiol 115:663-672.

Bouzat C, Gumilar F, del Carmen Esandi M, Sine SM (2002) Subunit-selective contribution to channel gating of the M4 domain of the nicotinic receptor. Biophys J 82:1920-1929.

Brams M, Pandya A, Kuzmin D, van Elk R, Krijnen L, Yakel JL, Tsetlin V, Smit AB, Ulens C (2011) A structural and mutagenic blueprint for molecular recognition of strychnine and d-tubocurarine by different Cys-loop receptors. PLoS biology 9:e1001034.

Breitinger HG, Villmann C, Rennert J, Ballhausen D, Becker CM (2002) Hydroxylated residues influence desensitization behaviour of recombinant alpha3 glycine receptor channels. Journal of neurochemistry 83:30-36.

Brejc K, van Dijk WJ, Klaassen RV, Schuurmans M, van der Oost J, Smit AB, Sixma TK (2001) Crystal structure of an ACh-binding protein reveals the ligand-binding domain of nicotinic receptors. Nature 411:269-276.

Bristow DR, Bowery NG, Woodruff GN (1986) Light microscopic autoradiographic localisation of [3H]glycine and [3H]strychnine binding sites in rat brain. European journal of pharmacology 126:303-307.

Burzomato V, Groot-Kormelink PJ, Sivilotti LG, Beato M (2003) Stoichiometry of recombinant heteromeric glycine receptors revealed by a pore-lining region point mutation. Receptors & channels 9:353-361.

Burzomato V, Beato M, Groot-Kormelink PJ, Colquhoun D, Sivilotti LG (2004) Single-channel behavior of heteromeric alpha1beta glycine receptors: an attempt to detect a conformational change before the channel opens. J Neurosci 24:10924-10940.

Butler AS, Lindesay SA, Dover TJ, Kennedy MD, Patchell VB, Levine BA, Hope AG, Barnes NM (2009) Importance of the C-terminus of the human 5-HT3A receptor subunit. Neuropharmacology 56:292-302.

Callister RJ, Graham BA (2010) Early history of glycine receptor biology in Mammalian spinal cord circuits. Frontiers in molecular neuroscience 3:13.

Campos-Caro A, Sala S, Ballesta JJ, Vicente-Agullo F, Criado M, Sala F (1996) A single residue in the M2-M3 loop is a major determinant of coupling between binding and gating in neuronal nicotinic receptors. Proc Natl Acad Sci U S A 93:6118-6123.

Carland JE, Cooper MA, Sugiharto S, Jeong HJ, Lewis TM, Barry PH, Peters JA, Lambert JJ, Moorhouse AJ (2009) Characterization of the effects of charged residues in the intracellular loop on ion permeation in alpha1 glycine receptor channels. J Biol Chem 284:2023-2030.

Castaldo P, Stefanoni P, Miceli F, Coppola G, Del Giudice EM, Bellini G, Pascotto A, Trudell JR, Harrison NL, Annunziato L, Taglialatela M (2004) A novel hyperekplexia-causing mutation in the pre-transmembrane segment 1 of the human glycine receptor alpha1 subunit reduces membrane expression and impairs gating by agonists. J Biol Chem 279:25598-25604.

Celić A, Martin NP, Son CD, Becker JM, Naider F, Dumont ME (2003) Sequences in the intracellular loops of the yeast pheromone receptor Ste2p required for G protein activation. Biochemistry-Us 42:3004-3017.

Celie PH, van Rossum-Fikkert SE, van Dijk WJ, Brejc K, Smit AB, Sixma TK (2004) Nicotine and carbamylcholine binding to nicotinic acetylcholine receptors as studied in AChBP crystal structures. Neuron 41:907-914.

Chakrapani S, Bailey TD, Auerbach A (2003) The role of loop 5 in acetylcholine receptor channel gating. J Gen Physiol 122:521-539.

Chakrapani S, Bailey TD, Auerbach A (2004) Gating dynamics of the acetylcholine receptor extracellular domain. J Gen Physiol 123:341-356.

Chattipakorn SC, McMahon LL (2002) Pharmacological characterization of glycine-gated chloride currents recorded in rat hippocampal slices. Journal of neurophysiology 87:1515-1525.

Chen X, Webb TI, Lynch JW (2009) The M4 transmembrane segment contributes to agonist efficacy differences between alpha1 and alpha3 glycine receptors. Molecular membrane biology 26:321-332.

Christie SB, Li RW, Miralles CP, Riquelme R, Yang BY, Wendou-Yu CE, Daniels SB, Cantino ME and De Blas AL (2002). Synaptic and extrasynaptic $GABA_A$ receptors and gephyrin clusters. Prog. Brain Res. 136, 157–180.

Clapham DE, Neher E (1984) Substance-P Reduces Acetylcholine-Induced Currents in Isolated Bovine Chromaffin Cells. J Physiol-London 347:255-277.

Collins T, Millar NS (2010) Nicotinic acetylcholine receptor transmembrane mutations convert ivermectin from a positive to a negative allosteric modulator. Mol Pharmacol 78:198-204.

Colquhoun D, Sakmann B (1985) Fast Events in Single-Channel Currents Activated by Acetylcholine and Its Analogs at the Frog-Muscle Endplate. J Physiol-London 369:501-&.

Colquhoun D, Ogden DC (1988) Activation of ion channels in the frog end-plate by high concentrations of acetylcholine. The Journal of physiology 395:131-159.

Colquhoun D, Hawkes AG (1990) Stochastic Properties of Ion Channel Openings and Bursts in a Membrane Patch That Contains 2 Channels - Evidence Concerning the Number of Channels Present When a Record Containing Only Single Openings Is Observed. Proc R Soc Ser B-Bio 240:453-477.

Colquhoun D, Hawkes AG, Srodzinski K (1996) Joint distributions of apparent open and shut times of single-ion channels and maximum likelihood fitting of mechanisms. Philos T R Soc A 354:2555-2590.

Colquhoun D, Hatton CJ, Hawkes AG (2003) The quality of maximum likelihood estimates of ion channel rate constants. J Physiol-London 547:699-728.

Colquhoun D, Dowsland KA, Beato M, Plested AJ (2004) How to impose microscopic reversibility in complex reaction mechanisms. Biophys J 86:3510-3518.

Colquhoun DaS, F. J. (1995) Fitting and statistical analysis of single-channel records. *Single-Channel Recording* Plenum Press, New York:438- 587.

Corradi J, Gumilar F, Bouzat C (2009) Single-Channel Kinetic Analysis for Activation and Desensitization of Homomeric 5-HT(3)A Receptors. Biophys J 97:1335-1345.

Corringer PJ, Le Novere N, Changeux JP (2000) Nicotinic receptors at the amino acid level. Annual review of pharmacology and toxicology 40:431-458.

Corringer PJ, Bertrand S, Galzi JL, Devillers-Thiery A, Changeux JP, Bertrand D (1999) Mutational analysis of the charge selectivity filter of the alpha7 nicotinic acetylcholine receptor. Neuron 22:831-843.

Crook J, Hendrickson A, Robinson FR (2006) Co-localization of glycine and gaba immunoreactivity in interneurons in Macaca monkey cerebellar cortex. Neuroscience 141:1951-1959.

Curtis DR, Hosli L, Johnston GA (1967) Inhibition of Spinal Neurones by Glycine. Nature 215:1502-1503.

Curtis DR, Hosli L, Johnston GA, Johnston IH (1968) Hyperpolarization of Spinal Motoneurones by Glycine and Related Amino Acids. Exp Brain Res 5:235-&.

Cymes GD, Grosman C (2008) Pore-opening mechanism of the nicotinic acetylcholine receptor evinced by proton transfer. Nature structural & molecular biology 15:389-396.

Cymes GD, Ni Y, Grosman C (2005) Probing ion-channel pores one proton at a time. Nature 438:975-980.

Czajkowski C (2005) Neurobiology - Triggers for channel opening. Nature 438:167-168.

Dang H, England PM, Farivar SS, Dougherty DA, Lester HA (2000) Probing the role of a conserved M1 proline residue in 5-hydroxytryptamine(3) receptor gating. Mol Pharmacol 57:1114-1122.

Dani JA, Eisenman G (1987) Monovalent and divalent cation permeation in acetylcholine receptor channels. Ion transport related to structure. J Gen Physiol 89:959-983.

Davies PA, Wang W, Hales TG, Kirkness EF (2003) A novel class of ligand-gated ion channel is activated by Zn2+. J Biol Chem 278:712-717.

Del Castillo J, Katz B (1957) Interaction at end-plate receptors between different choline derivatives. Proceedings of the Royal Society of London Series B, Containing papers of a Biological character Royal Society 146:369-381.

Dellisanti CD, Hanson SM, Chen L, Czajkowski C (2011) Packing of the extracellular domain hydrophobic core has evolved to facilitate pentameric ligand-gated ion channel function. J Biol Chem 286:3658-3670.

Dellisanti CD, Yao Y, Stroud JC, Wang ZZ, Chen L (2007) Crystal structure of the extracellular domain of nAChR alpha1 bound to alpha-bungarotoxin at 1.94 A resolution. Nature neuroscience 10:953-962.

Delpire E (2000) Cation-Chloride Cotransporters in Neuronal Communication. News in physiological sciences : an international journal of physiology produced jointly by the International Union of Physiological Sciences and the American Physiological Society 15:309-312.

Devignot V, Prado de Carvalho L, Bregestovski P, Goblet C (2003) A novel glycine receptor alpha Z1 subunit variant in the zebrafish brain. Neuroscience 122:449-457.

Dieudonne S (1995) Glycinergic synaptic currents in Golgi cells of the rat cerebellum. Proc Natl Acad Sci U S A 92:1441-1445.

Dumba JS, Irish PS, Anderson NL, Westrum LE (1998) Electron microscopic analysis of gamma-aminobutyric acid and glycine colocalization in rat trigeminal subnucleus caudalis. Brain research 806:16-25.

Dumoulin A, Triller A, Dieudonne S (2001) IPSC kinetics at identified GABAergic and mixed GABAergic and glycinergic synapses onto cerebellar Golgi cells. J Neurosci 21:6045-6057.

Dumoulin A, Rostaing P, Bedet C, Levi S, Isambert MF, Henry JP, Triller A, Gasnier B (1999) Presence of the vesicular inhibitory amino acid transporter in GABAergic and glycinergic synaptic terminal boutons. Journal of cell science 112 (Pt 6):811-823.

Dupre ML, Broyles JM, Mihic SJ (2007) Effects of a mutation in the TM2-TM3 linker region of the glycine receptor alpha1 subunit on gating and allosteric modulation. Brain research 1152:1-9.

Durisic N, Godin AG, Wever CM, Heyes CD, Lakadamyali M, Dent JA (2012) Stoichiometry of the human glycine receptor revealed by direct subunit counting. J Neurosci 32:12915-12920.

Edmonds B, Gibb AJ, Colquhoun D (1995) Mechanisms of Activation of Muscle Nicotinic Acetylcholine-Receptors and the Time-Course of End-Plate Currents. Annu Rev Physiol 57:469-493.

Ehrlich I, Lohrke S, Friauf E (1999) Shift from depolarizing to hyperpolarizing glycine action in rat auditory neurones is due to age-dependent Cl- regulation. The Journal of physiology 520 Pt 1:121-137.

Elenes S, Ni Y, Cymes GD, Grosman C (2006) Desensitization contributes to the synaptic response of gain-of-function mutants of the muscle nicotinic receptor. J Gen Physiol 128:615-627.

Elmslie FV, Hutchings SM, Spencer V, Curtis A, Covanis T, Gardiner RM, Rees M (1996) Analysis of GLRA1 in hereditary and sporadic hyperekplexia: a novel mutation in a family cosegregating for hyperekplexia and spastic paraparesis. Journal of medical genetics 33:435-436.

Ernst M, Brauchart D, Boresch S, Sieghart W (2003) Comparative modeling of GABA(A) receptors: limits, insights, future developments. Neuroscience 119:933-943.

Filippova N, Wotring VE, Weiss DS (2004) Evidence that the TM1-TM2 loop contributes to the r_1 GABA receptor pore. J Biol Chem 279:20906-20914.

Finer-Moore J, Stroud RM (1984) Amphipathic analysis and possible formation of the ion channel in an acetylcholine receptor. Proc Natl Acad Sci U S A 81:155-159.

Fredkin DR, Rice JA (1985) Aggregated Markov-Processes and Channel Gating Kinetics. J Res Nat Bur Stand 90:517-520.

Fujita M, Sato K, Sato M, Inoue T, Kozuka T, Tohyama M (1991) Regional distribution of the cells expressing glycine receptor beta subunit mRNA in the rat brain. Brain research 560:23-37.

Galzi JL, Changeux JP (1995) Neuronal Nicotinic Receptors - Molecular-Organization and Regulations. Neuropharmacology 34:563-582.

Galzi JL, Devillers-Thiery A, Hussy N, Bertrand S, Changeux JP, Bertrand D (1992) Mutations in the channel domain of a neuronal nicotinic receptor convert ion selectivity from cationic to anionic. Nature 359:500-505.

Gao F, Bren N, Burghardt TP, Hansen S, Henchman RH, Taylor P, McCammon JA, Sine SM (2005) Agonist-mediated conformational changes in acetylcholine-binding protein revealed by simulation and intrinsic tryptophan fluorescence. J Biol Chem 280:8443-8451.

Garcia-Alcocer G, Mejia C, Berumen LC, Miledi R, Martinez-Torres A (2008) Developmental expression of glycine receptor subunits in rat cerebellum. International journal of developmental neuroscience : the official journal of the International Society for Developmental Neuroscience 26:319-322.

Gee VJ, Kracun S, Cooper ST, Gibb AJ, Millar NS (2007) Identification of domains influencing assembly and ion channel properties in alpha 7 nicotinic receptor and 5-HT3 receptor subunit chimaeras. British journal of pharmacology 152:501-512.

Gentet LJ, Clements JD (2002) Binding site stoichiometry and the effects of phosphorylation on human alpha1 homomeric glycine receptors. The Journal of physiology 544:97-106.

Gonzalez-Gutierrez G, Grosman C (2010) Bridging the gap between structural models of nicotinic receptor superfamily ion channels and their corresponding functional states. Journal of molecular biology 403:693-705.

Gonzalez-Gutierrez G, Lukk T, Agarwal V, Papke D, Nair SK, Grosman C (2012) Mutations that stabilize the open state of the Erwinia chrisanthemi ligand-gated ion channel fail to change the conformation of the pore domain in crystals. Proc Natl Acad Sci U S A 109:6331-6336.

Graham D, Pfeiffer F, Simler R, Betz H (1985) Purification and characterization of the glycine receptor of pig spinal cord. Biochemistry-Us 24:990-994.

Greenfield LJ, Jr., Zaman SH, Sutherland ML, Lummis SC, Niemeyer MI, Barnard EA, Macdonald RL (2002) Mutation of the GABAA receptor M1 transmembrane proline increases GABA affinity and reduces barbiturate enhancement. Neuropharmacology 42:502-521.

Grenningloh G, Pribilla I, Prior P, Multhaup G, Beyreuther K, Taleb O, Betz H (1990a) Cloning and expression of the 58 kd beta subunit of the inhibitory glycine receptor. Neuron 4:963-970.

Grenningloh G, Rienitz A, Schmitt B, Methfessel C, Zensen M, Beyreuther K, Gundelfinger ED, Betz H (1987) The Strychnine-Binding Subunit of the Glycine Receptor Shows Homology with Nicotinic Acetylcholine-Receptors. Nature 328:215-220.

Grenningloh G, Schmieden V, Schofield PR, Seeburg PH, Siddique T, Mohandas TK, Becker CM, Betz H (1990b) Alpha-Subunit Variants of the Human Glycine Receptor - Primary Structures, Functional Expression and Chromosomal Localization of the Corresponding Genes. Embo J 9:771-776.

Groot-Kormelink PJ, Beato M, Finotti C, Harvey RJ, Sivilotti LG (2002) Achieving optimal expression for single channel recording: a plasmid ratio approach to the expression of alpha 1 glycine receptors in HEK293 cells. J Neurosci Meth 113:207-214.

Grosman C, Zhou M, Auerbach A (2000a) Mapping the conformational wave of acetylcholine receptor channel gating. Nature 403:773-776.

Grosman C, Salamone FN, Sine SM, Auerbach A (2000b) The extracellular linker of muscle acetylcholine receptor channels is a gating control element. J Gen Physiol 116:327-340.

Grudzinska J, Schemm R, Haeger S, Nicke A, Schmalzing G, Betz H, Laube B (2005) The beta subunit determines the ligand binding properties of synaptic glycine receptors. Neuron 45:727-739.

Grutter T, Prado de Carvalho L, Le Novere N, Corringer PJ, Edelstein S, Changeux JP (2003) An H-bond between two residues from different loops of the acetylcholine binding site contributes to the activation mechanism of nicotinic receptors. Embo J 22:1990-2003.

Guzman GR, Santiago J, Ricardo A, Marti-Arbona R, Rojas LV, Lasalde-Dominicci JA (2003) Tryptophan scanning mutagenesis in the alphaM3 transmembrane domain of the Torpedo californica acetylcholine receptor: functional and structural implications. Biochemistry-Us 42:12243-12250.

Hales TG, Dunlop JI, Deeb TZ, Carland JE, Kelley SP, Lambert JJ, Peters JA (2006) Common determinants of single channel conductance within the large cytoplasmic loop of 5-hydroxytryptamine type 3 and alpha4beta2 nicotinic acetylcholine receptors. J Biol Chem 281:8062-8071.

Hamill OP, Bormann J, Sakmann B (1983) Activation of multiple-conductance state chloride channels in spinal neurones by glycine and GABA. Nature 305:805-808.

Handford CA, Lynch JW, Baker E, Webb GC, Ford JH, Sutherland GR, Schofield PR (1996) The human glycine receptor beta subunit: primary structure, functional characterisation and chromosomal localisation of the human and murine genes. Brain research Molecular brain research 35:211-219.

Hansen SB, Sulzenbacher G, Huxford T, Marchot P, Taylor P, Bourne Y (2005) Structures of Aplysia AChBP complexes with nicotinic agonists and antagonists reveal distinctive binding interfaces and conformations. Embo J 24:3635-3646.

Harvey RJ, Schmieden V, Von Holst A, Laube B, Rohrer H, Betz H (2000) Glycine receptors containing the alpha4 subunit in the embryonic sympathetic nervous system, spinal cord and male genital ridge. The European journal of neuroscience 12:994-1001.

Harvey RJ, Depner UB, Wassle H, Ahmadi S, Heindl C, Reinold H, Smart TG, Harvey K, Schutz B, Abo-Salem OM, Zimmer A, Poisbeau P, Welzl H, Wolfer DP, Betz H, Zeilhofer HU, Muller

U (2004) GlyR alpha 3: An essential target for spinal PGE(2)-mediated inflammatory pain sensitization. Science 304:884-887.

Harvey VL, Caley A, Muller UC, Harvey RJ, Dickenson AH (2009) A Selective Role for alpha3 Subunit Glycine Receptors in Inflammatory Pain. Frontiers in molecular neuroscience 2:14.

Hassaine G, Deluz C, Grasso L, Wyss R, Tol MB, Hovius R, Graff A, Stahlberg H, Tomizaki T, Desmyter A, Moreau C, Li XD, Poitevin F, Vogel H, Nury H (2014) X-ray structure of the mouse serotonin 5-HT3 receptor. Nature 512:276-281.

Hawkes AG, Jalali A, Colquhoun D (1990) The Distributions of the Apparent Open Times and Shut Times in a Single Channel Record When Brief Events Cannot Be Detected. Philos T Roy Soc A 332:511-538.

Hawkes AG, Jalali A, Colquhoun D (1992) Asymptotic Distributions of Apparent Open Times and Shut Times in a Single Channel Record Allowing for the Omission of Brief Events. Philos T Roy Soc B 337:383-404.

Heindl C, Brune K, Renner B (2007) Kinetics and functional characterization of the glycine receptor alpha2 and alpha3 subunit. Neuroscience letters 429:59-63.

Hibbs RE, Gouaux E (2011) Principles of activation and permeation in an anion-selective Cys-loop receptor. Nature 474:54-U80.

Hibbs RE, Sulzenbacher G, Shi J, Talley TT, Conrod S, Kem WR, Taylor P, Marchot P, Bourne Y (2009) Structural determinants for interaction of partial agonists with acetylcholine binding protein and neuronal alpha7 nicotinic acetylcholine receptor. Embo J 28:3040-3051.

Hilf RJ, Dutzler R (2008) X-ray structure of a prokaryotic pentameric ligand-gated ion channel. Nature 452:375-379.

Hilf RJ, Dutzler R (2009) Structure of a potentially open state of a proton-activated pentameric ligand-gated ion channel. Nature 457:115-118.

Houston CM, Bright DP, Sivilotti LG, Beato M, Smart TG (2009) Intracellular chloride ions regulate the time course of GABA-mediated inhibitory synaptic transmission. J Neurosci 29:10416-10423.

Hubner CA, Stein V, Hermans-Borgmeyer I, Meyer T, Ballanyi K, Jentsch TJ (2001) Disruption of KCC2 reveals an essential role of K-Cl cotransport already in early synaptic inhibition. Neuron 30:515-524.

Imoto K, Busch C, Sakmann B, Mishina M, Konno T, Nakai J, Bujo H, Mori Y, Fukuda K, Numa S (1988) Rings of negatively charged amino acids determine the acetylcholine receptor channel conductance. Nature 335:645-648.

Jackson MB, Wong BS, Morris CE, Lecar H, Christian CN (1983) Successive Openings of the Same Acetylcholine-Receptor Channel Are Correlated in Open Time. Biophys J 42:109-114.

Jadey S, Auerbach A (2012) An integrated catch-and-hold mechanism activates nicotinic acetylcholine receptors. J Gen Physiol 140:17-28.

Jansen M, Bali M, Akabas MH (2008) Modular design of Cys-loop ligand-gated ion channels: functional 5-HT3 and GABA rho1 receptors lacking the large cytoplasmic M3M4 loop. J Gen Physiol 131:137-146.

Jonas P, Bischofberger J, Sandkuhler J (1998) Corelease of two fast neurotransmitters at a central synapse. Science 281:419-424.

Jones MV, Westbrook GL (1995) Desensitized states prolong GABAA channel responses to brief agonist pulses. Neuron 15:181-191.

Karlin A (1967) On the application of "a plausible model" of allosteric proteins to the receptor for acetylcholine. Journal of theoretical biology 16:306-320.

Karlin A (2002) Emerging structure of the nicotinic acetylcholine receptors. Nat Rev Neurosci 3:102-114.

Karlsson U, Druzin M, Johansson S (2011) Cl(-) concentration changes and desensitization of GABA(A) and glycine receptors. J Gen Physiol 138:609-626.

Kash TL, Dizon MJF, Trudell JR, Harrison NL (2004) Charged residues in the b_2 subunit involved in $GABA_A$ receptor activation. J Biol Chem 279:4887-4893.

Kelley SP, Dunlop JI, Kirkness EF, Lambert JJ, Peters JA (2003) A cytoplasmic region determines single-channel conductance in 5-HT3 receptors. Nature 424:321-324.

Keramidas A, Harrison NL (2010) The activation mechanism of alpha1beta2gamma2S and alpha3beta3gamma2S GABAA receptors. J Gen Physiol 135:59-75.

Keramidas A, Moorhouse AJ, Schofield PR, Barry PH (2004) Ligand-gated ion channels: mechanisms underlying ion selectivity. Progress in biophysics and molecular biology 86:161-204.

Keramidas A, Moorhouse AJ, French CR, Schofield PR, Barry PH (2000) M2 pore mutations convert the glycine receptor channel from being anion- to cation-selective. Biophys J 79:247-259.

Kneussel M, Betz H (2000) Receptors, gephyrin and gephyrin-associated proteins: novel insights into the assembly of inhibitory postsynaptic membrane specializations. The Journal of physiology 525 Pt 1:1-9.

Kneussel M, Loebrich S (2007) Trafficking and synaptic anchoring of ionotropic inhibitory neurotransmitter receptors. Biology of the cell / under the auspices of the European Cell Biology Organization 99:297-309.

Krashia P, Lape R, Lodesani F, Colquhoun D, Sivilotti LG (2011) The long activations of alpha2 glycine channels can be described by a mechanism with reaction intermediates ("flip"). J Gen Physiol 137:197-216.

Krishtal OA, Pidoplichko VI (1980) A Receptor for Protons in the Nerve-Cell Membrane. Neuroscience 5:2325-2327.

Krupp J, Larmet Y, Feltz P (1994) Postnatal change of glycinergic IPSC decay in sympathetic preganglionic neurons. Neuroreport 5:2437-2440.

Kuhse J, Schmieden V, Betz H (1990) Identification and Functional Expression of a Novel Ligand-Binding Subunit of the Inhibitory Glycine Receptor. J Biol Chem 265:22317-22320.

Kuhse J, Laube B, Magalei D, Betz H (1993) Assembly of the inhibitory glycine receptor: identification of amino acid sequence motifs governing subunit stoichiometry. Neuron 11:1049-1056.

Kuhse J, Kuryatov A, Maulet Y, Malosio ML, Schmieden V, Betz H (1991) Alternative splicing generates two isoforms of the alpha 2 subunit of the inhibitory glycine receptor. FEBS letters 283:73-77.

Laha KT, Ghosh B, Czajkowski C (2013) Macroscopic kinetics of pentameric ligand gated ion channels: comparisons between two prokaryotic channels and one eukaryotic channel. PloS one 8:e80322.

Langosch D, Thomas L, Betz H (1988) Conserved Quaternary Structure of Ligand-Gated Ion Channels - the Postsynaptic Glycine Receptor Is a Pentamer. P Natl Acad Sci USA 85:7394-7398.

Langosch D, Laube B, Rundstrom N, Schmieden V, Bormann J, Betz H (1994) Decreased Agonist Affinity and Chloride Conductance of Mutant Glycine Receptors Associated with Human Hereditary Hyperekplexia. Embo J 13:4223-4228.

Lape R, Colquhoun D, Sivilotti LG (2008) On the nature of partial agonism in the nicotinic receptor superfamily. Nature 454:722-727.

Lape R, Krashia P, Colquhoun D, Sivilotti LG (2009) Agonist and blocking actions of choline and tetramethylammonium on human muscle acetylcholine receptors. The Journal of physiology 587:5045-5072.

Lape R, Plested AJ, Moroni M, Colquhoun D, Sivilotti LG (2012) The alpha1K276E startle disease mutation reveals multiple intermediate states in the gating of glycine receptors. J Neurosci 32:1336-1352.

Lasalde JA, Tamamizu S, Butler DH, Vibat CR, Hung B, McNamee MG (1996) Tryptophan substitutions at the lipid-exposed transmembrane segment M4 of Torpedo californica acetylcholine receptor govern channel gating. Biochemistry-Us 35:14139-14148.

Law RJ, Henchman RH, McCammon JA (2005) A gating mechanism proposed from a simulation of a human alpha7 nicotinic acetylcholine receptor. Proc Natl Acad Sci U S A 102:6813-6818.

Le Novere N, Changeux JP (1999) The Ligand Gated Ion Channel Database. Nucleic acids research 27:340-342.

Lee WY, Sine SM (2004) Invariant aspartic Acid in muscle nicotinic receptor contributes selectively to the kinetics of agonist binding. J Gen Physiol 124:555-567.

Lee WY, Sine SM (2005) Principal pathway coupling agonist binding to channel gating in nicotinic receptors. Nature 438:243-247.

Leffler JE (1953) Parameters for the Description of Transition States. Science 117:340-341.

Leffler JE, Grunwald E (1963) Rates and Equilibria of Organic Reactions Wiley.

Legendre P (2001) The glycinergic inhibitory synapse. Cell Mol Life Sci 58:760-793.

Legendre P, Ali DW, Drapeau P (2000) Recovery from open channel block by acetylcholine during neuromuscular transmission in zebrafish. J Neurosci 20:140-148.

Leonard RJ, Labarca CG, Charnet P, Davidson N, Lester HA (1988) Evidence that the M2 membrane-spanning region lines the ion channel pore of the nicotinic receptor. Science 242:1578-1581.

Lewis TM, Sivilotti LG, Colquhoun D, Gardiner RM, Schoepfer R, Rees M (1998) Properties of human glycine receptors containing the hyperekplexia mutation alpha1(K276E), expressed in Xenopus oocytes. The Journal of physiology 507 (Pt 1):25-40.

Livesey MR, Cooper MA, Deeb TZ, Carland JE, Kozuska J, Hales TG, Lambert JJ, Peters JA (2008) Structural determinants of Ca2+ permeability and conduction in the human 5-hydroxytryptamine type 3A receptor. J Biol Chem 283:19301-19313.

Lobitz N, Gisselmann G, Hatt H, Wetzel CH (2001) A single amino-acid in the TM1 domain is an important determinant of the desensitization kinetics of recombinant human and guinea pig alpha-homomeric 5-hydroxytryptamine type 3 receptors. Mol Pharmacol 59:844-851.

Lobo IA, Mascia MP, Trudell JR, Harris RA (2004) Channel gating of the glycine receptor changes accessibility to residues implicated in receptor potentiation by alcohols and anesthetics. J Biol Chem 279:33919-33927.

Lohse MJ (1993) Molecular mechanisms of membrane receptor desensitization. Biochimica et biophysica acta 1179:171-188.

Lummis SCR, Beene DL, Harrison NJ, Lester HA, Dougherty DA (2005) A cation-pi binding interaction with a tyrosine in the binding site of the GABA(C) receptor. Chem Biol 12:993-997.

Lynch JW (2004) Molecular structure and function of the glycine receptor chloride channel. Physiol Rev 84:1051-1095.

Lynch JW (2009) Native glycine receptor subtypes and their physiological roles. Neuropharmacology 56:303-309.

Lynch JW, Rajendra S, Barry PH, Schofield PR (1995) Mutations affecting the glycine receptor agonist transduction mechanism convert the competitive antagonist, picrotoxin, into an allosteric potentiator. J Biol Chem 270:13799-13806.

Lynch JW, Jacques P, Pierce KD, Schofield PR (1998) Zinc potentiation of the glycine receptor chloride channel is mediated by allosteric pathways. Journal of neurochemistry 71:2159-2168.

Lynch JW, Rajendra S, Pierce KD, Handford CA, Barry PH, Schofield PR (1997) Identification of intracellular and extracellular domains mediating signal transduction in the inhibitory glycine receptor chloride channel. Embo J 16:110-120.

Ma DJ, Liu ZW, Li L, Tang P, Xu Y (2005) Structure and dynamics of the second and third transmembrane domains of human glycine receptor. Biochemistry-Us 44:8790-8800.

Maconochie DJ, Steinbach JH (1995) Block by acetylcholine of mouse muscle nicotinic receptors, stably expressed in fibroblasts. J Gen Physiol 106:113-147.

Maconochie DJ, Steinbach JH (1998) The channel opening rate of adult- and fetal-type mouse muscle nicotinic receptors activated by acetylcholine. The Journal of physiology 506 (Pt 1):53-72.

Magleby KL, Pallotta BS (1983) Burst Kinetics of Single Calcium-Activated Potassium Channels in Cultured Rat Muscle. J Physiol-London 344:605-623.

Malosio ML, Marquezepouey B, Kuhse J, Betz H (1991a) Widespread Expression of Glycine Receptor Subunit Messenger-Rnas in the Adult and Developing Rat-Brain. Embo J 10:2401-2409.

Malosio ML, Grenningloh G, Kuhse J, Schmieden V, Schmitt B, Prior P, Betz H (1991b) Alternative splicing generates two variants of the alpha 1 subunit of the inhibitory glycine receptor. J Biol Chem 266:2048-2053.

Mangin JM, Baloul M, Prado De Carvalho L, Rogister B, Rigo JM, Legendre P (2003) Kinetic properties of the alpha2 homo-oligomeric glycine receptor impairs a proper synaptic functioning. The Journal of physiology 553:369-386.

Marabelli A, Moroni M, Lape R, Sivilotti LG (2013) The kinetic properties of the alpha3 rat glycine receptor make it suitable for mediating fast synaptic inhibition. The Journal of physiology 591:3289-3308.

Matzenbach B, Maulet Y, Sefton L, Courtier B, Avner P, Guenet JL, Betz H (1994) Structural analysis of mouse glycine receptor alpha subunit genes. Identification and chromosomal localization of a novel variant. J Biol Chem 269:2607-2612.

Meier JC, Henneberger C, Melnick I, Racca C, Harvey RJ, Heinemann U, Schmieden V, Grantyn R (2005) RNA editing produces glycine receptor alpha3(P185L), resulting in high agonist potency. Nature neuroscience 8:736-744.

Melzer N, Villmann C, Becker K, Harvey K, Harvey RJ, Vogel N, Kluck CJ, Kneussel M, Becker CM (2010) Multifunctional basic motif in the glycine receptor intracellular domain induces subunit-specific sorting. J Biol Chem 285:3730-3739.

Meyer G, Kirsch J, Betz H, Langosch D (1995) Identification of a gephyrin binding motif on the glycine receptor beta subunit. Neuron 15:563-572.

Mihic SJ, Ye Q, Wick MJ, Koltchine VV, Krasowski MD, Finn SE, Mascia MP, Valenzuela CF, Hanson KK, Greenblatt EP, Harris RA, Harrison NL (1997) Sites of alcohol and volatile anaesthetic action on GABA(A) and glycine receptors. Nature 389:385-389.

Miller PS, Aricescu AR (2014) Crystal structure of a human GABAA receptor. Nature 512:270-275.

Miyazawa A, Fujiyoshi Y, Unwin N (2003) Structure and gating mechanism of the acetylcholine receptor pore. Nature 423:949-955.

Miyazawa A, Fujiyoshi Y, Stowell M, Unwin N (1999) Nicotinic acetylcholine receptor at 4.6 A resolution: transverse tunnels in the channel wall. Journal of molecular biology 288:765-786.

Monod J, Wyman J, Changeux JP (1965) On the Nature of Allosteric Transitions: A Plausible Model. Journal of molecular biology 12:88-118.

Moore MJ, Caspary DM (1983) Strychnine blocks binaural inhibition in lateral superior olivary neurons. J Neurosci 3:237-242.

Moroni M, Biro I, Giugliano M, Vijayan R, Biggin PC, Beato M, Sivilotti LG (2011) Chloride ions in the pore of glycine and GABA channels shape the time course and voltage dependence of agonist currents. J Neurosci 31:14095-14106.

Mowrey DD, Cui T, Jia Y, Ma D, Makhov AM, Zhang P, Tang P, Xu Y (2013) Open-Channel Structures of the Human Glycine Receptor alpha1 Full-Length Transmembrane Domain. Structure.

Mukhtasimova N, Free C, Sine SM (2005) Initial coupling of binding to gating mediated by conserved residues in the muscle nicotinic receptor. J Gen Physiol 126:23-39.

Mukhtasimova N, Lee WY, Wang HL, Sine SM (2009) Detection and trapping of intermediate states priming nicotinic receptor channel opening. Nature 459:451-454.

Mulle C, Lena C, Changeux JP (1992) Potentiation of nicotinic receptor response by external calcium in rat central neurons. Neuron 8:937-945.

Nikolic Z, Laube B, Weber RG, Lichter P, Kioschis P, Poustka A, Mulhardt C, Becker CM (1998) The human glycine receptor subunit alpha3. Glra3 gene structure, chromosomal localization, and functional characterization of alternative transcripts. J Biol Chem 273:19708-19714.

Nury H, Bocquet N, Le Poupon C, Raynal B, Haouz A, Corringer PJ, Delarue M (2010) Crystal structure of the extracellular domain of a bacterial ligand-gated ion channel. Journal of molecular biology 395:1114-1127.

Paas Y, Gibor G, Grailhe R, Savatier-Duclert N, Dufresne V, Sunesen M, de Carvalho LP, Changeux JP, Attali B (2005) Pore conformations and gating mechanism of a Cys-loop receptor. Proc Natl Acad Sci U S A 102:15877-15882.

Pan J, Chen Q, Willenbring D, Yoshida K, Tillman T, Kashlan OB, Cohen A, Kong XP, Xu Y, Tang P (2012) Structure of the pentameric ligand-gated ion channel ELIC cocrystallized with its competitive antagonist acetylcholine. Nature communications 3:714.

Peters JA, Kelley SP, Dunlop JI, Kirkness EF, Hales TG, Lambert JJ (2004) The 5-hydroxytryptamine type 3 (5-HT3) receptor reveals a novel determinant of single-channel conductance. Biochemical Society transactions 32:547-552.

Pfeiffer F, Betz H (1981) Solubilization of the glycine receptor from rat spinal cord. Brain research 226:273-279.

Pfeiffer F, Graham D, Betz H (1982) Purification by affinity chromatography of the glycine receptor of rat spinal cord. J Biol Chem 257:9389-9393.

Picton AJ, Fisher JL (2007) Effect of the alpha subunit subtype on the macroscopic kinetic properties of recombinant GABA(A) receptors. Brain research 1165:40-49.

Pitt SJ, Sivilotti LG, Beato M (2008) High Intracellular Chloride Slows the Decay of Glycinergic Currents. J Neurosci 28:11454-11467.

Pless SA, Millen KS, Hanek AP, Lynch JW, Lester HA, Lummis SC, Dougherty DA (2008) A cation-pi interaction in the binding site of the glycine receptor is mediated by a phenylalanine residue. J Neurosci 28:10937-10942.

Plested AJ, Groot-Kormelink PJ, Colquhoun D, Sivilotti LG (2007) Single-channel study of the spasmodic mutation alpha1A52S in recombinant rat glycine receptors. The Journal of physiology 581:51-73.

Pourcho RG (1996) Neurotransmitters in the retina. Current eye research 15:797-803.

Probst A, Cortes R, Palacios JM (1986) The distribution of glycine receptors in the human brain. A light microscopic autoradiographic study using [3H]strychnine. Neuroscience 17:11-35.

Protti DA, Gerschenfeld HM, Llano I (1997) GABAergic and glycinergic IPSCs in ganglion cells of rat retinal slices. J Neurosci 17:6075-6085.

Purohit P, Mitra A, Auerbach A (2007) A stepwise mechanism for acetylcholine receptor channel gating. Nature 446:930-933.

Racca C, Gardiol A, Triller A (1997) Dendritic and postsynaptic localizations of glycine receptor alpha subunit mRNAs. J Neurosci 17:1691-1700.

Racca C, Gardiol A, Triller A (1998) Cell-specific dendritic localization of glycine receptor alpha subunit messenger RNAs. Neuroscience 84:997-1012.

Rajendra S, Lynch JW, Pierce KD, French CR, Barry PH, Schofield PR (1994) Startle disease mutations reduce the agonist sensitivity of the human inhibitory glycine receptor. J Biol Chem 269:18739-18742.

Rajendra S, Lynch JW, Pierce KD, French CR, Barry PH, Schofield PR (1995) Mutation of an arginine residue in the human glycine receptor transforms beta-alanine and taurine from agonists into competitive antagonists. Neuron 14:169-175.

Rayes D, De Rosa MJ, Sine SM, Bouzat C (2009) Number and locations of agonist binding sites required to activate homomeric Cys-loop receptors. J Neurosci 29:6022-6032.

Reichling DB, Kyrozis A, Wang J, MacDermott AB (1994) Mechanisms of GABA and glycine depolarization-induced calcium transients in rat dorsal horn neurons. The Journal of physiology 476:411-421.

Revah F, Bertrand D, Galzi JL, Devillers-Thiery A, Mulle C, Hussy N, Bertrand S, Ballivet M, Changeux JP (1991) Mutations in the channel domain alter desensitization of a neuronal nicotinic receptor. Nature 353:846-849.

Rivera C, Voipio J, Payne JA, Ruusuvuori E, Lahtinen H, Lamsa K, Pirvola U, Saarma M, Kaila K (1999) The K+/Cl- co-transporter KCC2 renders GABA hyperpolarizing during neuronal maturation. Nature 397:251-255.

Rovira JC, Vicente-Agullo F, Campos-Caro A, Criado M, Sala F, Sala S, Ballesta JJ (1999) Gating of alpha3beta4 neuronal nicotinic receptor can be controlled by the loop M2-M3 of both alpha3 and beta4 subunits. Pflugers Archiv : European journal of physiology 439:86-92.

Sakmann B, Patlak J, Neher E (1980) Single Acetylcholine-Activated Channels Show Burst-Kinetics in Presence of Desensitizing Concentrations of Agonist. Nature 286:71-73.

Sato K, Kiyama H, Tohyama M (1992) Regional distribution of cells expressing glycine receptor alpha 2 subunit mRNA in the rat brain. Brain research 590:95-108.

Sauguet L, Shahsavar A, Poitevin F, Huon C, Menny A, Nemecz A, Haouz A, Changeux JP, Corringer PJ, Delarue M (2014) Crystal structures of a pentameric ligand-gated ion channel provide a mechanism for activation. Proc Natl Acad Sci U S A 111:966-971.

Saul B, Kuner T, Sobetzko D, Brune W, Hanefeld F, Meinck HM, Becker CM (1999) Novel GLRA1 missense mutation (P250T) in dominant hyperekplexia defines an intracellular determinant of glycine receptor channel gating. J Neurosci 19:869-877.

Schmitt B, Knaus P, Becker CM, Betz H (1987) The Mr 93,000 polypeptide of the postsynaptic glycine receptor complex is a peripheral membrane protein. Biochemistry-Us 26:805-811.

Shiang R, Ryan SG, Zhu YZ, Hahn AF, O'Connell P, Wasmuth JJ (1993) Mutations in the alpha 1 subunit of the inhibitory glycine receptor cause the dominant neurologic disorder, hyperekplexia. Nature genetics 5:351-358.

Sieghart W (1995) Structure and pharmacology of gamma-aminobutyric acid A receptor subtypes. Pharmacological reviews 47:181-234.

Sine SM (2002) The nicotinic receptor ligand binding domain. Journal of neurobiology 53:431-446.

Sine SM, Claudio T, Sigworth FJ (1990) Activation of Torpedo acetylcholine receptors expressed in mouse fibroblasts. Single channel current kinetics reveal distinct agonist binding affinities. J Gen Physiol 96:395-437.

Singer JH, Talley EM, Bayliss DA, Berger AJ (1998) Development of glycinergic synaptic transmission to rat brain stem motoneurons. Journal of neurophysiology 80:2608-2620.

Sixma TK (2007) Nicotinic receptor structure emerging slowly. Nature neuroscience 10:937-938.

Sixma TK, Smit AB (2003) Acetylcholine binding protein (AChBP): A secreted glial protein that provides a high-resolution model for the extracellular domain of pentameric ligand-gated ion channels. Annu Rev Bioph Biom 32:311-334.

Song C, Corry B (2010) Ion conduction in ligand-gated ion channels: Brownian dynamics studies of four recent crystal structures. Biophys J 98:404-411.

Song YM, Huang LY (1990) Modulation of glycine receptor chloride channels by cAMP-dependent protein kinase in spinal trigeminal neurons. Nature 348:242-245.

Spitzmaul G, Corradi J, Bouzat C (2004) Mechanistic contributions of residues in the M1 transmembrane domain of the nicotinic receptor to channel gating. Molecular membrane biology 21:39-50.

Spurny R, Billen B, Howard RJ, Brams M, Debaveye S, Price KL, Weston DA, Strelkov SV, Tytgat J, Bertrand S, Bertrand D, Lummis SC, Ulens C (2013) Multisite binding of a general anesthetic to the prokaryotic pentameric Erwinia chrysanthemi ligand-gated ion channel (ELIC). J Biol Chem 288:8355-8364.

Spurny R, Ramerstorfer J, Price K, Brams M, Ernst M, Nury H, Verheij M, Legrand P, Bertrand D, Bertrand S, Dougherty DA, de Esch IJ, Corringer PJ, Sieghart W, Lummis SC, Ulens C (2012) Pentameric ligand-gated ion channel ELIC is activated by GABA and modulated by benzodiazepines. Proc Natl Acad Sci U S A 109:E3028-3034.

Stevens DR, Gerber U, McCarley RW, Greene RW (1996) Glycine-mediated inhibitory postsynaptic potentials in the medial pontine reticular formation of the rat in vitro. Neuroscience 73:791-796.

Sunesen M, de Carvalho LP, Dufresne V, Grailhe R, Savatier-Duclert N, Gibor G, Peretz A, Attali B, Changeux JP, Paas Y (2006) Mechanism of Cl- selection by a glutamate-gated chloride (GluCl) receptor revealed through mutations in the selectivity filter. J Biol Chem 281:14875-14881.

Takahashi T, Momiyama A (1991) Single-channel currents underlying glycinergic inhibitory postsynaptic responses in spinal neurons. Neuron 7:965-969.

Takahashi T, Momiyama A, Hirai K, Hishinuma F, Akagi H (1992) Functional correlation of fetal and adult forms of glycine receptors with developmental changes in inhibitory synaptic receptor channels. Neuron 9:1155-1161.

Tasneem A, Iyer LM, Jakobsson E, Aravind L (2005) Identification of the prokaryotic ligand-gated ion channels and their implications for the mechanisms and origins of animal Cys-loop ion channels. Genome biology 6:R4.

Thompson AJ, Lester HA, Lummis SC (2010) The structural basis of function in Cys-loop receptors. Quarterly reviews of biophysics 43:449-499.

Thompson AJ, Alqazzaz M, Ulens C, Lummis SC (2012) The pharmacological profile of ELIC, a prokaryotic GABA-gated receptor. Neuropharmacology 63:761-767.

Tia S, Wang JF, Kotchabhakdi N, Vicini S (1996) Distinct deactivation and desensitization kinetics of recombinant GABAA receptors. Neuropharmacology 35:1375-1382.

Todd AJ (1990) An electron microscope study of glycine-like immunoreactivity in laminae I-III of the spinal dorsal horn of the rat. Neuroscience 39:387-394.

Todd AJ (1996) GABA and glycine in synaptic glomeruli of the rat spinal dorsal horn. The European journal of neuroscience 8:2492-2498.

Todd AJ, Watt C, Spike RC, Sieghart W (1996) Colocalization of GABA, glycine, and their receptors at synapses in the rat spinal cord. J Neurosci 16:974-982.

Triller A, Cluzeaud F, Pfeiffer F, Betz H, Korn H (1985) Distribution of glycine receptors at central synapses: an immunoelectron microscopy study. The Journal of cell biology 101:683-688.

Ulens C, Hogg RC, Celie PH, Bertrand D, Tsetlin V, Smit AB, Sixma TK (2006) Structural determinants of selective alpha-conotoxin binding to a nicotinic acetylcholine receptor homolog AChBP. P Natl Acad Sci USA 103:3615-3620.

Unwin N (1995) Acetylcholine receptor channel imaged in the open state. Nature 373:37-43.

Unwin N (2005) Refined structure of the nicotinic acetylcholine receptor at 4A resolution. Journal of molecular biology 346:967-989.

Unwin N, Fujiyoshi Y (2012) Gating Movement of Acetylcholine Receptor Caught by Plunge-Freezing. Journal of molecular biology 422:617-634.

Unwin N, Miyazawa A, Li J, Fujiyoshi Y (2002) Activation of the nicotinic acetylcholine receptor involves a switch in conformation of the alpha subunits. Journal of molecular biology 319:1165-1176.

van den Pol AN, Gorcs T (1988) Glycine and glycine receptor immunoreactivity in brain and spinal cord. J Neurosci 8:472-492.

Van Hooft JA, Vijverberg HP (1995) Phosphorylation controls conductance of 5-HT3 receptor ligand-gated ion channels. Receptors & channels 3:7-12.

Velisetty P, Chakrapani S (2012) Desensitization mechanism in prokaryotic ligand-gated ion channel. J Biol Chem 287:18467-18477.

Verdoorn TA, Draguhn A, Ymer S, Seeburg PH, Sakmann B (1990) Functional properties of recombinant rat GABAA receptors depend upon subunit composition. Neuron 4:919-928.

Vernino S, Amador M, Luetje CW, Patrick J, Dani JA (1992) Calcium modulation and high calcium permeability of neuronal nicotinic acetylcholine receptors. Neuron 8:127-134.

Villmann C, Oertel J, Melzer N, Becker CM (2009) Recessive hyperekplexia mutations of the glycine receptor alpha1 subunit affect cell surface integration and stability. Journal of neurochemistry 111:837-847.

Wang HL, Cheng X, Sine SM (2012) Intramembrane proton binding site linked to activation of bacterial pentameric ion channel. J Biol Chem 287:6482-6489.

Wang HL, Milone M, Ohno K, Shen XM, Tsujino A, Batocchi AP, Tonali P, Brengman J, Engel AG, Sine SM (1999) Acetylcholine receptor M3 domain: stereochemical and volume contributions to channel gating. Nature neuroscience 2:226-233.

Webb TI, Lynch JW (2007) Molecular pharmacology of the glycine receptor chloride channel. Current pharmaceutical design 13:2350-2367.

Weiss DS, Magleby KL (1989) Gating Scheme for Single Gaba-Activated Cl- Channels Determined from Stability Plots, Dwell-Time Distributions, and Adjacent-Interval Durations. J Neurosci 9:1314-1324.

Werman R, Davidoff RA, Aprison MH (1967) Inhibition of Motoneurones by Iontophoresis of Glycine. Nature 214:681-&.

Werman R, Davidoff RA, Aprison MH (1968) Inhibitory of glycine on spinal neurons in the cat. Journal of neurophysiology 31:81-95.

Wilkins ME, Hosie AM, Smart TG (2005) Proton modulation of recombinant GABA(A) receptors: influence of GABA concentration and the beta subunit TM2-TM3 domain. The Journal of physiology 567:365-377.

Wilson G, Karlin A (2001) Acetylcholine receptor channel structure in the resting, open, and desensitized states probed with the substituted-cysteine-accessibility method. Proc Natl Acad Sci U S A 98:1241-1248.

Wu WL, Ziskind-Conhaim L, Sweet MA (1992) Early development of glycine- and GABA-mediated synapses in rat spinal cord. J Neurosci 12:3935-3945.

Wyllie DJ, Behe P, Colquhoun D (1998) Single-channel activations and concentration jumps: comparison of recombinant NR1a/NR2A and NR1a/NR2D NMDA receptors. The Journal of physiology 510 (Pt 1):1-18.

Xiu XA, Puskar NL, Shanata JAP, Lester HA, Dougherty DA (2009) Nicotine binding to brain receptors requires a strong cation-pi interaction. Nature 458:534-U510.

Ye JH (2008) Regulation of excitation by glycine receptors. Results and problems in cell differentiation 44:123-143.

Young AB, Snyder SH (1973) Strychnine binding associated with glycine receptors of the central nervous system. Proc Natl Acad Sci U S A 70:2832-2836.

Young GT, Zwart R, Walker AS, Sher E, Millar NS (2008) Potentiation of alpha7 nicotinic acetylcholine receptors via an allosteric transmembrane site. Proc Natl Acad Sci U S A 105:14686-14691.

Zarbin MA, Wamsley JK, Kuhar MJ (1981) Glycine receptor: light microscopic autoradiographic localization with [3H]strychnine. J Neurosci 1:532-547.

Zhang H, Karlin A (1997) Identification of acetylcholine receptor channel-lining residues in the M1 segment of the b-subunit. Biochemistry-Us 36:15856-15864.

Zimmermann I, Dutzler R (2011) Ligand activation of the prokaryotic pentameric ligand-gated ion channel ELIC. PLoS biology 9:e1001101.

Zimmermann I, Marabelli A, Bertozzi C, Sivilotti LG, Dutzler R (2012) Inhibition of the prokaryotic pentameric ligand-gated ion channel ELIC by divalent cations. PLoS biology 10:e1001429.

Acknowledgements

I would like to express my gratitude to Prof. Lucia Sivilotti for giving me the opportunity to work on these projects and for all the advice, criticism, help and knowledge that she has given me during these years of working with her.

I am grateful to Remi Lape and David Colquhoun (Dc) for everything they have taught me, for sharing their exceptional skills with me and for all the advice and support they have given me. Also, I would like to thank Mirko Moroni, Elliot Hurdiss, Timo Greiner and Fathma for making the lab a friendly place to work in.

Finally, my thanks to my family and to Cristina and Mattia Kalevi, for their love and sacrifices, their support, trust and their endless patience.